8-18-2014 12:00 AM

Design and Assessment of an Experimental Test Setup For Use in Studies on the Vibrational Response of the Head to Impact

Claudia M. Blandford
The University of Western Ontario

Supervisor
Dr. Thomas Jenkyn
The University of Western Ontario

Graduate Program in Mechanical and Materials Engineering
A thesis submitted in partial fulfillment of the requirements for the degree in Master of Engineering Science

DESIGN AND ASSESSMENT OF AN EXPERIMENTAL TEST SETUP FOR USE IN STUDIES ON THE VIBRATIONAL RESPONSE OF THE HEAD TO IMPACT

(Thesis format: Integrated Article)

by

Claudia M. Blandford

Graduate Program in Mechanical and Materials Engineering

A thesis submitted in partial fulfillment
of the requirements for the degree of
Masters of Engineering Science

The School of Graduate and Postdoctoral Studies
The University of Western Ontario
London, Ontario, Canada

Abstract

With the mortality, disability and socioeconomic costs associated with head injury, head impact biomechanics is important to developing injury criterions and safety tolerances. However, the current state of knowledge is contradictory and vague. This thesis will contribute to research done on the vibrational response of the head to impact by discussing two studies. The first will describe the design, implementation and validation of a head impactor setup specific for the study of the frequency response of the skull. An impactor capable of producing sub-5ms duration, sub-fracture impacts was successfully designed. The apparatus was validated by comparing the results of a protocol to the results published in established literature and a repeatability study was done to prove the repeatability and reproducibility of the impactor. The second part discusses the effects of various factors on the frequency response of the head. Strain gauge data were transformed to the frequency domain and frequency peaks were extracted. Resonant frequencies were then identified by a cluster analysis. ANOVA tests were used to determine the significance of factors on changes to the frequency response. Individual specimen differences were found to have a significant effect on the vibrational response observed, whereas the impact location was found to effect the frequency power ratios only, and not the resonant frequency values. The presence of fracture was also found to have an effect on the overall vibrational response, however the impact energy was not found to have a significant effect.

Keywords: head impact, impact apparatus, repeatability, sub-fracture cranial impacts, vibrational response, skull

Co-Authorship Statement

The research presented in this document was done as a collaborative effort from several individuals. The contributions of those involved are greatly appreciated and are as follows:

Chapter 1: Claudia Blandford - wrote the manuscript, Thomas Jenkyn revised the manuscript.

Chapter 2: Claudia Blandford - wrote the manuscript, Mark Neuert, Arjang Yazdani and Thomas Jenkyn revised a version of the materials and methods section of the manuscript.

Chapter 3: Claudia Blandford - wrote the manuscript, Mark Neuert, Arjang Yazdani and Thomas Jenkyn revised the paper submitted to Journal of Cranio-Facial Surgery on which this chapter is based.

Chapter 4: Claudia Blandford - wrote the manuscript, Thomas Jenkyn revised the manuscript.

Acknowlegements

I would like to acknowlege several individuals for their contributions to, and support of, this work. First of all, I would like to thank Dr. Thomas Jenkyn for being my supervisor and providing me with the opportunity to further my education and develop my skills. My advisory committee members of Jim Johson and Arjang Yazdani provided great mentorship, as well as constant reminders that my project, although preliminary and wrought with troubleshooting difficulties was ultimately interesting. Chris Vandelaar from the university machine shop and Eugen Porter of the university electronics shop gave invaluable advice in the building of the impactor device itself. I would also like to thank the members of the WOBL lab for getting me started, and for the members of the HULC lab for giving us a space to complete our research as well as friendly advice on cadaver experiments (like strain gauging on bone). Noteably Louis Ferreira provided extra assistance in instrumentation selection, and Bjarni Trygvasson must be thanked for his generous procurement of a state of the art data acquisitioning devices. Anne McDonald also deserves a significant acknowledgment, for she spent hours manually examining over 500 frequency spectra and Januvi Jagatheswaran deserves credit for testing some of the early stages of the data processing code. For personal support throughout the perpetuating timeline of this project I have to thank my family and friends (Vanessa Béland) and housemates (Natasha Caminsky). For mentorship and advice at all stages of this endeavour, I would like to thank Mark Neuert. He has been a patient mentor to me as well as an inspiration when I lost interest. Most of all he consistently managed to confirm to me that things will work out in both research and in life if you have the passion and curiosity enough to stay engaged.

Contents

List of Figures

List of Tables

List of Appendices

Chapter 1

Introduction

1.1 STUDY RATIONALE

With up to half of all trauma deaths associated with head injury (Jennett, 1996), it is widely recognized as a serious health problem in western countries (Jennett, 1996). Not only is the associated mortality high, but people involved in road accidents, falls, assaults or any of the other common causes of head injury experience high rates of disability (O'Riordain et al., 2003) as well as contribute to significant socioeconomic costs (Brands, 2002). This significant effect of head injury has inspired a number of studies investigating head impact biomechanics and continues to enforce the need for future research.

The project presented in this document will attempt to supplement the current knowledge state of head impact biomechanics by addressing a few holes in the literature. First of all, several acceleration based head impact studies have already been performed compared to the relatively small body of vibrational response based work (McLean and Anderson, 1997). Therefore, I propose to address this research area by designing an impactor capable of producing repeatable, short duration, subfracture impacts. With this device I can not only confirm the previously reported values of skull natural frequency and its dependency on the specimen, but also determine the effect of impact site location and impact energy on these values. Furthermore, by designing the impactor to be capable of initiating a fracture, I can also study the effect of fracture on the vibrational response of the skull. To the authors knowledge, these fac-

tors have not yet been studied and they will be helpful to increase knowledge of the vibrational dynamics of the head, to validate future finite element models as well as potentially inspire a new direction of inquiry into head injury mechanisms.

1.2 THE HUMAN SKULL AND HEAD IMPACTS

1.2.1 Anatomy and Function

The human skull is an important structure associated with many necessary biomechanical functions. Most significantly the skull surrounds and protects the brain, however it is also a structure that protects the initial stages of the digestive and respiratory tracts, provides an attachment points for muscles controlling eyes and jaw movements, as well as underlines aesthetic and recognizable features of the human face (Martini et al., 2006). Of the twenty-two bones found in the human skull, eight make up the cranium and fourteen are associated with the face.

The cranium is primarily responsible for brain protection, as its eight bones are fused by immoveable joints called sutures creating a spherical shell case in which the brain is located. These eight bones are the occipital bone (1), the parietal bones (2), the temporal bones (2), the frontal bone (1), the sphenoid (1) and the ethmoid (1). These bones are all illustrated in Figure 1.1 and are briefly described in the explanation that follows. The occipital bone is the posterior base of the skull and contains the foramen magnum, a large circular opening in which the vertebral column inserts to connect the spinal and cranial cavities (Martini et al., 2006). Adjacent to the occipital bone on either side are the temporal (inferior) and parietal (superior) bones forming the skulls lateral walls. Both the parietal and temporal bones are attachment points for the masticatory muscles. In addition, the temporal bones support the zygomatic arch of the cheek and protect the inner ear as evidenced by the external acoustic meatus (ear canal) (Martini et al., 2006). The frontal bone forms the superior anterior wall of the skull and comprises the forehead and the superior orbits which protect the eye (Martini et al., 2006). The bones discussed thus far are classified as flat bones (Martini et al., 2006) that are described as

having two parallel surfaces of stiff cortical bone (internal and external tables) sandwiching a spongy bone diploë. The bone that forms the cranial floor and separates the face from the brain cavity is called the sphenoid, a symmetric wing shaped bone that extends from one temporal bone to the other. Externally it is only evident as a small slice of bone wedged between the frontal bone, the faces zygomatic bone and the temporal bone. The last cranial skull bone, the ethmoid connects the sphenoid to the frontal skull and also provides structure to the medial orbit and roofs the nasal cavity (Martini et al., 2006).

The fourteen bones that make up the face are illustrated in Figure 1.2 the maxillae (2), the palatine bones (2), the nasal bones (2), the inferior nasal conchae (2), the zygomatic bones (2), the lacrimal bones (2), the vomer (1) and the mandible (1). The largest of the facial bones is the maxilla, a bone that forms the upper jaw and inferior orbit. The frontal process is a wing of the maxilla that sweeps up to the frontal bone between the eye and the nasal bone and forms the medial orbital floor (Martini et al., 2006). Posterior to the maxilla, anterior to the sphenoid is the L-shaped palatine bones that form the back part of the mouth roof. They also extend up framing the lateral nasal cavity and provide support for the inferior-medial orbit. The bone wedged between the cranial ethmoid and sphenoid that protrudes anteriorly is called the vomer and forms the nasal cavity floor and separates this cavity with a vertical ridge called the nasal septum. The zygomatic bones are very prominent aesthetic features of the face and they are also known as cheekbones. It also forms the inferior lateral orbit and joins with the frontal bone to complete the orbital rim as well as extends posteriorly to articulate with the sphenoid forming part of the orbital floor. This bone is also connected to the maxillary bone to its medial side and laterally to the temporal bone via the zygomatic arch. These four articulations can be described as the tetrapods supporting the most prominent feature of the zygomatic bone, the malar eminence (Zingg et al., 1992). The nasal bones and inferior nasal conchae make up the delicate structures of the nose and nasal cavities, and the lacrimal bones are the last bones described to contribute to the orbital floor. Finally, the mandible forms the lower jaw.

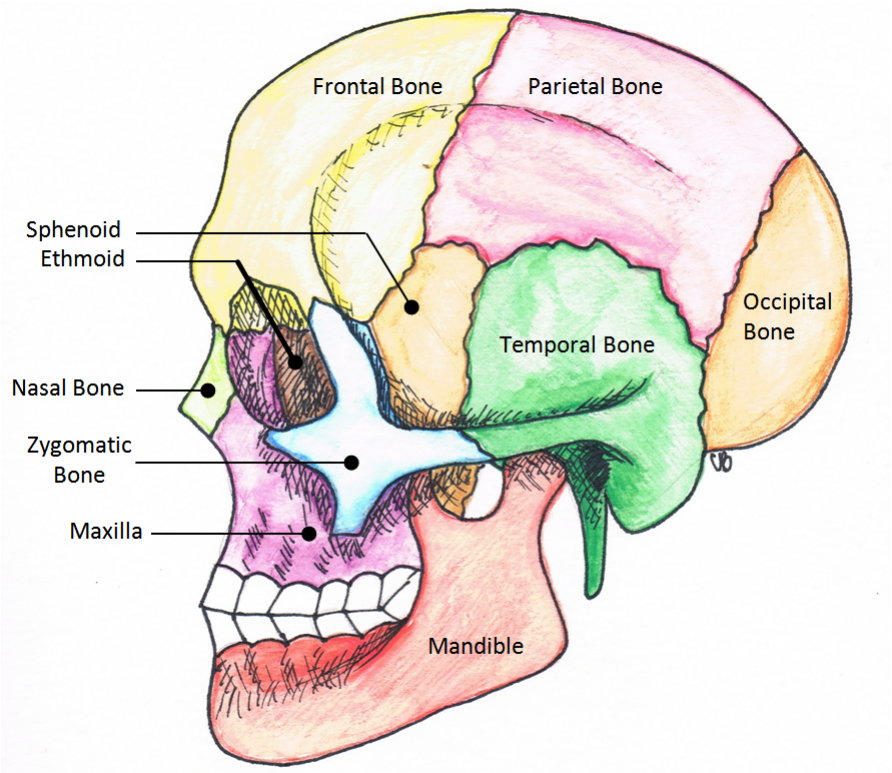

Figure 1.1: Lateral view of human skull

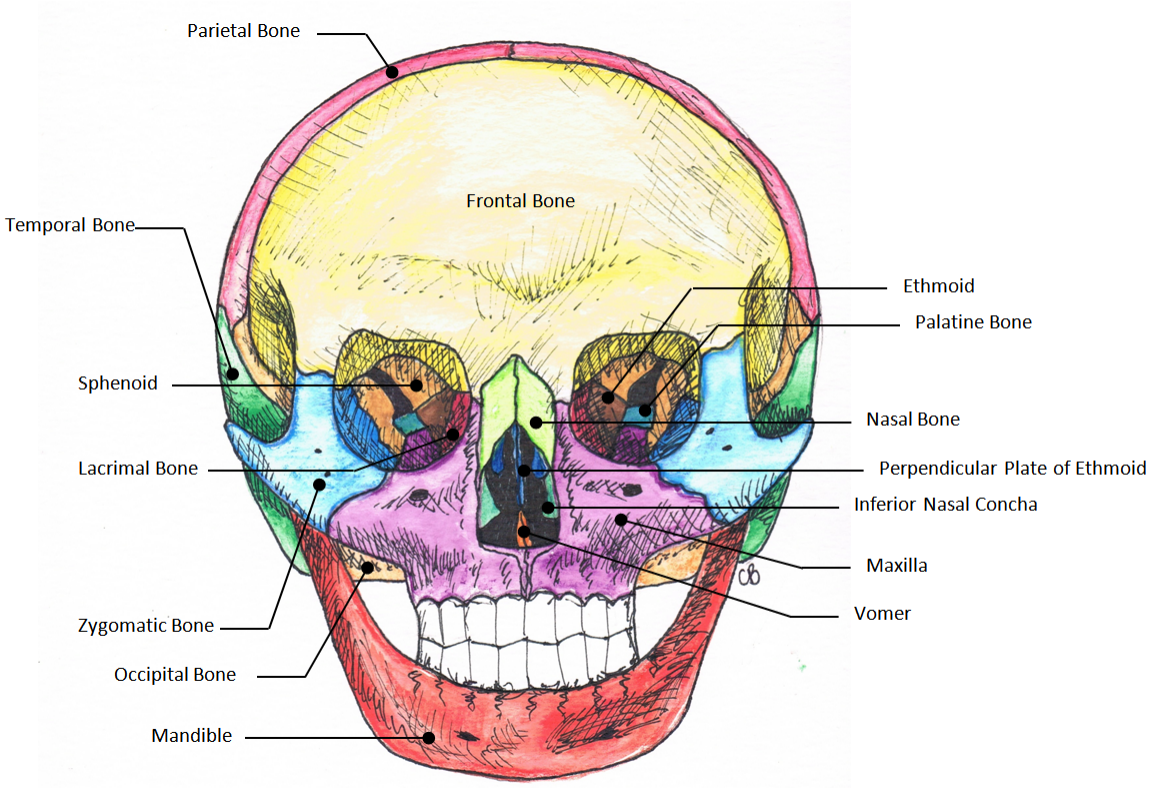

Figure 1.2: Frontal view of human skull

1.2.2 Material Properties and Structure of the Human Skull

The mechanical properties of the human skull have been studied intermittently since the early 1970s, and conclusions on the structure and its behaviour under loading are briefly summarized in this section. The cranial bones are considered to be a sandwich structure, consisting of an inner and outer layer of cortical bone sandwiching a porous, lightweight, trabecular layer called the diploë (Martini et al., 2006). This sandwich structure combined with differing properties of the calcified suture lines where the individual cranial bones come together render the skull non-homogeneous and anisotropic (Misra and Chakraborty, 2005). The mechanical properties of the cranial structure have been studied in a number of projects, the results of which have been found to vary due to a few factors that will be discussed later (Misra and Chakraborty, 2005). That being said, unembalmed post mortem human specimens are typically considered as a composite material of transverse isotropy (Misra and Chakraborty, 2005) with the following properties. The radial compression modulus is 0.4-2.6 GPa, a tangential compression modulus of 2.6-5.6 GPa, and a tangential tension modulus of 5.4-8.8 GPa with a Poissons ratio of 0.19-0.22 (Misra and Chakraborty, 2005; McElhaney et al., 1970).

Factors that can affect the values previously described include age and gender as well as specimen preparation techniques such as embalming or drying of the skull (Misra and Chakraborty, 2005). Age generally decreases the modulus and stress of bone by 20-30% between the ages of 20 and 80 (Yamada, 1970) however a few recent studies have found little statistical significance correlating age to weakened cranial biomechanical properties (Raymond et al., 2009a; Yoganandan et al., 1991; Rhee et al., 2001). Gender is another factor with varying reported significance; a 2009 study found no statistical significance between the parietal bones of men and women (Raymond et al., 2009a), but a 1968 study by Gadd suggested women have weaker facial bones (Hampson, 1995). Low concentrations of formaldehyde used in an embalming process has been found to minimally affect the mechanical properties (McElhaney et al., 1970; Delye et al., 2007) whereas bone drying is found to have a more drastic impact on the mechanical properties of bone in general. Specifically, as bone dries, strain to failure

decreases (Reilly and Burstein, 1974) and the elastic modulus is around 20% higher (Franke, 1956).

Strain rate can also affect the modulus and strength values as it is a widely accepted fact that the human skull responds viscoelastically to loading (Robbins and Wood, 1969; McElhaney et al., 1970; Misra and Chakraborty, 2005; Motherway et al., 2009). Stiffness and strength is found to increase with loading rate (Motherway et al., 2009) which is a significant observation in the context of impact testing, as different impact speeds are often tested. This viscoelasticity may also contribute to the varying recorded values of mechanical properties such as force to fracture which can differ by as much as 6000N between quasi-static (0.002m/s) and rapid (7.5m/s) loading conditions (Yoganandan et al., 1995).

1.2.3 Head Impacts and Associated Injuries

Head and facial impact injuries are known to have a number of detrimental effects including mortality, disability, as well as financial and resource costs on healthcare (O'Riordain et al., 2003). These injuries, often the result of motor vehicle accidents, falls, and assaults, can cause serious health risks by inducing brain injuries such as haematomas, contusions and diffuse axonal (concussion) injuries (O'Riordain et al., 2003). Research attempting to study these injuries must simulate the impact conditions of these clinically realistic events, the characteristics of which will be discussed in this section.

Much research has been done in attempt to characterize the impact conditions based on the either the severity of injury or the type of injury sustained and although there is still much debate among researchers as to the ideal way of classifying impacts and head tolerances (Melvin et al., 1993) an idea of the types of impacts generally studied and their real world effects can be obtained from these classifications.

Generally, closed head impacts are characterized by the impact acceleration, and the impact duration (McLean and Anderson, 1997). These quantities are the result of several notable inputs, such as the weight and size of the impactor, the velocity at impact, the impact stiffness

and the constraint of the specimen (Melvin et al., 1993). Short impacts are commonly called ballistic impacts and occur when a projectile of low mass strikes the skull with a high velocity, causing a propagating strain wave front through the head (Brands, 2002). These wave fronts are hypothesized to be a significant factor in many head injury mechanisms, but this has not been adequately confirmed in the literature (Brands, 2002). These short impulsive impacts have also been shown to excite the skull to vibrate transiently at its natural frequencies (Willinger et al., 1994; Khalil and Viano, 1979; Gurdjian et al., 1970), causing the skull to deform according to mode shapes (Khalil and Viano, 1979). Activities that can induce short impacts can include slips and falls where the head rapidly connects with stiff ground, or during sporting events where a ball or other projectile at high speed contacts the head. This type of impact has also been reported to occur when police use non-lethal ballistic missiles in law enforcement (Raymond et al., 2009b).

Long impacts are generally caused by lower velocity impacts with large masses and can be further lengthened by decreasing the impact stiffness through the use of padding. These impacts do not excite vibrational modes of the skull and are instead hypothesized to cause deeper tissue injuries caused by brain shear due to the inertial forces arising with the longer impacts (Willinger et al., 1995). Head impacts as a result of car accidents generally fall in this category as there is significant padding in the car interior slowing the impact and increasing it's duration.

Overall, the head can experience a large variety of impact conditions depending on the circumstances of the accident. From an experimental design standpoint, this means that the researcher must consider the impact most relevant to the question at hand, and develop procedures to ensure the desired impact conditions are met.

1.3 HEAD IMPACT APPARATUSES

1.3.1 Review of Apparatuses Used in Previous Studies

The validity of head impact studies depends heavily on the apparatus used to deliver the impact, as the goal of trauma biomechanics is to relate the input energy created by the apparatus to the output kinematics observed (Hardy, 1993). Thus in order to accurately reproduce and study the injury inducing impact, the apparatus must be designed to accomodate the impact particulars. Several varied approaches have been used in the past to simulate the head impacts described in Section 1.2.3 including drop tests, pneumatic and hydraulically driven impact devices as well as a few other apparatus designs. In this section I will discuss the details of these tests as well as review the advantages and disadvantages of these methodologies.

Vertical Drop Testing Apparatuses

Drop and guided fall tests are the most frequently used testing method for head impact studies (Verschueren et al., 2007), and it was also one of the first testing methods to be used in head impact biomechanics. Generally, the drop test consists of an instrumented specimen that is constrained to a vertical drop track. The specimen is then raised to a desired height or energy level and left to drop onto an instrumented surface.

The earliest example, like that used by Gurdjian in as early as the 1950s, was simply a free fall drop of a skull coated in a strain-sensitive lacquer, without even the use of a force plate or vertical track (Gurdjian et al., 1949). With these methods, Gurdjian qualitatively studied linear skull fractures and concluded that fractures initiated at the locations of maximum outbending. By the 1970s this methodology was improved to include a vertical guide track in a study by Hodgson (Hodgson et al. 1970 as cited in Verschueren et al. (2007)).

Yoganandan et al. in a 1991 study used a vertical guided fall testing system that was 7.6 m high with a carriage designed to fix intact cadaver heads at any superior/inferior and medial lateral orientations to impact the specimens at a specific site. This carriage was supported

by bearings and guided by a vertical monorail with two side outrigger mechanisms to prevent rotation of the carriage about the vertical axis. This device was capable of delivering controlled impacts at speeds of up to 12 m/s. An accelerometer mounted on the skull along with a load cell and a potentiometer placed under the impact surface provided the force and deformation information of the impact, gathered at a sampling rate of 8000Hz. Impact velocity was also collected in this study (Yoganandan et al., 1991). This setup is a typical example of a modern drop testing setup, and as it is a setup similar to those used by other notable head impact studies of the 21st century (Rhee et al., 2001; Vander Vorst et al., 2004).

Generalizing the following Table 1.1, which is a summary of drop and guided fall impact apparatuses, the modern drop tower is a well tested methodology for head impact testing. Recorded impact velocities generally range between 0-10 m/s with the lower velocities used in sub-fracture testing, the higher ones recorded in tests studying fracture. Load cells and accelerometers are instruments found in nearly all cases giving convenient and well established access to impact biomechanics such as the force and time history for various impacts. The apparatus is relatively simple to design and construct as gravity is used as the source of input energy. However apparatuses of this nature have certain established disadvantages as well. First of all, some of the biomechanical information of interest is inferred assuming idealized conditions. For example, none of the apparatuses discussed calculated the velocity directly, and measured it only through the assumption that a perfect free-fall occurred. Considering the potential energy losses due to friction in the vertical track the velocities reported may have extra associated uncertainty. Deformation is another variable that is not easily measured by these devices. Reported values are generally either the displacement of the impact surface or the deformation obtained by double integrating the accelerometer curve. In the former case, this displacement is not an accurate portrayal of the local deformation experienced by the specimen. Double integration also has flaws as it is known to amplify measurement errors arising from accelerometer drift and also has depends on assumed initial conditions (Slifka, 2004). The biomechanical event simulated by these devices has also been called into question by Ver-

Source	**Description**	**Measured Variables: values (instrumentation)**	**Calculated Variables: values (method)**
Gurdjian et al. 1949	Skull coated with a stresscoat lacquer is dropped to free fall onto slab of 160lb steel	weight of head; height of drop: 101-244cm	energy absorbed to fracture: 45-100J (calc using weight and height); impact velocity: 4-7m/s (free fall eq with height)
Hodgson et al. 1970	Guided fall device	impact force; linear head acceleration (accelerometer)	——-
Yoganandan et al. 1991	7.6m monorail device with carriage to fix specimen	head acceleration (tri-axial accelerometer); impact force (load cell); surface deformation (potentiometer) *sampled at 8000Hz	impact velocity: 0-12m/s (from dropped height)
Rhee et al. 2001	Same as Yoganandan et al. 1991	head acceleration (tri-axial accelerometer); impact force (load cell)	impact velocity: 2-7m/s (from height dropped)
Vander Vorst et al. 2004	Free fall drop test with flat durometer impact targets	impact force (load cell); impat duration: 3-9ms (load cell) *sampled at 12.5kHz	impact velocity: 2-10m/s (from height dropped)
Yoganandan et al 2004	Same as Yoganandan et al. 1991	head acceleration (accelerometer); impact force (load cell); impact duration: 8ms *sampled at 12.5kHz	impact velocity: 5-8m/s (from height of drop); deformation of skull (double integration of accel curve); energy absorved to fracture (integration of force-deflection curve); HIC (from head acceleration and impact duration)

Table 1.1: Drop tower impact apparatuses in previous studies

schueren et al. (2007) who suggests that the excess weight of the carriage or the specimen-track fixture can cause a crushing event upon impact, squeezing the specimen between the impact surface and the moving part of the drop tower (Verschueren et al., 2007). This issue can be eliminated in the free fall techniques of Gurdjian (1949) and Vander Vorst (2004) however lacking constraints on the specimens orientation can lead to uncertainty of the impact site.

Pneumatic and Hydraulic Impact Apparatuses

Another class of impact testing apparatuses are those that involve pneumatic or hydraulic propulsion. These tests tend to consider much higher impact velocities and smaller impact durations and are most often found in studies concerning blunt ballistic impacts. However, there exist a few examples that utilize the lower speeds and longer impact durations comparable to those of the guided fall tests discussed in the previous section.

One of the earliest ballistics tests was for a study done in 1967 by Hodgson (Hodgson, 1967). This test setup consisted of an entire cadaver specimen constrained to a swinging chair and a pneumatic piston device. This device accelerated solid metal impactors between 2 and 16 pounds through an air cylinder driven with compressed air. The impactor is instrumented with an accelerometer to obtain the force history data, and a set of magnetic probes at the end of the air cylinder are used to calculate the impactor velocity. The cadaver is also instrumented with an accelerometer opposite the impact site to measure head acceleration. This pneumatic cannon was capable of producing impacts with variable speeds (0.5-8.5m/s) by adjusting the weight of the impactor and the pressure of the air cannon, as well as variable impact times (2-25ms) by adjusting the padding on the impactor end effector.

More modern examples of a ballistic impactor can be found in studies by Viano et al. (2004) and Raymond et al. (2009). Both of these devices consisted of a projectile accelerated through a cylinder by a pressure vessel. These projectiles weighed anywhere between 25-30g (Viano et al., 2004) or 103g (Raymond et al., 2009b,a) and were instrumented with an accelerometer to obtain impact force in both cases. Both setups also included a high speed camera to record

the kinematics and in the case of Viano, this data is also used to calculate the deformation at maximum force.

The ballistics tests are a useful methodology for studying high speed, blunt impacts, such as those found in cases of less-lethal law enforcement ballistics (Raymond et al., 2009a) or blunt shrapnel injuries in a military context. These high speed, short duration impacts would also be useful for studying the vibrational response of an impact to a specimen, as this type of impact will be closest to that of a delta function assuming no mechanical damage is issued upon impact. Despite these advantages, the repeatability of ballistic test devices often decrease as impact velocity is lowered. For example, in 2009 a Raymond et al. study found relative standard deviations of 4% for impact speeds of 35m/s, but a relative standard deviation of 13% was found when the impact speed was reduced to 20m/s, suggesting that these devices are not ideally suited for studying lower speed impacts (Raymond et al., 2009b). These devices are also much more complicated and costly to design and build especially if a high level of precision was desired for a range of different impact speeds.

Hydraulic and pneumatically driven impactors have also been used to test at lower speeds ranging from a quasi-static loading rate to impact speeds comparable to those of the aforementioned drop towers. A 1969 study simulated impacts with a pneumatically powered Instron machine (Melvin et al., 1969) and in 1995 Yoganandan et al. describes a study using and a hydraulic piston impactor (Yoganandan et al., 1995). Characteristic of both these designs is that the impact is induced by the cylinder itself rather than a separate, moveable mass. This design provides the advantages of being a more controllable and repeatable system, and is also capable of directly measuring the local deformation via the piston position. Unfortunately, due to the pneumatic/hydraulic nature of the pistons driving force, the rebound of the piston off the specimen is hindered, leading to longer impact times, making it a poor choice in the study of specimen vibrational responses. Another disadvantage to note in the 1995 Yoganandan et al. setup is his use of a rigid specimen constraint. Contrary to the guided fall device setups which used no constraints or the minimally constrained, invertedly hung specimen used in the ballis-

tics tests, Yoganandan fixed his specimens rigidly at the distal end with a U-shaped clamped bracket with screws tightening into the auditory meatii. Although this setup provides some advantage of precisely defining the impact site, the stress distribution is not comparable to a clinically realistic neck constraint.

Other Notable Devices

Recently, a few other notable impactor designs have been developed, including a double pendulum testing device, a horizontal impact simulation and a variation on the drop tower design.

The double pendulum apparatus was designed in 2007 by Verschueren et al to eliminate the difficulties in measuring local deformation and to accurately simulate inertial effects of a body undergoing head impacts (Verschueren et al., 2007). This device consists of two aligned pendulums, one made of steel weighing 14.3kg that is raised and dropped to strike a blow on the inverted specimen fixed to the second aluminium pendulum. This device can measure impact force with a force sensor on the impacting pendulum as well as the local deformation with a laser displacement sensor attached to the impactor pendulum arm combined with a reflective device mirrored onto the specimen supporting pendulum (Verschueren et al., 2007). The researchers concluded that as long as vibrational effects captured by the displacement laser were minimal, accurate local deformation measurements could be made (Verschueren et al., 2007). Furthermore because each pendulum arm was over 1m long, and that the specimen was fixed via a steel strut and resin through the foramen magnum, this device is well equipped to simulate a more clinically realistic impact condition in the context of neck stiffness and inertial effects. However, it should also be noted that the authors themselves concluded based on high speed video and additional displacement lasers that neither inertial effects of the body nor the neck force acting on the head have an effect on the fracture tolerance of the head (Verschueren et al., 2007). This suggests that the additional weight and structure characteristic of this device is not necessary for simulating clinically realistic fracture tests. Furthermore, these inertial effects make it a poor device for simulating the short duration impacts necessary for studying

the vibrational effects, as the pendulums momentum increases the impact duration to over 8ms.

A testing device designed by Hardy et al. in 2007 consists of horizontally accelerating an inverted specimen fixed onto a subassembly carriage on horizontal rails. The acceleration of the carriage is driven by a pneumatically controlled piston and the impact occurs when the specimen-carriage subassembly connects with a stationary target (Hardy et al., 2007). Thus, this device is comparable to both the pneumatic driven impactors of Yoganandan et al. (1995) and the guided fall apparatuses. For example, the impact speeds tested were similar to those of the guided fall devices at 3-4m/s but the potential crushing effects of drop test devices are mitigated because the effects of gravity are removed. That being said, the repeatability issues associated with the use of a pneumatic device still stand as do the difficulties in obtaining a short impact time and data for a vibrational response study.

The last device to be reviewed is a device similar to the guided fall apparatuses discussed in the first section. However, instead of fixing the specimen on a moveable carriage, the drop tower apparatus designed by Kroman et al. in 2011 consists of a free falling mass onto a stationary specimen. Specifically, an 8.58kg weight instrumented with a load cell is dropped from 1.96-2.82m and allowed to contact the specimen (Kroman et al., 2011). This specimen is loosely supported by wooden beam design to fail at the slightest increase in pressure, eliminating the crushing biomechanical effects characteristic of traditional guided fall and drop test devices. Little information on the impact speeds and impact durations are available for this device, but considering that the duration of contact is dependent on the performance of the loose support, repeatable impacts in the context of subfracture testing would be difficult to obtain.

1.3.2 General Considerations of Impact Apparatus Design

In general, an impact apparatus design must provide an accurate simulation of clinically realistic impact conditions and events. This requires considerations to the specimen fixture, the precision and control of input variables, the input energy source as well as the instrumentation used for data collection. In general, the goals of an impact apparatus design should reflect the

objectives of the research studied.

Specimen fixture should not be rigidly constrained as in the setup of the 1995 Yoganandan et al. experiment, as this can alter the stress distribution of the impact on the head (Yoganandan et al., 1995). That being said, Verschueren concluded that rotational effects of head occur significantly after the maximum experienced load (Verschueren et al., 2007), suggesting that as long as the specimen is supported at a location comparable to the natural neck (ie the foramen magnum) the stiffness of this support is less critical to the experimental outcome.

Precision and control of the impact event is more important to experiments requiring repeated tests, such as those used in subfracture specimen testing. For example, research aiming to study a fracture event will be interested only in the single trial that fracture occurred, whereas repeated tests on the same specimen will require precise input variables to ensure that all repeated tests are as comparable as possible. These input variables include the impact location on the specimen, the velocity at impact, and the mass of the impactor weight.

The input energy source is another factor to consider. We have discussed apparatuses using gravity and pneumatic pressures as well as the advantages and disadvantages of each. Namely, gravity will be a more consistent source of energy providing the guiding track has minimal energy losses, whereas the pneumatic devices are useful to increase the force and speed at which a projectile is launched.

The instrumentation used for data collection will probably be most specific to individual research goals; however there are a few general factors for consideration. Sampling rate is a significant aspect of data collection, and the rate used must be rapid enough to capture the impact event. Although most historical studies have captured at rates of around 10-20 kHz (Viano et al., 2004; Raymond et al., 2009b; Yoganandan et al., 2004; Vander Vorst et al., 2004; Hardy et al., 2007), increased sampling rates of up to 65kHz have been used (Verschueren et al., 2007). Impact force is measured in all head impact studies, and is generally captured using accelerometers (Raymond et al., 2009b; Viano et al., 2004; Hardy et al., 2007) or load cells (Yoganandan et al., 1991; Rhee et al., 2001; Vander Vorst et al., 2004; Yoganandan et al.,

2004). Some of the output variables such as impact velocity and deformation have been collected both through calculations as well as directly. In the case of vertical test setups, a free fall calculation (Gurdjian et al., 1949; Yoganandan et al., 1991; Verschueren et al., 2007) may be a fairly accurate alternative to a velocity trap (Hodgson, 1967; Viano et al., 2004; Raymond et al., 2009b), especially if there is minimal energy losses in the guide track. Deformation measurements has been calculated by double integrating the accelerometer curve (Yoganandan et al., 2004) and through high speed video frames (Raymond et al., 2009b; Viano et al., 2004) neither of which have proven to be a very accurate option (Verschueren et al., 2007). Direct deformation measurements are also very difficult to obtain and have only been collected through a laser deflection system (Verschueren et al., 2007) and piston motion of a quasi-static test (Yoganandan et al., 1995).

There are advantages and disadvantages to all instrumentation available, and they must be considered thoroughly in a head impact apparatus design.

1.4 RESPONSE OF THE HEAD TO IMPACT

The main goal of head impact studies is to define human injury tolerances towards head impacts for use in developing safety standards. To do this, the response of the human head to impact must be studied. The prevailing focus of the literature is the head kinetics, including the deformation, accelerations, and global kinematics responses of the head to impact and with this information a few injury mechanisms are proposed. This next section will briefly summarize the state of knowledge in head injury biomechanics by outlining a few key studies.

1.4.1 Skull Fracture Response

Linking the biomechanical response of the head to skull fracture has the largest body of investigative literature, with the most common being the fracture response to impact forces and velocities. Nahum in 1968 was the first to assign a tolerance value to skull fracture at 4000N

for frontal skull bone and 2000N for temporo-parietal bone based on fracture forces in tests ranging from 2670-8850N (frontal) and 2215-5930 (temporo-parietal) (Melvin et al., 1993). Fracture values in this range have been reported by several other studies (Shneider and Nahum, 1972; Allsop et al., 1988; Yoganandan et al., 2004; Delye et al., 2007) however this range is so large that several researchers are pursuing fracture tolerances based on alternate biomechanical parameters. Some of these include energy absorbed to fracture (Delye et al., 2007), strain to fracture (Raymond et al., 2009b), or velocity of impact (Rhee et al., 2001) with values of 22-24J (Delye et al., 2007), 2000-6000 $\mu\epsilon$ (Raymond et al., 2009b), and 3.5m/s (Rhee et al., 2001) respectively.

1.4.2 Brain Injury Response

Because brain injury has been found to occur in subfracture cases, researchers have also looked into subfracture impacts and their effects on the brain. Early human head tolerance criterions considered only head acceleration (angular and linear) as an injury mechanism but when competing studies came back with contradictory results, researchers at Wayne State University developed the Head Injury Criterion (HIC) which included a dependence on the impact duration as well (McLean and Anderson, 1997). This is still the most widely accepted injury criterion today and suggests that clinically realistic injuries are the result of short-acting, high accelerations, as opposed to long, low acceleration impacts (McLean and Anderson, 1997). This conclusion has been supported specifically in the case of skull fracture injuries, but results have been inconclusive in the context of brain injury leading many researchers to reject HIC as an injury criterion in favour of mechanisms relating to specific lesion types (McLean and Anderson, 1997). Some of these proposed mechanisms suggest that haematomas are more likely to occur with high acceleration (over 200g's) and short durations (less than 3.5 ms) (Genarrelli and Thibault 1982 in O'Riordain et al. (2003)) as the brain will most likely move relative to the skull. Diffuse axonal injuries and concussion on the other hand have been argued to be caused by slower impacts at lower accelerations, where the motion of the brain with the skull

can cause deep tissue damage (Willinger et al., 1994).

Overall, brain injury mechanisms are still crudely understood and it is difficult to determine the impact response of the head in the context of injury mechanisms and tolerances.

1.4.3 Vibrational Response of the Head to Impact

While many acceleration based injury mechanism theories have been proposed throughout the history of head impact studies, a few researchers have taken a different approach by studying the vibrational response of the head upon impact. These vibration studies are significant not only for injury mechanisms they hypothesize, but because they also describe an important aspect of the dynamic characteristics of the head and skull which can be used to validate analytical or finite element models.

The first head vibration research was studied not in the context of head impacts, but concerned with the role of bone conduction in hearing. In 1948 Békésy measured the skull movement of live patients at the frontal and occipital regions with transducers, and vibrated the frontal region with a vibrating piston (Békésy, 1948). He concluded that the first resonant of the skull was at 1800Hz, and used this value to examine effectiveness of hearing protection devices. Later, in 1951 he conducted a similar study and found two resonant frequencies, at 800Hz and 1600Hz, suggesting that the initial frequency reported may have actually been the second frequency of the skull (Khalil and Viano, 1979). This work initiated head vibration research despite future criticisms of loose boundary conditions due to living subjects (Khalil and Viano, 1979), inconsistent vibrator preload due to the methodology of simply pressing and holding the instrument onto the subject (Stalnaker et al., 1971), as well as the fact that the transducers were placed on top of skin and soft tissue leading to the question of the effects of vibrating soft tissue on the transducer signal (Franke, 1956).

Franke (1956), and Stalnaker et al. (1971) were interested in the vibrational response of the head to quantify its dynamic characterisitics for use in analytical and continuum models. They focussed on evaluating the mechanical impedance of the head and obtained results significantly

different to the earlier studies by Békésy. By using a vibrating piston and an electromagnetic shaker respectively, Franke and Stalnaker et al. measured the local head motion of cadaver head and skulls and determined the first and second resonant frequencies to be significantly lower. Franke determined the first resonant frequency of a dry skull to be 820Hz and hypothesized that the added mass and damping contributed to his resonant findings of the cadaver head of 600Hz and 900Hz (Franke, 1956). The cadaver tests done by Stalnaker et al. supported these low values, as he reported two resonant frequencies of 166Hz and 820Hz. Stalnaker et al. also concluded that a specimen without a scalp or cranial contents did not alter these resonant frequencies despite contributing to increased damping (Stalnaker et al., 1971).

In 1970, Gurdjian and Hodgson were the first to conduct vibrational tests in an effort to hypothesize head injury mechanisms. With impedance sensors rigidly anchored to the frontal, occipital, and left parietal bone, as well as the vertex of the head, this study measured the local skull movement with differing impact lengths. Their study suggested that with long impacts that excite only the low frequencies below 200Hz, the empty cadaver head acts as a rigid body and no vibrational response was noted. Tests done by applying sinusoidal forces suggested that an antiresonant mode at 313Hz could contribute to contrecoup injury as the high impedance found at the frontal bone impact site was compared to the larger deflections of the occipital site. A large amplification ratio was found at a second resonant mode of 880Hz, which was later confirmed by impact tests to be excited with short impacts on the order of 3ms (Gurdjian et al., 1970).

Concerned about the lack of higher frequency investigations and mode shape characterization as well as the arbitrary boundary conditions and driving point motions of the past studies, Khalil et al. extensively explored the vibrational characterisitics of two dry skulls. He did this by measuring the local acceleration of several points of each skull upon a short impulsive impact on soft rubber foam to simulate a free support condition. He made several conclusions on the vibrational response of the head including a first resonant frequency at 1385 (skull 1) and 1640 (skull 2), and that the vibrational response of each skull was unique. That

is, the number of resonant frequencies found differed (11 for skull 1, 6 for skull 2), and the mode shapes corresponding to each resonant frequency differed between skulls. Khalil et al. also discussed the low resonant frequency values previously reported in the literature and suggested that added mass due to various support conditions and the rigid attachment of excitation methods (impedance sensors, vibrator preloads etc.) may have contributed to inaccurately low values (Khalil and Viano, 1979).

Between the 1979 and 1995, limited research was done on the subject of vibrational response on the skull, except for Fujiwara et al. in 1989. This group performed a modal analysis upon impact with 13 accelerometers and a rigidly supported head and alluded to a contrecoup injury mechanism caused by the inbending and outbending of the skull upon periodic deformation. He also determined that the inbending-outbending motion occurred at frequency of 380Hz suggesting this to be a resonant frequency (Fujiwara et al., 1989).

More recently, Hakansson et al. studied the head frequency response of live human subjects by using titanium bone conducting hearing aids as a vibrator. This study confirmed that of Khalil et al., as he found resonant frequencies and the frequency response to vary largely between patients. The lowest frequency response he recorded was between 828Hz and 1164 Hz with a second between 981Hz and 1417Hz (Hakansson et al., 1994). This study, although brilliant in its methods of finding the resonant frequencies of the skull, does not look at the vibrational response upon impact. Because most trauma is due to an impact event, it is more clinically relevant to study the vibrational response in this context, as impact characteristics such as different sites and energy levels are not taken accounted for in this methodology.

The last study that will be discussed in this section is that of Willinger et al. (1995). From mechanical impedance measurements he performed on a live human subject he discovered a resonant frequency at 150Hz and an accompanying decoupling of a 1.5kg mass. He used this data as inputs to one analytical and two finite element models. With these models, Willinger et al. concluded that impacts that excite mainly the lower frequencies (long impacts) cause the brain to move with the head motion causing a gradient state of stress and deep tissue

strain. Short shocks on the other hand that excite this 150Hz resonant cause a decoupling of the brain mass from the skull and can cause relative displacement, leading to haematomas, and contusions (Willinger et al., 1995). These conclusions are useful on a macroscopic scale and in the context of head injury mechanisms, however the authors did not consider the effects of higher vibrational modes, such as those reported in Khalil et al. (1979) and Hakansson et al. (1994).

The current state of knowledge is far from defining the response of the human head to impact, let alone the injury mechanisms associated with these dynamic characteristics. That being said, several notable studies have laid the groundwork necessary for continued study in this research area.

1.5 ANALYSIS TECHNIQUES AND CALCULATIONS

Several methods were used to collect, reduce and analyse the presented data. Some of these techniques are complex enough to warrant extra explanation which will be discussed in this section. Specifically, the calculation of strain and principal strain from strain gauges, discrete fourier transform techniques for studying the frequency domain of the collected temporal strain data, as well as statistical methods of analysis of variance (ANOVA) tests and cluster analyses used to classify the data and present conclusions.

1.5.1 Strain Gauges and Calculations

Foil strain gauges are instruments commonly used to measure strain and mechanical motion. The electrical resistance of the gauge material is proportional to the strain the material experiences, and this property can be utilized to measure the instantaneous spatial-average strain of an object over the surface to which the gauge is securely bonded (Wilson, 1996). It is a useful instrument in the field of shock and vibration as a gauge recording can also determine the time-history of an impact event from which frequency response can be obtained (Wilson,

1996).

Basic strain gauge theory is centered around the relationship between change in resistance and change in foil length and hinges on the gauge factor to describe this proportionality.

$$GF = \frac{\Delta R/R}{\epsilon} \tag{1.1}$$

where

$\Delta R/R$ is the change in gauge resistance over unstrained resistance

ϵ is the strain of the wire

GF is the gauge factor of the strain gauge

The gauge factor is found to be approximately +2.0 for common strain gauges with constantan filament materials (Wilson, 1996).

A strain gauge is typically wired to a data acquisition system using a wheatstone bridge (Figure 1.3) which serves the dual function of both providing an electric current (excitation voltage) as well as measuring the voltage drop across the gauge indicating changes in the strain state. Specifically, the wheatstone bridge is wired such that the following relationship holds true.

$$V_{out} = V_{ex}[\frac{R_3}{R_3 + R_g} - \frac{R_2}{R_1 + R_2}] \tag{1.2}$$

where

V_{out} is the output voltage

V_{ex} is the excitation voltage

R_1, R_2, R_3 is the resistance of fixed value resistors

R_g is the variable gauge resistance

From this equation, we can see that when $R_1/R_2 = R_g/R_3$, V_{out} becomes zero. This is defined as a balanced bridge and it is then simple to obtain the strain value using equation 1.1. However, it is often difficult to balance the bridge, and, especially in the case of dynamic testing where

the relative strain change is of more interest than the absolute strain magnitude, unbalanced bridges are compensated for by using additional calculations.

Equation 1.2 will hold for both the strained and unstrained cases, providing us with a way of describing the voltage ratio between the strained and unstrained cases, specifically:

$$V_r = (\frac{V_{out}}{V_{ex}})_{strained} - (\frac{V_{out}}{V_{ex}})_{unstrained} \tag{1.3}$$

where

V_r is the difference of the ratios between the unstrained and strained cases

Subsitituting equation 1.2 in for the two V_{out}/V_{ex} terms we can derive the following equation.

$$\Delta R_g/R_g = \frac{-4 * V_r}{1 + 2 * V_r} \tag{1.4}$$

where

ΔR_g is the resistance change between the strained and the unstrained states

With $\Delta R_g/R_g$ defined, we can use equation 1.1 to solve for our strain with an unbalanced bridge.

These simple equations are part of the reason strain gauges are such a popular measurement tool, however they are subject to a few limitations. Temperature effects are a major concern in many strain gauge applications as many strain sensitive materials vary their resistance with temperature as well. Fortunately these effects are negligible in dynamic impact testing as temperature changes occur on a time scale significantly larger than strain changes occuring during a 5ms impact. Furthermore, the analyses done for this thesis involve only the frequency response of relative changes between strain states. Therefore, limitations affecting the accuracy of the gauge, such as added resistance of lead wires or transverse strain effects are unecessary to account for.

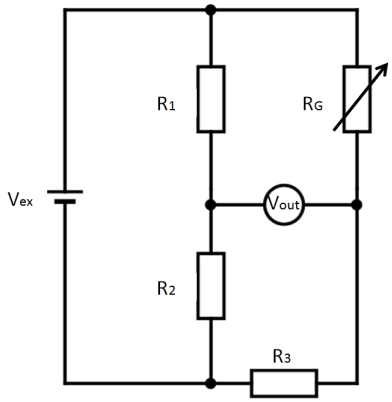

Figure 1.3: Diagram of a wheatstone bridge circuit

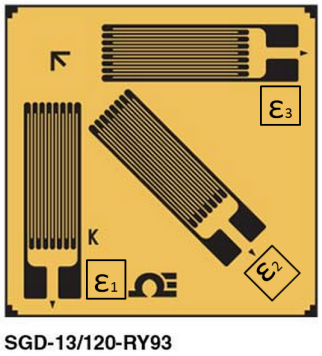

Figure 1.4: Diagram of a three element strain gauge

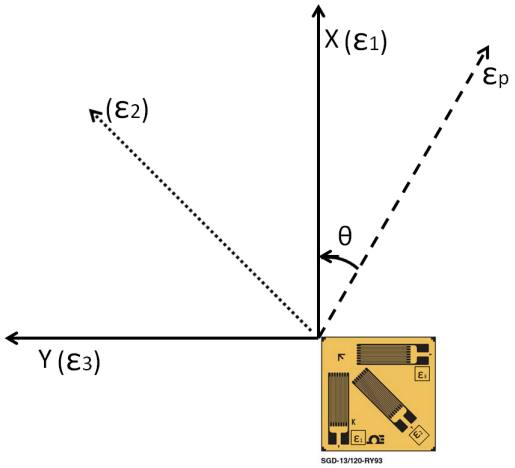

Figure 1.5: The principal direction angle is calculated with the three known strain values and is the clockwise rotation of the principal strain axis by angle θ to the original gauge orientation

Because the strain direction at the several gauge locations tested in this study are unknown, three element gauges (both stacked rosettes and triaxial gauges) were used to obtain the principal strain. A three element gauge is essentially three superimposed uniaxial gauges directed 45 degrees from each other, as illustrated in Figure 1.4. The strain is measured from each direction simultaneously in the same way a measurement would be recorded by a uniaxial gauge. However, the precise positioning and direction of these three gauges make it possible to perform additional calculations using these three measurements to obtain the principal strains at each location. These additional calculations are essentially transformation equations that describe the strain state in the orientation with which only normal strains are present. These strains are defined as the principal strains and are calculated with the following equations.

$$\epsilon_{P,Q} = \frac{\epsilon_1 + \epsilon_3}{2} \pm \frac{1}{sqrt2} \sqrt{(\epsilon_1 - \epsilon_2)^2 + (\epsilon_2 - \epsilon_3)^2} \tag{1.5}$$

where

$\epsilon_{P,Q}$ are the principal strains

$\epsilon_{1,2,3}$ are the strains measured from the three superimposed directions on the strain gauge, numbered counterclockwise (as in Figure 1.4)

The principal angle can also be calculated using the same transformation theory, and this angle describes the angle between the principal axis and the axis to which the reference strains ($\epsilon_{1,2,3}$) are calculated. Figure 1.5 illustrates this angle that is calculated with the following equation.

$$\theta = \frac{1}{2} \arctan\left(\frac{2\epsilon_2 - \epsilon_1 - \epsilon_3}{\epsilon_1 - \epsilon_3}\right) \tag{1.6}$$

where

θ is the clockwise rotation angle of the principal strain axes to the original gauge orientation

$\epsilon_{1,2,3}$ are the strains measured from the three superimposed directions on the strain gauge, numbered counterclockwise (as in Figure 1.4)

1.5.2 Discrete Fourier Transform

In order to extract the frequency response information from the strain gauge data, a discrete fourier transform (DFT) was used to transfer the time domain strain history data into that of the frequency domain. The DFT is implemented to reduce computational time in the case of sampled data and can also transform aperiodic functions if used correctly (Richardson, 1978). The DFT also reduces the computational time compared to the classic fourier transform by employing the fast fourier transform (FFT) algorithm which limits the resolution between frequencies identified. Because the data transformed for this work consisted of discrete sampled data, and that the sample window of data transformed was large enough to provide adequate resolution, it was the DFT and not the basic fourier transform that was used for data processing.

Fundamentally, a discrete dataset is a continuous dataset $x(t)$ that is bounded by a finite time window and multiplied by a sampling function. The time window function defines the interval between which the transform will be performed, and the sampling function is essentially an impulse train of unit amplitude occuring at every Δt where Δt is the time between samples ($\frac{1}{f_s}$, where f_s is the sampling rate). These modifications to the continuous function ensue modifications to the fourier transform and these modifications to the fourier transform result in the DFT. Specifically, the time window bounds the integral in the fourier transform, and the impulse train alters the integral to a summation, as the integrand exists only at the sample points (Mandal and Asif, 2007). Thus, the fourier transform of the original signal $x(t)$:

$$X(j\omega) = \int_{-\infty}^{\infty} x(t)\mathrm{e}^{-j\omega t}\mathrm{d}t \tag{1.7}$$

becomes

$$X(n) = \sum_{k=0}^{N-1} x[k]\mathrm{e}^{-j\frac{2\pi}{N}kn}(n = 0 : N-1) \tag{1.8}$$

where

N is the number of samples in the time window

k is the individual sample delimiter

n is the fundamental frequency and its harmonics (including $n = 0$, the average when $\omega = 0$)

Equation 1.8 can also be expressed as a transform matrix $X = Wx$ where W is an NxN matrix equal to

$$W = \frac{1}{\sqrt{N}} \begin{bmatrix} 1 & 1 & 1 & 1 & \cdots & \omega^{N-1} \\ 1 & \omega & \omega^2 & \omega^3 & \cdots & \omega^{2(N-1)} \\ 1 & \omega^2 & \omega^4 & \omega^6 & \cdots & \omega^{3(N-1)} \\ \vdots & \vdots & \vdots & \vdots & \ddots & \vdots \\ 1 & \omega^{N-1} & \omega^{2(N-1)} & \omega^{3(N-1)} & \cdots & \omega^{(N-1)(N-1)} \end{bmatrix} \tag{1.9}$$

where $\omega = e^{\frac{-2\pi j}{N}}$ and the first row and column of this matrix is 1 because when $n = 0$ the complex exponential is reduced to $e^{-j\frac{2\pi}{N}*0} = 1$.

With this matrix we can observe an important property of the complex exponential $e^{\frac{-2\pi j}{N}}$. There exists complex conjugate symmetry where $\omega^{N-n} = \omega^{-n} = [\omega^n]*$ where $*$ denotes the complex conjugate.

Although equation 1.8 accurately describes the magnitudes of the DFT coefficients for the signal $x(t)$, the conventional way of displaying a frequency spectrum is to solve for $x_n(k)$ by taking the coefficients $X(n)$ solved for by equation 1.8 and solving equation 1.10. This will determine the component of a particular frequency within a particular sample.

$$x[k] = \frac{1}{N} \sum_{n=0}^{N-1} X[n] e^{j\frac{2\pi}{N}nk} \tag{1.10}$$

To speed up the calculation of this equation, the FFT reduces the computation time by splitting up the even and odd indexed sequences:

$$x[k] = \frac{1}{N} \left(\sum_{r=0}^{N/2-1} X[2r] e^{j\frac{2\pi}{N/2}kr} + \sum_{r=0}^{N/2-1} X[2r+1] e^{j\frac{2\pi}{N/2}k(2r+1)} \right) \tag{1.11}$$

where

$n = 2r$

$n = 2r + 1$

r is (n = 0 : N/2 -1)

This splitting can be repeated p times by splitting the index r into even and odd components, as long as the sample size is divisible by 2^p. For this reason, the sample size N in a DFT algorithm are generally a power of 2. Although this method drastically reduces the computation time, it also affects the resolution of the frequency spectra obtained to $df = \frac{f_s}{N}$. Also important to note is that the maximum resolvable frequency is the Nyquist frequency of $\frac{f_s}{2}$. This is because $X[n]$ coefficients are complex and the $x[k]$ values are assumed to be real, so this equation uses complex conjugate symmetry to combine the terms $X[n]$ and $X[N-n]$ to produce two frequency components only one of which is considered valid as the higher frequency is aliased from the first.

This operation is most accurate when the time window selected is equal to the fundamental frequency (or an integer number of cycles of the waveform) of a periodic function. This is because the fourier series waveform is essentially a continuous repetition of the signal bounded by the window selected. If the window is not selected appropriately, discontinuities can occur and the DFT will attempt to account for these discontinuities by ”smearing” the frequency spectrum, resulting in non-zero outputs at frequencies not actually present in the signal. If the function $x(t)$ is not periodic, care must be taken in selecting the window to avoid leakage effects. Filtering the data with the use of different window functions can minimize these effects as they can taper the samples towards zero values at both endpoints, eliminating the discontinuities. The research in this document was concerned with transient signals that decayed to zero within every window, so a simple rectangular windowing function was found to be appropriate (Richardson, 1978).

A second pitfall commonly found with DFTs is aliasing. This occurs when initial samples are too spaced out to capture high frequency components in the real signal. Increasing the sam-

pling rate to a value larger or equal to twice the known bandwidth (Nyquist rate) of the signal will prevent aliasing. However, if the bandwidth of the signal is unknown, an analogue low pass filter can limit the bandwidth so that the Nyquist rate can be calculated and the signal samples as found. The bandwidth of the studies presented in this document is approximately 5000Hz and the sampling frequency of 50 000Hz is ample enough to avoid any aliasing (Richardson, 1978).

It is with the theory discussed in this section that the custom written software (Matlab™, The Mathworks, Natick, MA, USA) (see Appendix C.3) was developed to process the time-domain strain data into the frequency spectra analysed in this research.

1.5.3 Statistical Tools

ANOVA tests

Analysis of variance (ANOVA) tests are common statistical methods used in hypothesis testing of quantitative results of experimental units (Devore, 2012). It is primarily used to determine the effect of differing treatments of separate datasets. Information on this subject is easily accessible, so this section will be very brief in its discussion of the basic principles and interpretation of ANOVA results.

Essentially, ANOVA tests compare the means of two populations and assess the probability that the two populations arise from the same underlying base population. If there is a high probability that the difference in the means of two populations arise simply from randomness, the less likely that the differing treatment of the two populations have a significant effect. To do this, the ANOVA test is formally set up by defining a null hypothesis, H_0, as the case where the two means are assumed to arise from different sampling of a single population. It then computes a test statistic called the F-ratio that describes the ratio between the found variance between a group of averages and the expected variance between a group of averages. If the F-ratio is near 1, the null hypothesis is supported and if not, the null hypothesis is rejected and

a significant effect is found. However this statistic has the disadvantage that it is difficult to determine the point at which the F-ratio is "near" one. To relate this statistic to theories of significance levels, the ANOVA test also returns a p-value. The p-value is the probability of obtaining a value of the test statistic at least as contradictory to H_0 as the value calculated from the available sample, assuming H_0 is true (Devore, 2012). This is essentially saying that a large p-value indicates that there is an increased chance that there is no statistical difference between your treatments, and the null hypothesis is not rejected. A low p-value then indicates significant effects between two treatments as the p-value is essentially equal to the probability of rejecting H_0 when H_0 is true. Thus the p-value can quantify the confidence in our assessment by defining the significance level. Commonly used significance levels are $\alpha = 0.05, 0.01, and 0.1$ with p-values falling below the α significance level as significant to that level.

Cluster Analysis

Cluster analysis techniques are classificatory sorting strategies used to classify data under a set of distinct categories. These strategies are used for many applications, particularly in marketing, sciences and engineering (Halkidi et al., 2001), and are used to find underlying populations in a given dataset. In this study, resonant frequencies were collected from over 500 strain histories, of which each history identified 0-3 separate resonant frequencies. The cluster analysis is used to identify the total number of resonant frequencies found from these individual frequency snapshots by subjecting the entire dataset of frequencies to a cluster analysis to identify the underlying individual resonant frequency populations.

Although there are a few differing types of cluster analyses used, this section will focus on agglomerative hierarchical clustering algorithms, as not only is this type a commonly used clustering method (Mooi and Sarstedt, 2011) and is available in SPSS software, but it is also the method selected for the analysis presented in this research. Hierarchical algorithms are clustering techniques that group datapoints in an iterative way that successively merges the most similar clusters into larger ones. This process can be illustrated by a dendogram which

exposes the merges at each successive level. This is illustrated in Figure 1.6 and shows how no matter where the dendogram is cut, each data point is assigned to a particular cluster.

In order to accurately construct this dendogram, an objective measure of similarity must be selected in order to identify the merging pair at each level of succession. Euclidean distance is the most commonly used similarity measure, as it is the direct straight line distance between two points. Alternative measures include the city-block distance or the Chebychev distance neither of which change the results for the one dimensional data presented in the research of this document. Once a similarity measure is selected, a proximity matrix organizes the similarity of every data point pair and the most similar pair is merged to form a cluster.

Because the initial level of an agglomerative heirarchical cluster analysis considers each individual data point a unique cluster, calculation of the similarity measure between two cluster bodies is straight-forward, as it is simply the distance btween two data points. Once a cluster is formed, a linkage criteria must be defined in order to identify the point of a cluster that will be used to measure the distance between one cluster body and another. The simplest linkage criterions include the nearest neighbour linkage and farthest neighbour linkage, where the distance between two cluster bodies is defined as the the distance between their closest or furthest elements respectively. Although simple, these linkages are generally rejected in most analyses due to their extreme behaviour. For example, nearest-neighbour linkage has a tendency to chain clusters together, resulting in a large smeared clusters (Lance and Williams, 1967). The furthest-neighbour linkage on the other hand has extreme space-dilating properties, which can faultily increase the perceived distance between two clusters (Blashfield, 1976). As a midground between the two extreme linkage criterions are average linkage criterions whcih include the centroid method and the between groups linkage. The centroid method calculates a centroid of a particular cluster and the distance is calculated from that point. It is a linkage criterion that is popular because it does not dilute or contract the perceived space between groups, however it has the disadvantage that characteristic properties of cluster outliers are lost (Lance and Williams, 1967). An unweighted strategy such as the between group method con-

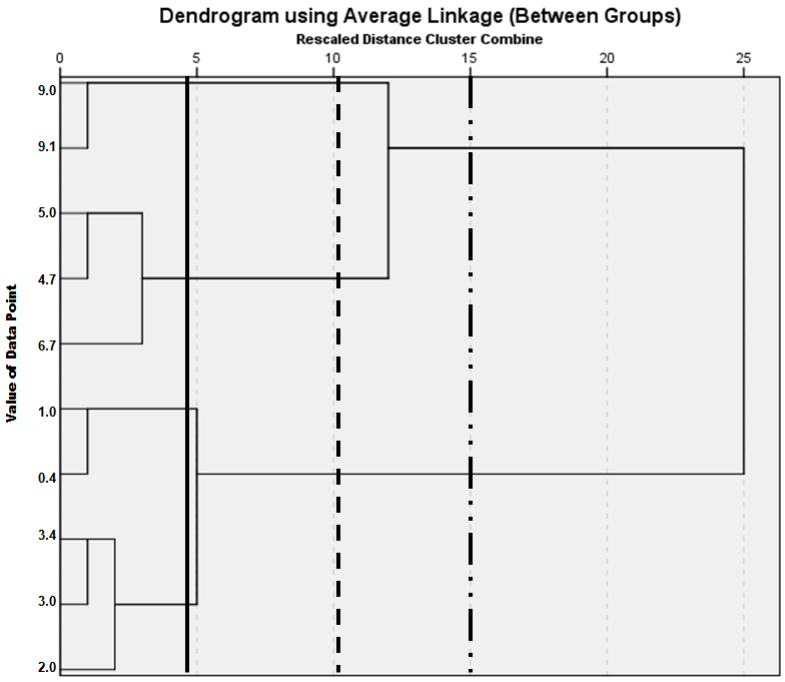

Figure 1.6: Example of a dendogram. Note how at each vertical bar (solid, dashed, and double dashed) there is a unique number of clusters. Specifically, at the solid line, 4 clusters are defined, at the dashed line 3 clusters are defined and at the double dashed line, 2 clusters are defined.

siders the properties of all elements of a cluster, as the distance between clusters is calculated as an average of the distance between every element of each cluster. Although this method is significantly more computationally expensive, it has been suggested that this method identified the most accurate groupings of known clusters better than any other critera (Blashfield, 1976). The research presented in this document selected between-groups linkage criteria for its space conserving treatment of distance as well as its historical performance.

The final step in the cluster analysis is to determine the optimal number of clusters. This is one disadvantage of the hierarchical cluster analysis type, however there are several guidelines that can be used to identify a reasonable number of clusters for a particular dataset. A method commonly used is to find the knee of a curve where the number of clusters is plotted against the distance closed to merge two clusters. This is ultimately determining where large distances are closed to obtain only one less cluster. Various methods to find the knee of the curve include the largest magnitude difference between two points, the largest ratio difference between two points, the point on the curve that is furthest from a line fitted to the entire curve or the data point with the largest second derivative (Salvador and Chan, 2004). Because the knee of a curve is defined primarily as the point of maximum curvature (Salvador and Chan, 2004), the largest second derivative was used to determine the number of clusters in the analyses presented in this research. However, these methods are objective algorithms that do not take into account the nature of the data being studied. For example, the data being clustered in this research are the frequency peak values of strain gauge frequency spectra. If the optimal number of clusters involved merging frequencies separated by more or less hertz than was generally observed between peaks on the spectra, the data point where the second derivative was second largest was used instead to identify the optimal number of clusters.

1.6 OBJECTIVES AND HYPOTHESES

The specific objectives of this study are as follows:

1. To design and implement a head impact apparatus and experimental protocol with consideration for constraints of space, cost and development time that is capable of producing repeatable, short duration impacts with a large range of energy inputs on variable impact sites of a human cadaver skull.

2. To determine the effect of different specimen, impact site, impact energies and fracture on the frequency response of the skull upon impact.

The hypotheses associated with these objectives are:

1. A head impact apparatus capable of impacts under 5ms in duration with input energy levels of 0.5-1500J can be designed. This apparatus will also be able to accommodate various impact sites of the specimen and measure the force applied at each impact.

2. This impact apparatus will produce repeatable and reproducible impacts with consistent impact conditions

3. The frequency response of the skull to impact will be unique to the specimen tested and dependent on its geometery and stiffness. The location of the impact site will not affect the frequency spectrum nor the power ratio of the response. An increase in impact energy will also have little effect on the frequencies collected and the power ratio of the response.

4. The frequencies excited upon impact of a specific gauge will be repeatable between trials of consistent impact conditions, and will be independent of impact site or impact energy. However I expect different frequencies excited upon impact to be picked up by different gauges.

5. There will be a notable difference in the frequency response of the same specimen before and after a facial fracture.

1.7 THESIS OVERVIEW

This thesis explores the design and development of a head impact apparatus, for use in studying the vibrational response of the human skull upon impact. Chapter 2 describes the design process of the impact apparatus, as well as outlines the repeatability and reproducibility of the impacts produced with the goal of validating the design and confirming comparisons between impact apparatuses used in past studies. Chapter 3 is concerned with the vibrational response of the skull to subfracture impacts on the intact specimens. Using strain gauges I will evaluate the effect of specimen, impact location and impact energy to the frequency domain of the strain response. It will also have a section outlining how the presence of a facial fracture might affect the resonant frequencies of the skull. Finally, Chapter 4 will summarize this body of work and discuss the strengths and limitations of these studies as well as possible directions for future research.

Bibliography

DL Allsop, CY Warner, MG Wille, DC Schneider, and AM Nahum. Facial impact response: A comparison of the hybrid iii dummy and human cadaver. *32nd Stapp*, 1988.

Georg Békésy. Vibration of the head in a sound field and its role in hearing by bone conduction. *Journal of the Acoustical Society of America*, 1948.

Roger K Blashfield. Mixture model tests of cluster analysis: Accuracy of four agglomerative hierarchical methods. *Psychological Bulletin*, 1976.

D Brands. Predicting brain mechanics during closed head impact: Numerical and constitutive aspects, 2002.

Hans Delye, Peter Verschueren, Bart Depreitere, Ignaas verpoest, Baniel Berckmans, Jos Vander Sloten, Georges Van Der Perre, and Jan Goffin. Biomechanics of frontal skull fracture. *Journal of Neurotrauma*, 2007.

Jay L Devore. *Probability and Statistics for Engineering and the Sciences*. Brooks/Cole, 2012.

Ernst Franke. Response of the human skull to mechanical vibration. *Journal of the Acoustical Society of America*, 1956.

S Fujiwara, Y Yanagida, and Y Mizoi. Impact-induced intracranial pressure cause by an accelerated motion of the head or by skull deformation: An experimental study using physical models of the head and neck, and ones of the skull. *Forensic Science International*, 1989.

E Gurdjian, V Hodgson, and L Thomas. Studies on mechanical impedance of the human skull: Preliminary report. *Journal of Biomechanics*, 1970.

E S Gurdjian, John E Webster, and Herbert R Lissner. Studies on skull fracture with particular reference to engineering factors. *American Journal of Surgery*, 78:736–742, 1949.

Bo Hakansson, Anders Brandt, and Peder Carlsson. Resonance frequencies of the human skull in vivo. *Journal of the Acoustical Society of America*, 1994.

Maria Halkidi, Yannis Batistakis, and Michalis Vazirgiannis. On clustering validation techniques. *Journal of Intelligent Information Systems*, 2001.

David Hampson. Facial injury: A review of biomechanical studies and test procedures for facial injury and assessment. *Journal of Biomechanics*, 1995.

Warren Hardy. *Accidental Injury: Biomechanics and Prevention*, chapter 2 Instrumentation in Experimental Design, pages 12–48. Springer-Verlag, New York, NY, 1 edition, 1993.

Warren Hardy, Matthew Mason, Craig Foster, Chirag Shah, James Kopacz, King Yang, and Albert King. A study of the response of the human cadaver head to impact. *Stapp Car Crash Journal*, 2007.

Voight R. Hodgson. Tolerance of the facial bones to impact. *American Journal of Anatomy*, 1967.

Bryan Jennett. Epidemiology of head injury. *Journal of Neurology, Neurosurgery and Psychiatry*, 1996.

T Khalil and D Viano. Experimental analysis of the vibrational characteristics of the human skull. *Journal of Sound and Vibration*, 1979.

A Kroman, T Kress, and D Porta. Fracture propagation in the human cranium: A re-testing of popular theories. *Clinical Anatomy*, 2011.

G N Lance and W T Williams. A general theory of classificatory sorting strategies: Hierarchical systems. *The Computer Journal*, 1967.

Mrinal Mandal and Amir Asif. *Continuous and Discrete Time Signals and Systems*, chapter 12. Discrete Fourier Transform, pages 525–564. Cambridge University Press, New York, NY, 2007.

Frederic Martini, Michael Timmons, and Robert Tallitsch. *Human Anatomy*, chapter 7. Benjamin Cummings, Glenview, IL, 7th edition, 2006.

James H McElhaney, John L Fogle, John W Melvin, Russell R Haynes, Verne L Roberts, and Nabih M Alem. Mechanical properties of cranial bone. *Journal of Biomechanics*, 1970.

A J McLean and Robert WG Anderson. *Head Injury: Pathophysiology and Management of Severe Closed Injury*, chapter 2 Biomechanics of Closed Head Injury, pages 25–37. Chapman and Hall Medical, New York, NY, 1 edition, 1997.

J Melvin, P Fuller, R Daniel, and G Pavliscak. Human head and knee tolerance to localized impacts. In *Society of Automotive Engineers Mid-Year Meeting*, volume 2, Chicago IL, May 1969.

John W Melvin, James W Lighthall, and Kazunari Ueno. *Accidental Injury: Biomechanics and Prevention*, chapter 12 Brain Injury Biomechanics, pages 268–291. Springer-Verlag, 1 edition, 1993.

JC Misra and S Chakraborty. *Mathematical Models for Bioengineering and Probabilistic Systems*, chapter 1 Modelling of Head Impact Problems, pages 1–26. Narosa Publishing House, New York, NY, 1 edition, 2005.

Erik Mooi and Marko Sarstedt. *A Concise Guide to Market Research*, chapter 9 Cluster Analysis, pages 537–284. Springer-Verlag, Heidelberg, GER, 2011.

Julie A Motherway, Peter Verschueren, Georges Van der Perre, Jos Vander Sloten, and Michael D Gilchrist. The mechanical properties of cranial bone: The effect of loading rate and cranial sampling position. *Journal of Biomechanics*, 2009.

K O'Riordain, P M Thomas, J P Phillips, and M D Gilchrist. Reconstruction of real world head injury accidents resulting from falls using multibody dynamics. *Clinical Biomechanics*, 2003.

David Raymond, Gregory Crawford, Chris Van Ee, and Cynthia Bir. Development of biomechanical response corridors of the head to blunt ballistic temporo-parietal impact. *Journal of Biomechanical Engineering*, 2009a.

David Raymond, Chris Van Ee, Gregory Crawford, and Cynthia Bir. Tolerance of the skull to blunt ballistic temporo-parietal impact. *Journal of Biomechanics*, 2009b.

D T Reilly and A H Burstein. The mechanical properties of cortical bone. *Journal of Bone and Joint Surgery America*, 1974.

John S Rhee, Lisa Posey, Narayan Yoganandan, and Frank Pintar. Experimental trauma to the malar eminence: Fracture biomechanics and injury patterns. *Otolaryngology - Head and Neck Surgery*, 125:351–355, 2001.

Mark H Richardson. Fundamentals of the discrete fourier transform. *Sound and Vibration Magazine*, 1978.

D H Robbins and J L Wood. Determination of mechanical properties of the bones of the skull. *Experimental Mechanics*, 1969.

Stan Salvador and Philip Chan. Determining the number of clusters/segments in hierarchical clustering/segmentation algorithms. In *16th IEEE International Conference on Tools with Artificial Intelligence*, 2004.

DC Shneider and AM Nahum. Impact studies of facial bones and skull. *16th Stapp*, 1972.

Lance D Slifka. An accelerometer based approach to measuring displacement of a vehicle body. Master's thesis, University of Michigan, 2004.

Richard Stalnaker, John Fogle, and James McElhaney. Driving point impedance characteristics of the head. *Journal of Biomechanics*, 1971.

Michael Vander Vorst, Philemon Chan, Jiangyue Zhang, Narayan Yoganandan, and Frank Pintar. A new biomechanically-based criterion for lateral skukll fracture. *Annual Proceedings/Advancement of Automotive Medicine*, 48:181–195, 2004.

P Verschueren, H Delye, B Depreitere, C Van Lierde, B Haex, D Berckmans, I Verpoest, J Goffin, J Vander Sloten, and G Van Der Perre. A new test set-up for skull fracture characterisation. *Journal of Biomechanics*, 40:3389–3396, 2007.

David C Viano, Cynthia Bir, Tim Waliko, and Don Sherman. Ballistic impact to the forehead, zygoma and mandible: Comparison of human and frangible dummy face biomechanics. *The Journal of Trauma: Injury, Infection and Critical Care*, 2004.

R Willinger, L Taleb, and C Kopp. Modal and temporal analysis of head mathematical models. *Journal of Neurotrauma*, 1995.

Ryan Willinger, A J McLean, and C M Kopp. Mechanisms of brain injury derived from mathematical modelling and epidemiological data. *Accident Analysis and Prevention*, 1994.

Earl J Wilson. *Harris' Shock and Vibration Handbook*, chapter 17. Strain Gage Instrumentation. McGraw-Hill, Chicago IL, 5 edition, 1996.

Hiroshi Yamada. *Strength of Biological Materials*, chapter 3.1 Mechanical Properties of Locomotor Organs and Tissues: Bone, pages 19–79. Narosa Publishing House, New York, NY, 1 edition, 1970.

Narayan Yoganandan, Anthony Sances, Frank Pintar, Dennis Maiman, David Hemmy, Sandford Larson, and Victor Haughton. Traumatic facial injuries with steering wheel loading. *The Journal of Trauma*, 31:699–710, 1991.

Narayan Yoganandan, Frank Pintar, Anthony Sances Jr., Patrick Walsh, Channing Ewing, Daniel Thomas, and Richard Snyder. Biomechanics of skull fracture. *Journal of Neurotrauma*, 1995.

Narayan Yoganandan, Jiangyue Zhang, and Frank Pintar. Force and acceleration corridors from lateral head impact. *Traffic Injury Prevention*, 5:368–373, 2004.

Markus Zingg, Kurt Laerach, Joseph Chen, Khalid Chowdhury, Thierry Vuillemin, Franz Sutter, and Joram Raveh. Classification and treatment of zygomatic fractures: a review of 1025 cases. *Journal of Oral Maxillofacial Surgery*, 50:778–790, 1992.

Chapter 2

Design and Development of a Head Impactor System

2.1 INTRODUCTION

There have been several different approaches to simulate head impact conditions as it was discussed in Section 1.3. Comparisons among these known designs as well as a concern for the objectives of the specific research question at hand suggest the priorities and constraints of our new design. For example, to study the vibrational response of the head upon impact, it is necessary to produce impacts with a duration of under 5ms in order to excite multiple frequency modes of the skull (Willinger et al., 1995). Also, a natural head constraint must be considered to both distribute the impact stress in a way that allows for some nodding and tilting (Verschueren et al., 2007) as well as to ensure that constraints do not interfere with the vibrational response (Khalil and Viano, 1979). This chapter will discuss the details of the design and validation of a head impact apparatus capable of producing impacts with a duration of less than 5ms, and with a force application range of 0.5-1500N to apply both subfracture and fracture conditions. Furthermore, the design will aim for repeatable and reproducible impacts with consistent impact conditions, suggesting a need for precise loading and control

methods. Because a large majority of previously reported head impact studies focuses on the biomechanics of skull fracture, the impactor design must have capabilities for fracture both for use in future studies, as well as to validate the design against previously published literature. These goals will be accomplished with consideration for a minimal budget, as well as the spatial constraints of the lab and a requirement that it be mobile.

2.2 MATERIALS AND METHODS

Considering the differing impact apparatus designs previously discussed, it was decided that a drop tower apparatus with a free falling projectile was an appropriate general concept, based on the advantages and disadvantages outlined in Table 2.1. This design would be inexpensive and simple, as there would be no need to design a controllable input energy source as consistent as gravity. This design would also be more mobile than the traditional head drop towers, because a fixed, robust track to constrain the head would be unnecessary; as only a track sturdy enough to guide a 1-3kg projectile will be needed.

The general concept decided, the physical, instrumental and procedural aspects of both the impact apparatus and the experimental design was considered. Figure 2.1 is a photograph of the apparatus that can be referred to during the following sections.

2.2.1 Impact Apparatus Physical Design

Track and Base

The base of the impact apparatus is a 0.8m steel I-beam welded to a 0.74 x 0.255m steel base. Pipe clamps connected to I-beam clamps via a vertical threaded rod support 1.17m of transparent PVC tube vertically, about 15cm away from the I-beam base. The length of tubing was decided in conjunction with the projectile design in order to hit desired force levels and is described in Section 2.2.1. 1/4 inch holes corresponding to the size of a removable pin were bored into the PVC piping to define drop height points. These height points combined with the

Table 2.1: Advantages and Disadvantages of various devices and methods used in simulating head impacts.

Apparatus Type	Advantages	Disadvantages
Drop Testing	Simple design; Consistent input energy source (gravity)	Unspecified impact location; Crushing effect (if guided fall device)
Ballistic Devices	Short duration impacts	Lack of precision at lower speeds; Forceful; Expensive
Quasi-Static Testing	Deflection measurements	Rigid constraints; Long impacts
Pendulum Impactor	Inertial effects; Deflection measurements	Long impacts; Large lab space needed
Drop Testing	Consistent input energy source (gravity); Smaller forces; Short impacts	No deflection measurements

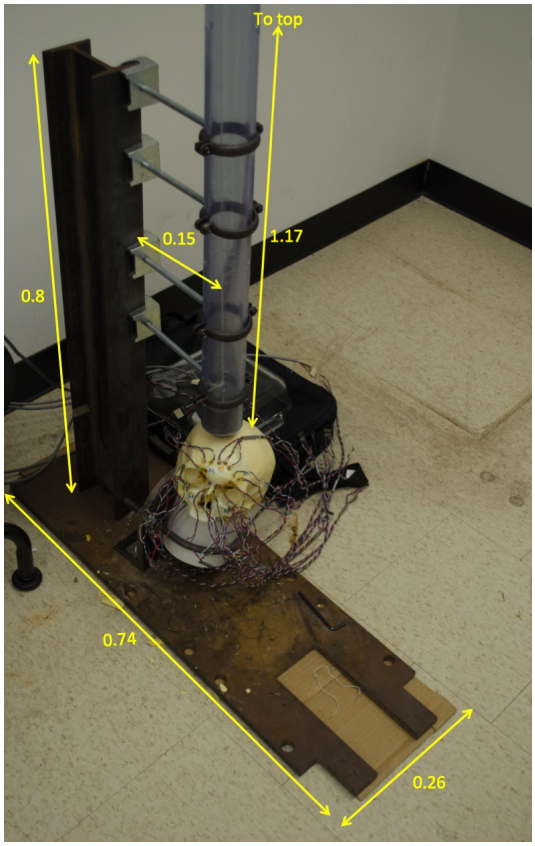

Figure 2.1: Vertical dropped projectile tower apparatus with a specimen in position for an impact at impact site 4. Dimensions are in meters.

variability of sliding the tubing up and down the pipe clamps makes any potential drop height accessible. The base was also perforated with a matrix of 5mm diameter holes in order to bolt the specimen containing bracket at various positions. Attached to two of the pipe clamps is a rigidly fixed laser pointer for use in aligning the specimen during testing.

Projectile

The impactor projectile was designed according to predicted force capabilities along with a consideration for a short impact requirement. Assuming negligible loss during free fall, as well as an impact time of no greater than 5ms, conservation of momentum was used to calculate the resultant force with various height/weight combinations. The following considerations were assessed in choosing an optimal combination. The height of the tubing was to be less than 1.5m due to spatial constraints, and the impactor projectile was to be as light as possible in order to maintain our 5ms impact duration assumption as well as to ensure that impacts will excite high frequency vibrations of the skull. Furthermore, the maximum force that was aimed for was to be capable of initiating fracture to some areas of the face such as the zygoma or the maxilla. These bones have known force tolerances between 489N-2000N (Hampson, 1995) suggesting a target for a maximum impact force of around 1500N. These design specifications and assumptions led to the selection of a 1.5kg steel projectile dropped at 1.4m, however preliminary tests with this setup indicated that the impact duration was generally more than 3-4ms prompting a reduction of the projectile mass to 0.713kg. A threaded attachment of 0.727kg was designed to increase the mass of the projectile if needed for cranial fracture studies, increasing the force capabilities of the impactor to around 4000N. The final design is depicted in Figure 2.2 with the dimensions, additional mass and the ball peen end effector.

Head Constraint Bracket

A custom design bracket was developed to hold the specimen rigid in a range of positions. Illustrated in Figure 2.3, it was cut from an L-shaped piece of steel and it was machined with

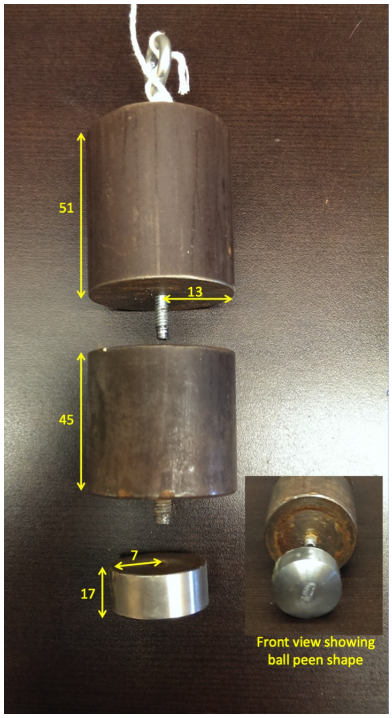

Figure 2.2: The projectile was designed as depicted here. The top mass is the additional attachment weighing 0.727kg. This was not used during testing. The total weight of the middle section and the ball pean end effector equalled 0.713kg and was the projectile used for all testing. Note how the end effector is attached by a threaded rod, allowing future studies to easily alter the end effector. All dimensions listed are in millimeters.

Figure 2.3: Custom bracket designed for specimen constraint

a series of 14 1/4 inch diameter holes on the base and a 4 inch diameter circular slot on the vertical section. The base holes were designed for variability in positioning the bracket on the base of the apparatus support, as any one of those holes could be aligned with one of the holes on the base matrix and thus change the specimen position simply by shifting the entire bracket one hole over. Since the specimens were potted in a 4 inch diameter pot (as will be discussed in Section 2.2.3), the 4 inch diameter circular slot was designed to accept a u-bolt that can be tightened against this steel support and the specimen pot. The edges of the vertical section were also rounded to minimize any contact between the edges of the bracket and the specimen.

2.2.2 Data Collection and Instrumentation

Accelerometers

The impact accelerations were recorded using a linear accelerometer (Measurement Specialties, Aliso Viejo, CA, USA). For specimen 1622, this accelerometer had loading range specifications of up to 200g's with a ratiometric sensitivity of 0.8mV/g's to an excitation voltage of 10 Vdc. The accelerometer used for the rest of the specimens had a dynamic range of 2000g's and a ratiometric sensitivity of 0.15mV/g's at 10Vdc. Although the impacts acquired using the 200g's accelerometer exceeded its limit, controlled impact tests with both accelerometers mounted concluded that no appreciable difference was recorded between the two accelerometers for impacts up to 500g's. The sensitivities of these accelerometers were specified by the manufacturer to have accuracies of +/-1/2dB and +/-2% in the frequency range tested for the 200g's and 2000g's accelerometers respectively.

Strain Gauges

Strain gauges were placed on each specimen in order to record the specimen deformation history upon impact. Each specimen had a combination of 350Ω linear and triaxial rosette strain gauges (Omega Engineering Canada, Montreal, QC, CAN) anchored to the specimens accord-

ing to the procedure outlined in appendix B.1. Each gauge was wired to a quarter bridge circuit as well as an extra 120Ω resistor in series to reduce the current and avoid gauge burnout. Strain gauge measurements were also processed using calculations specific for unbalanced bridges as only the relative strain changes upon impact are of interest. The equations used for these calculations as well as a diagram of the bridge circuits can be found in appendix B.

Data Acquisition System

The accelerometers and strain gauges were connected to and recorded by a data acquisition system (QDAC Systems, Waterloo, ON, CAN). Specimen 1622 was tested with an 8 channel model, and the other specimens were tested with a 16 channel model. All strain gauge signals were recorded with a gain of 10 and the accelerometer signal during the testing of specimen 1622 was also recorded with a gain of 10. Both QDAC systems had built in software defining the analogue and digital filter bandwidths (100 kHz and 5kHz at 50kHz sampling rate respectively) and had a gain accuracy of +/- 0.1% and a recorded resolution of 24bits. Since the event to be captured is of very short duration, a sampling rate of 50kHz was selected. The Nyquist-Shannon sampling frequency suggests that this sampling rate is appropriate for capturing frequencies up to 25 000 Hz. According to past skull vibrational response studies 25 000 Hz is more than enough to study up to 19 natural frequencies found below 10 kHz (Hakansson et al., 1994; Khalil and Viano, 1979).

Velocity Sensor

The impact velocity was captured at the base of the tube guide with an optical velocity trap. Two (Honeywell, Morristown, NJ, USA) photo emitter and photo transistor pairs were anchored 17mm apart on a wood and metal bracket. Each pair consisted of an emitter on one end of the bracket and a transistor across from it, with the second trap placed opposite the first to eliminate the potential of one emitter influencing the other transistor. The emitters and transistors were powered by and wired to a Parallax Propeller™chip (Rocklin, CA, USA) via a series

of resistors to create a digital switch altered when the projectile blocked the emitter from the transistor. The Propeller chip monitored the state of the switch at 80MHz and output the time in microseconds between the switch of the first and second photo emitter and photo transistor pair. This in conjunction with the known distance between the two pairs indicated the velocity at which the impactor projectile exited the guiding tube.

2.2.3 Experimental Procedures

Specimen Preparation

Six fresh frozen cadaveric head specimens were used for this study (mean age: 80 +- 12 years; 2 female, 4 male). CT scans were made of each specimen prior to skull preparation. Each specimen then had all soft tissue removed by a process of surgical dissection followed by denuding in a University of Guelph colony of Dermestidae beetles. Once only boney anatomy remained, the skulls were bleached and disinfected for our use. The skulls were then prepared with seventeen strain gauges. Skull 1622 was outfit with nine overlapping rosette gauges and eight uniaxial gauges (Omega, Montreal, QC, Canada) according to Figure 2.4a and the gauge configuration for the rest of the skulls is illustrated in Figure 2.4b with five rosette, six overlapping rosette gauges and uniaxial gauges (Omega, Montreal, QC, Canada). This second configuration was selected to accomodate the use of more triaxial gauges, to measure the strain directions at more locations. The gauges were applied following institutional protocols for gauging on bone (in Appendix B.1).

Specimen support conditions have been discussed in the literature as a significant consideration of impact testing. Much criticism has been directed to the 1995 Yoganandan et al. study and their use of a rigid constraint (Yoganandan et al., 1995) as this likely altered the stress distribution of the skull upon impact (Verschueren et al., 2007). Furthermore, to study the vibrational response of the skull to impact, Khalil et al. (1979) assumed a free support condition in order to reduce the amount of damping as well as to eliminate excess experimental variables

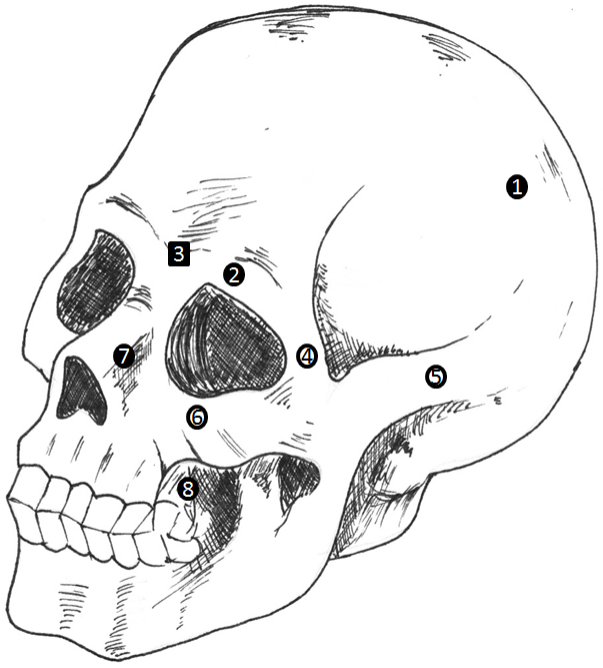

(a) Gauge locations for specimen 1622

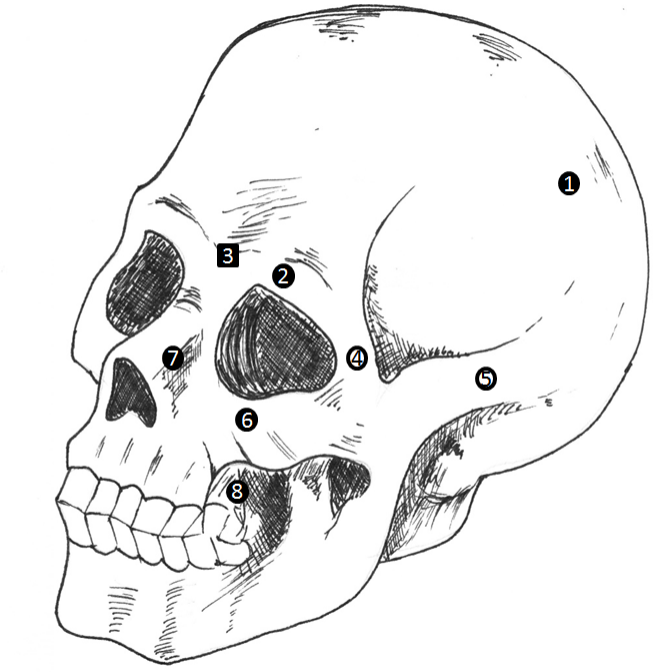

(b) Gauge locations for specimens 1625 through 1653

Figure 2.4: Gauge locations for specimens, Solid markers stand for triaxial gauges, open markers for uniaxial gauges. Circular markers means a second gauge is placed at the same location on the contralateral side and square markers indicate that a gauge is placed solely at that location. Two additional uniaxial gauges were placed on the left and right pterygoid plates of all specimens. The numbers represent the label assigned to each gauge. The pterygoid plates are obstructed from view by the maxilla in the figure, and so these gauges are not explicitly shown, but carry a number label of 9.

(Khalil and Viano, 1979). The design selected was a compromise with a design that constrained the head with a neck-like support. That is, to secure each specimen in a 4 inch diameter, 4 inch deep PVC pipe, two holes were drilled through the base of the occipital bone, about 1 to 2 cm laterally from the foramen magnum, where the bone was thickest. This location was selected to be more physiologically accurate, since the in vivo head is supported in a similar location by the neck. A 5/16th inch diameter carriage bolt was placed through each hole and secured using a steel washer-nut assembly. Rubber washers and grommets were placed in between the steel washers and bone surface to protect the bone itself and to allow nodding and some tilting motion. The 3 inch protruding ends of these bolts were then secured in the pipe filled with Denstone™cement. Enough clearance was left between the PVC pipe and the specimen so that any nodding motion did not cause impingement.

Experimental Setup and Testing Protocol for Repeatability and Reproducibility Validation

Once the specimen and pot were appropriately oriented under the impact zone and secured with the bracket, a laser mark was noted on the specimen to ensure consistent impacts. The testing protocol was then started which consisted of subfracture impact loadings on five saggital sites (illustrated in Figure 2.5). All skulls except specimen 1625 were impacted at the left parietal bone (site 5), the left posterior frontal bone (site 4), the left anterior frontal bone at the brow (site 3), the left inferior orbit (site 2) and the left malar eminence (site 1). Specimen 1625 was impacted in the same locations mirrored to the right side. Due to the channel constraints of the data acquisition units, several gauge configurations were required to obtain at least one set of data from each gauge. In this case, a set of data is defined as three trials each for two different heights. The procedure consisted of three impacts to a specific site with one configuration of gauges being sampled. The height was then changed for three more impacts to the same site and this entire process was repeated with another configuration of gauges plugged in until all gauges were sampled at least once.

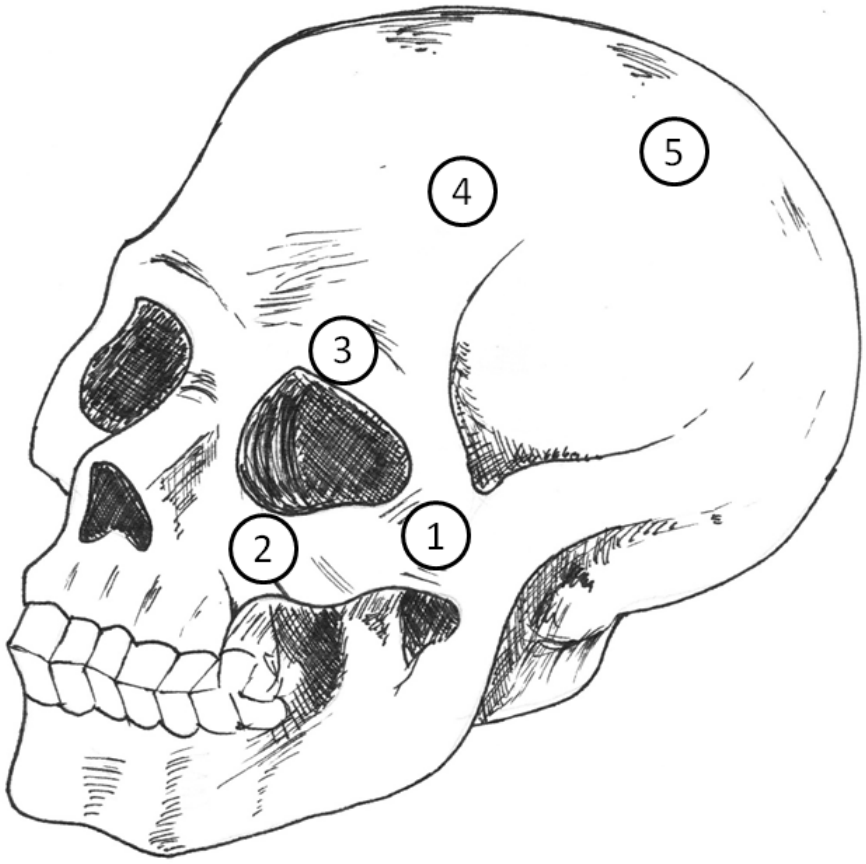

Figure 2.5: Impact site locations for all skulls except specimen 1625 (1625 was impacted on the contralateral, right side)

Once all of this data was collected, the specimen was reoriented to one of the other four sites and the procedure was repeated. A tree diagram in Figure 2.6 shows the order of these tests. Between each strike of an impact site the laser marking was realigned with the marking on the specimen to ensure consistent impacts, however the diligence with which this was performed varied according to operator. An entire site was repeated on a few occasions to assess the effect of operator on the results. A detailed outline of the procedure followed for each skull is provided in Appendix A. The gauge and accelerometer voltage values were saved for post processing (see next section).

Post Processing for Repeatability and Reproducibility Validation

Custom written software (Matlab™, The Mathworks, Natick, MA, USA) (see Appendix C) was used to convert the accelerometer voltage data to impact force data. The means and standard deviations of three variables: the peak force attained, the area under the force-time curve (impact energy) and the impact duration was then inspected. The means and standard deviations were calculated for three levels of repeatability: between each set of three trials, between all trials of consistent height/site combination as well as between the initial three trial hits at a specific site and the final three trial hits of a specific site. The percent deviation value ultimately reported is defined as the relative standard deviation, and these values will be reported for each level of repeatability and for each calculation of impact force, impact energy and impact duration. Any noticeable error events during testing trials, such as unexplainable signal artifacts, obvious skull shifting or double bounces, were recorded to identify discrepancies in the repeatability results. Furthermore, the consistency of the force-time curve shape was evaluated by calculating the root mean square error (RMSE) of each trial against the average curve of all trials.

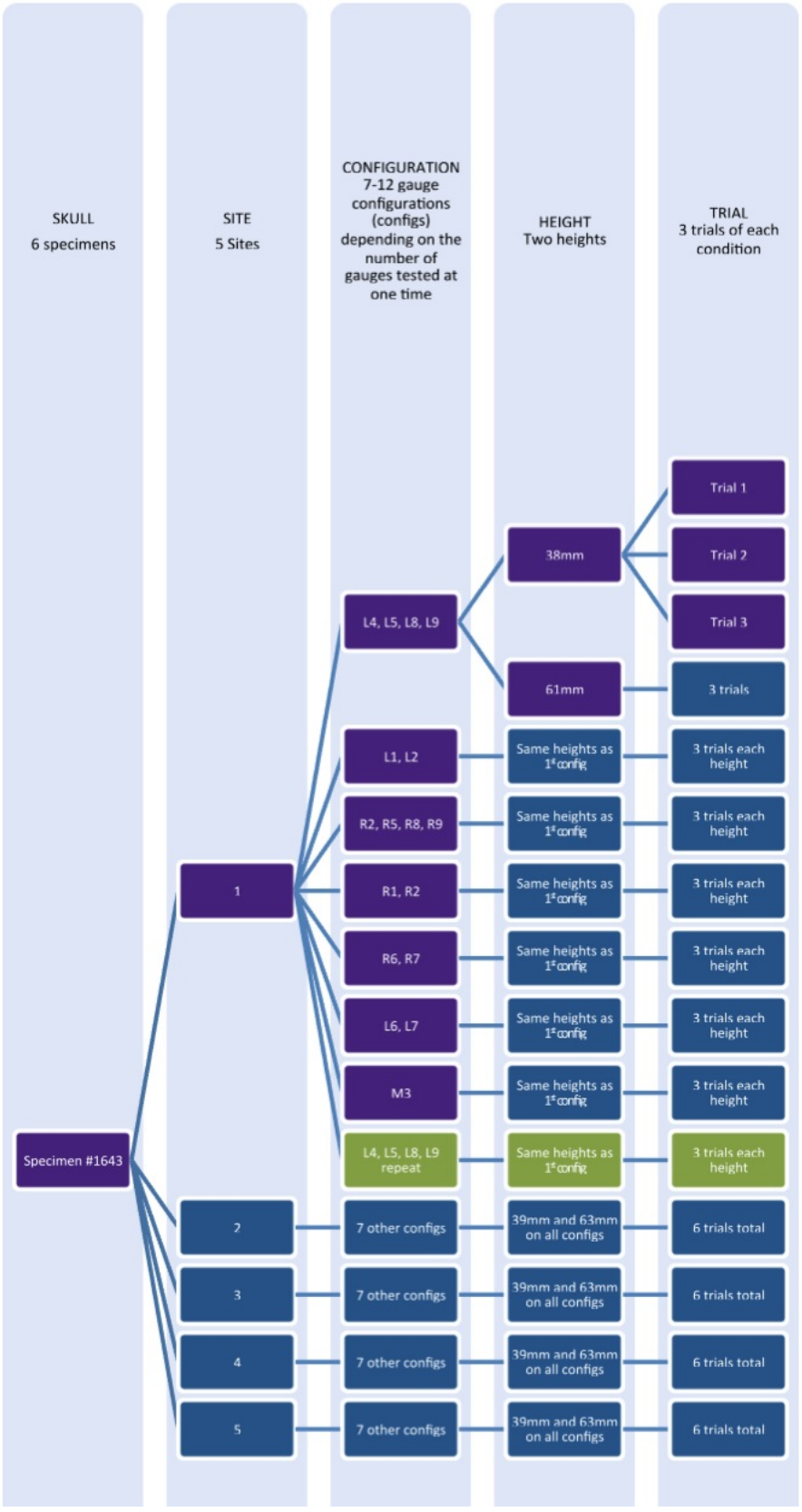

Figure 2.6: Diagram of protocol followed. The purple boxes describes the full protocol, the blue boxes summarize any repeated protocol, and the green boxes show the protocol followed for reproducibility testing. The overall labels provide a general description of each level of the protocol hierarchy

Experimental Setup and Testing Protocol for Fracture Study

In anticipation of future head impact studies involving cranio-facial fracture, a second testing protocol for each skull was completed to evaluate the impactor and the experimental setup in another frequently studied context. Once the subfracture protocol was completed, a fracture protocol was planned for five of the six specimens (1625, 1641, 1643, 1652, 1653). The fracture site chosen was the malar eminence (Site 1) and the specimen was oriented appropriately. Additional setup included anchoring a second accelerometer underneath the zygoma. Only one triaxial gauge (on maxilla) and three linear gauges (linear gauges on lateral orbit, zygomatic arch and pterygoid plate) on the same side as impact were monitored for strain input. Impact height was increased incrementally until damaged occurred. If the damage was localized and superficial (pitting or crushing of the bone surface only) the contralateral malar eminence was tested at 12-15cm above the last height tested in an attempt to induce structural damage in a single trial.

Both accelerometer curves were post processed. The impactor accelerometer signal was used to derive impact force and the zygomatic accelerometer was used to derive the zygomas deformation upon impact through double integration using Matlabs cumtrapz function. With these two curves, the time variable was eliminated and a force-deflection curve was computed. With this information, biomechanical data such as force to fracture and deflection to fracture was noted. Complete fracture was identified as the point on the force-deflection where the force deflection curve ceased to rise.

2.3 RESULTS

2.3.1 System Performance

The impactor apparatus designed performed well in consideration of our initial goals. Quantitatively, the subfracture protocol produced facial impacts of between 117-800N and cranial

impacts of 511-2035N. Impact durations of all strikes were between 0.56ms and 4.2ms with the facial strikes having longer impact durations (1.1ms-4.2ms) than the cranial impacts (0.56ms-1.2ms). All 5 sites were accessible for impact. Velocity at impact ranged from 0.36 to 1.89 m/s for subfracture protocol as found with the velocity sensor. The velocity sensor was incapable of calculating velocity for fracture protocol because of the high speeds, however free fall calculations estimate peak velocities at between 2.88 and 3.36m/s.

The flexible support provided by the rubber washers in the specimen constraint setup allowed for flexion and extension of the head by about 30 degrees and lateral bending to about 5 degrees.

2.3.2 Fracture Study

The fracture studies confirmed the ability of the impactor to induce facial fractures. Specimen 1625, 1641, 1643, 1652 and 1653 fractured at forces of 631N, 1015N, 1548N, 720N and 1548N respectively. The force-deflection curves of specimens 1625 and 1641 are illustrated in Figure 2.7. The zygoma accelerometer dislodged upon impact on specimen 1643 and was found to be damaged for the data collection of specimens 1652 and 1653. The deflection to fracture of specimen 1625 was found to be 0.97mm and of specimen 1641, 0.66mm.

2.3.3 Repeatability and Reproducibility of Impactor Device

The percent deviation values of the subfracture repeatability protocol for the first, second and third levels of repeatability are illustrated in Figures 2.9, 2.10 and 2.11 respectively and printed in tables in Appendix E.2. These standard deviations values arise from extracted characteristics of the accelerometer curve of the accelerometer anchored on the projectile, which is shown in Figure 2.8. During testing, four distinct trials were found to have a noticeable error event that drastically affected the repeatability results. The processing code allowed for these trials to be removed from the following summary of the first level repeatability results; however they

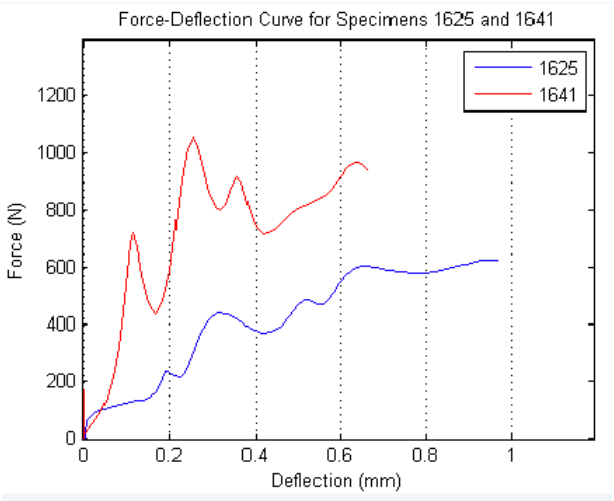

Figure 2.7: Force-Deflection curve for specimens 1625 and 1641 until fracture

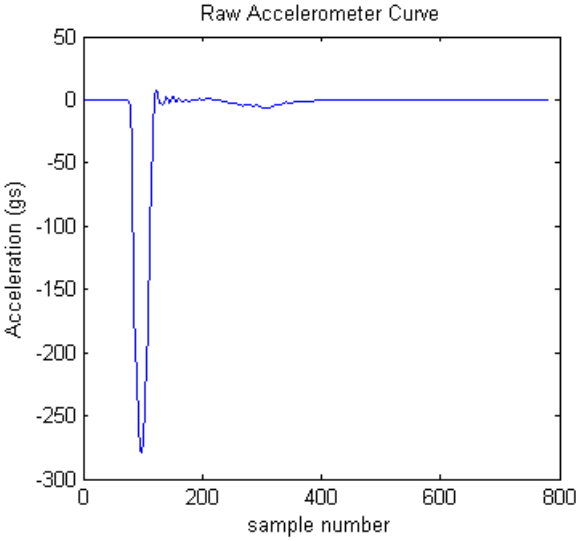

Figure 2.8: This figure shows the raw accelerometer data obtained from a representative specimen 1622 at height 2, site 4 and trial 1. By multiplying by mass we get a force-time curve from which the peak force (minimum value), impact energy (area under impact peak) and impact duration (width of impact peak) values were obtained, and the relative standard deviations of these parameters of each trial was assessed and presented as confirmation of the system's repeatability.

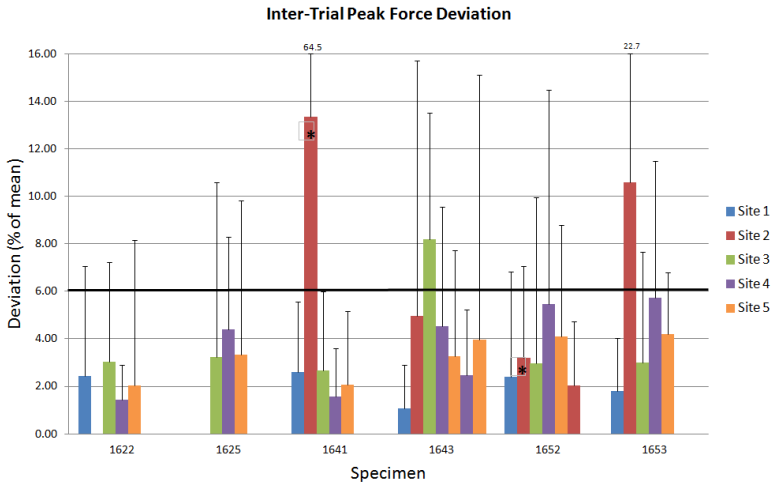

(a) Peak force deviations

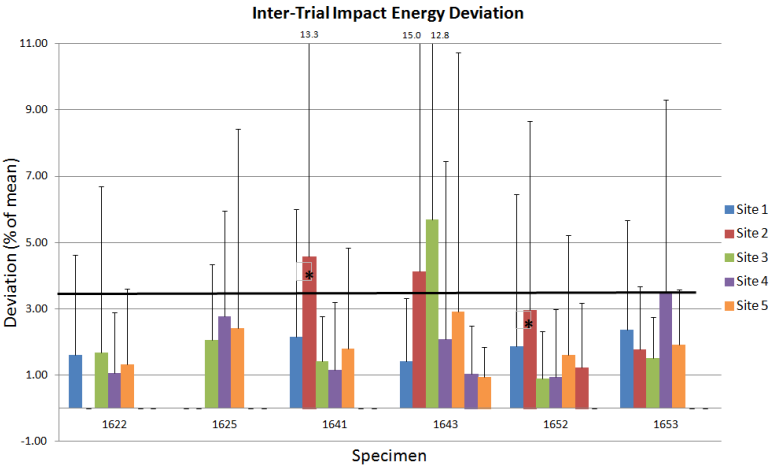

(b) Impact energy deviations

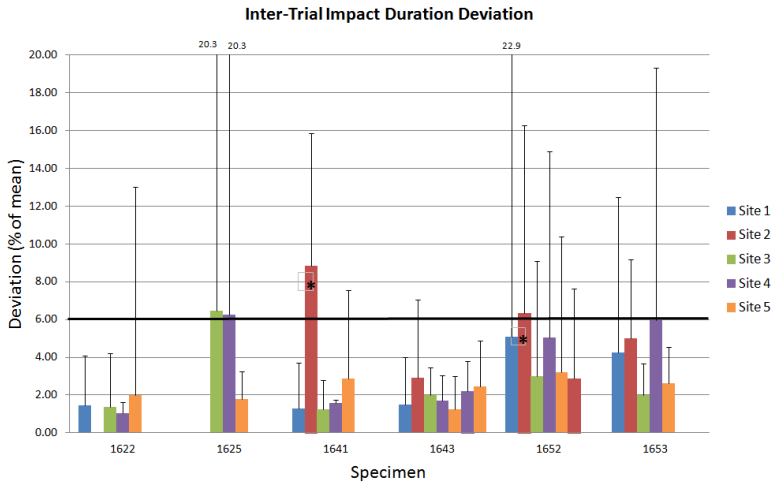

(c) Impact duration deviations

Figure 2.9: First-level repeatability deviations. Mean deviation values are indicated by the bar levels. Solid line indicates threshold below which 90% of the data resides. Error bars indicate the maximum deviation found. The asterisk values indicate trials where double strikes or other inconsistent impact events occured.

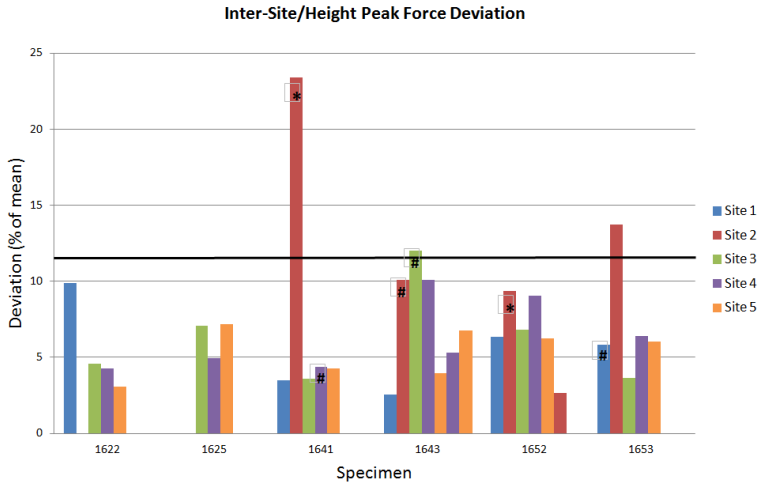

(a) Peak force deviations

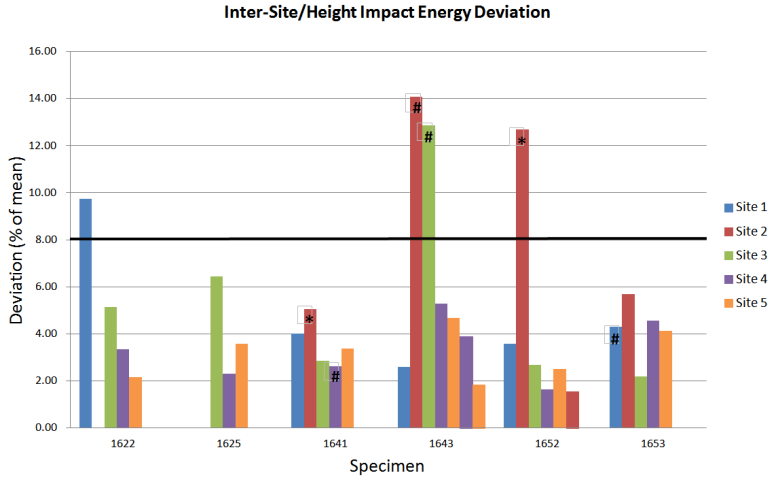

(b) Impact energy deviations

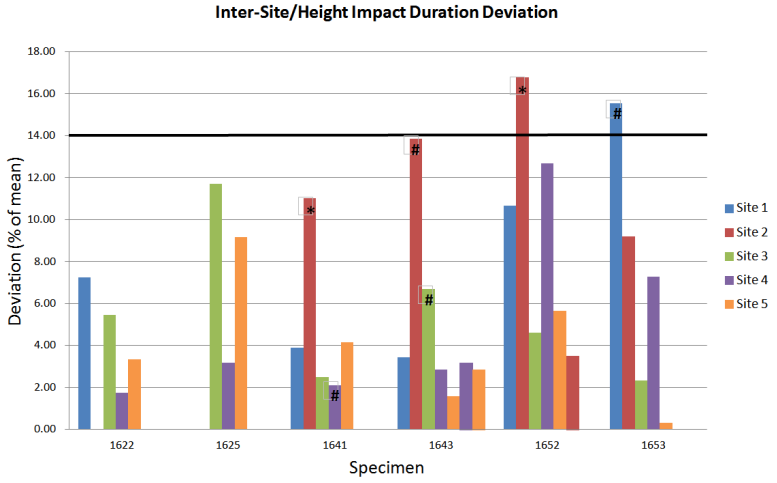

(c) Impact duration deviations

Figure 2.10: Second-level repeatability deviations. Mean deviation values are indicated by the bar levels. Solid line indicates threshold below which 90% of the data resides. The asterisk values indicate trials where double strikes or other inconsistent impact events occured, and the hashtag symbol indiactes when an impact event occurred for a specific trial within that set.

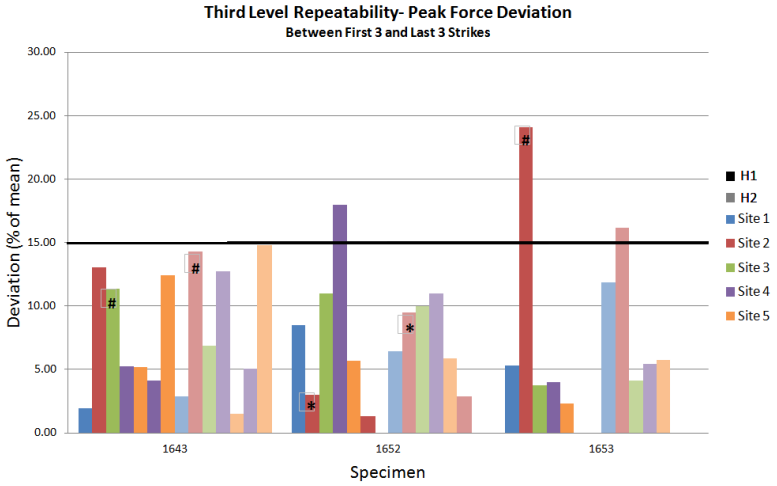

(a) Peak force deviations

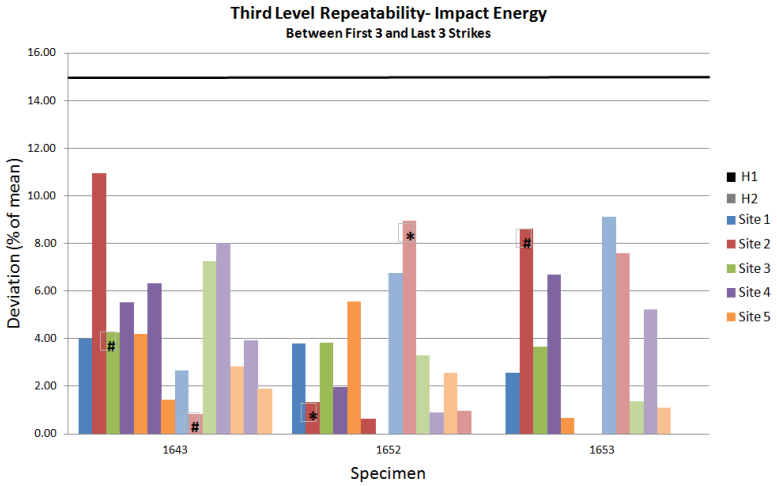

(b) Impact energy deviations

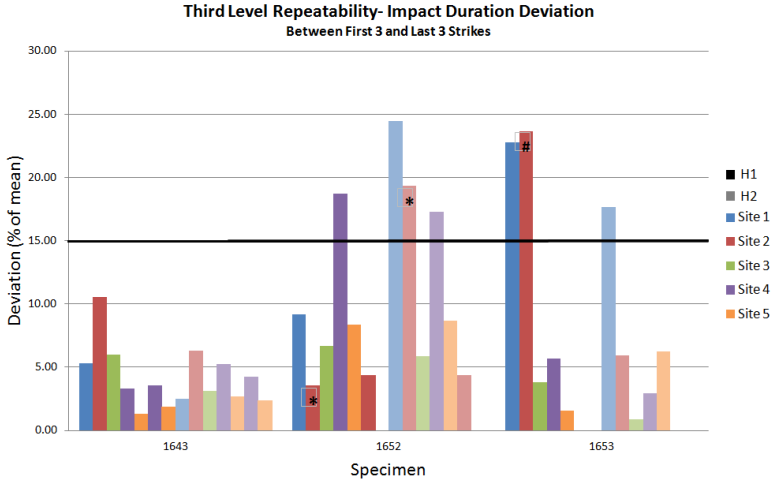

(c) Impact duration deviations

Figure 2.11: Third-level repeatability deviations. Mean deviation values are indicated by the bar levels. Solid line indicates threshold of significant deviations (15%). The asterisk values indicate trials where double strikes or other inconsistent impact events occured, and the hashtag symbol indiactes when an impact event occurred for a specific trial within that set.

were inherent to the calculations of subsequent levels of repeatability and should be considered a source of error. Two other sites were found to produce impact events with a double peak inconsistently throughout data collection accounting for large deviations in repeatability. Because these were not confined to a single trial, they were not removed from the analysis of any level of repeatability and should be considered a source of error.

Figure 2.9 shows that for the first level of repeatability, 90 percent of all trials had an average deviation of less than 6% for the peak force and impact duration, which reduced to 3.5% for impact energy. Maximum deviations for 90 percent of peak force and impact energy values were found to be under 16% and 11% respectively. The maximum deviations for impact duration were slightly larger with a value of 19%. The second level of repeatability suggests that 90 percent of all trials with a consistent height/site combination had standard deviations of less than 12%, 9%, and 14% for peak force, impact energy and impact duration respectively. There was little difference between the repeatability results of differing heights (see Figure 2.12a). The third level of repeatability illustrates how repeated testing will effect a measurement. Significant deviations (over 15%) of the peak force and impact energy across all heights and sites only occurred in three instances, for which known error events occurred during the most significant of these three. The remaining deviations tended to be quite small, between 2%-9%. The impact duration had more significant deviation between the first and the last trials with seven of the thirty six height-site combinations over 15% but the rest of the values below 10% deviation.

The RMSE values for the first level of repeatability for all specimens, sites and heights ranged between 1.55N (specimen 1652, Site 2 repeated, Height 1, Gauges L4, L5, L9) and 132.63N (specimen 1625, Site 3, Height 1, Gauge L7, L8). For reference, a plot showing each trial as well as the average to which the errors were calculated are plotted for both of these values along with a plot representative of the average RMSE value of the trials for all specimens, sites and heights in Figure 2.13. This average RMSE value was found to be 27.72N. All RMSE values of the first level of repeatability are printed in Table 2.2. Unfortunately

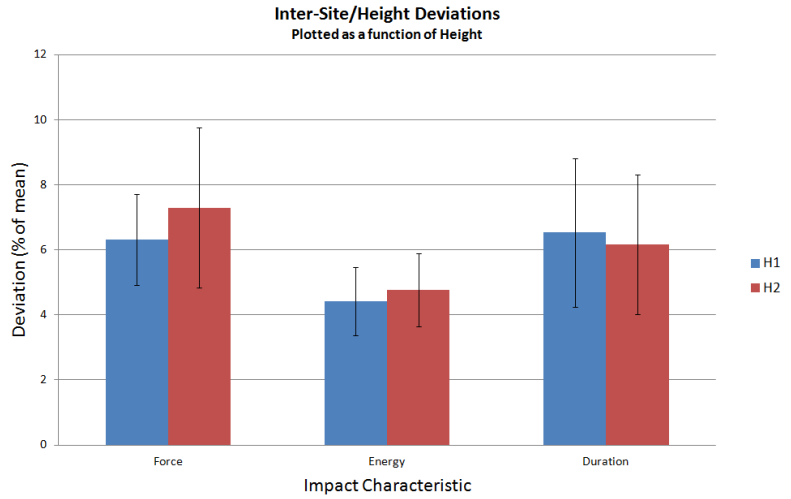

(a) Average impact deviaion of all sites and characteristics (impact force, impact energy and impact duration) per height

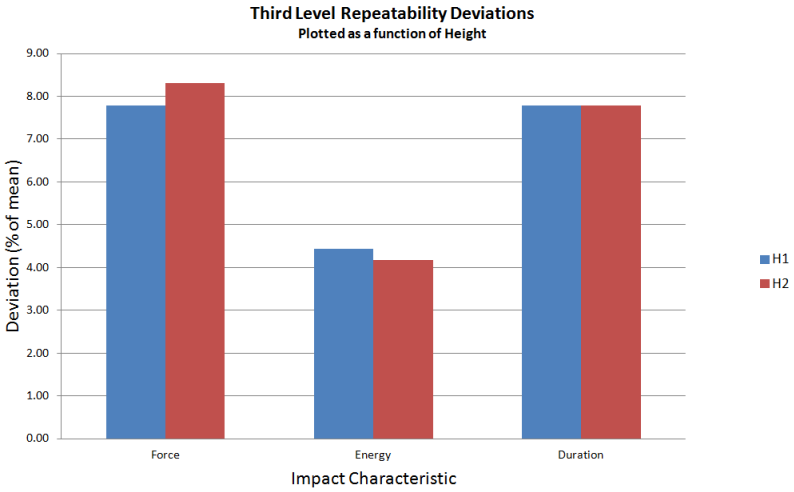

(b) Average impact deviation of the first and last three strikes of all sites and characteristics (impact force, impact energy and impact duration) per height

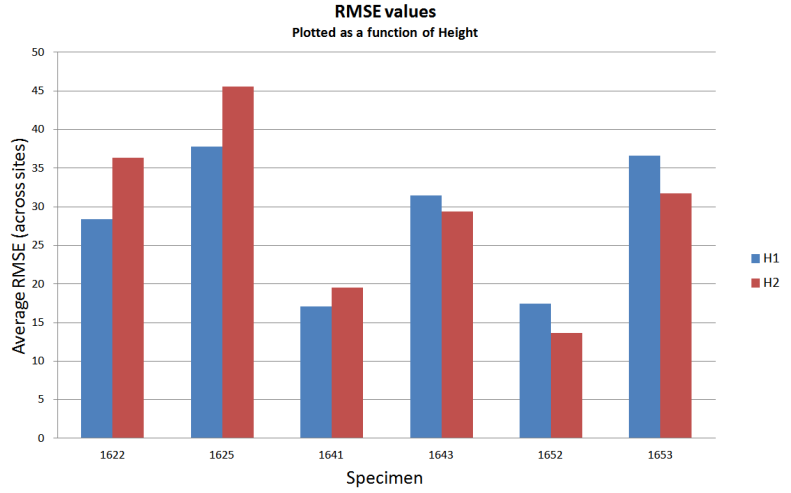

(c) Average RMSE values for each specimen plotted per height

Figure 2.12: Height comparison of deviation values.

Table 2.2: Average RMSE values of first level repeatability study. An asterisk indicates that a double strike was found inconsistently throughout trials, a # symbol indicates there was one distinct trial where a noticeable event occurred potentially affecting repeatability and r designates a repeated site (with increased focus on laser use).

Specimen	Site	RMSE H1 (N)	RMSE H2 (N)
1622			
	1	15.31	18.49
	3	40.34	35.46
	4	25.74	49.92
	5	32.28	41.43
1625			
	3	52.77	38.53
	4	36.39	53.88
	5	24.25	44.28
1641			
	1	17.36	15.18
	2*	8.34	15.54
	3	19.36	24.75
	4#	15.98	17.37
	5	24.51	24.84
1643			
	1	4.67	3.28
	2#	8.58	12.31
	3#	35.18	28.93
	4	57.14	36.42
	4r	33.06	37.00
	5	28.64	27.31
	5r	53.00	60.46
1652			
	1	3.47	4.24
	2*	2.44	3.98
	2r	2.46	2.47
	3	31.65	26.72
	4	48.92	23.70
	5	15.91	20.59
1653			
	1#	5.36	5.49
	2	14.18	14.59
	3	35.48	24.42
	4	77.06	65.09
	5	50.76	49.19

Table 2.3: Average RMSE values of third level repeatability study. r designates a repeated site (with increased focus on laser use).

Specimen	Site	RMSE H1 (N)	RMSE H2 (N)
1643			
	5	44.49	62.82
	4	74.03	92.60
	3	52.91	52.59
	2	23.27	22.08
	1	7.54	8.76
	4r	59.08	78.87
	5r	60.87	102.59
1652			
	5	53.47	50.65
	4	101.59	135.81
	3	65.78	65.67
	2	4.64	4.64
	1	9.87	11.19
	2r	4.11	5.54
1653			
	5	46.55	79.71
	4	101.99	80.10
	3	48.07	51.24
	2	44.76	42.78
	1	15.61	23.29

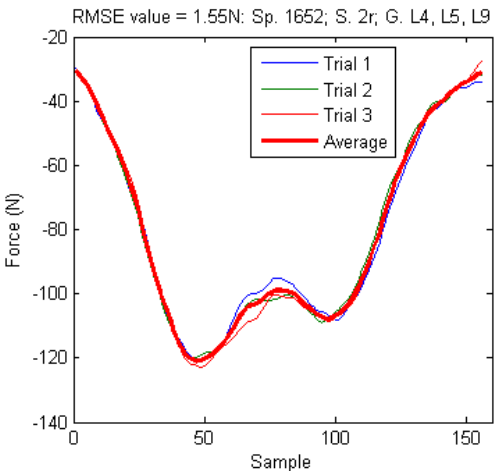

(a) Sample curve of best case: RMSE = 1.55

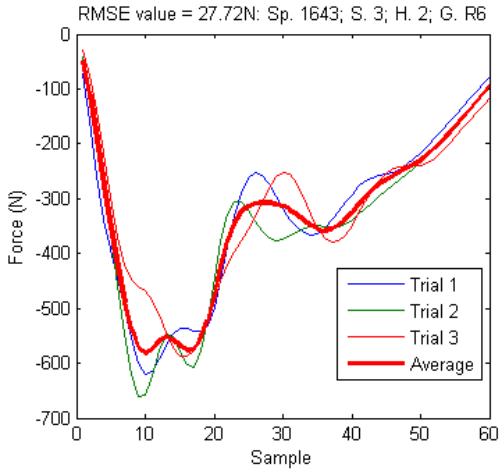

(b) Sample curve of average case: RMSE = 27.72

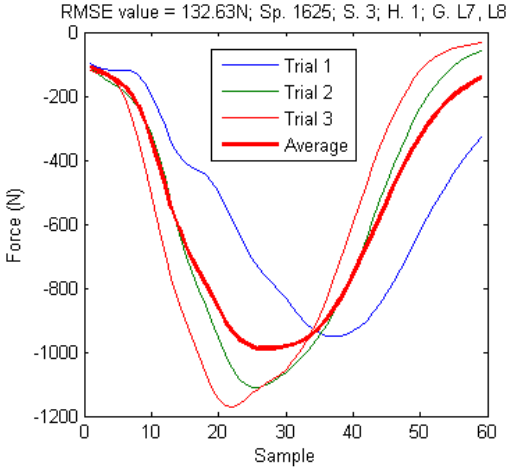

(c) Sample curve of worst case: RMSE = 132.63

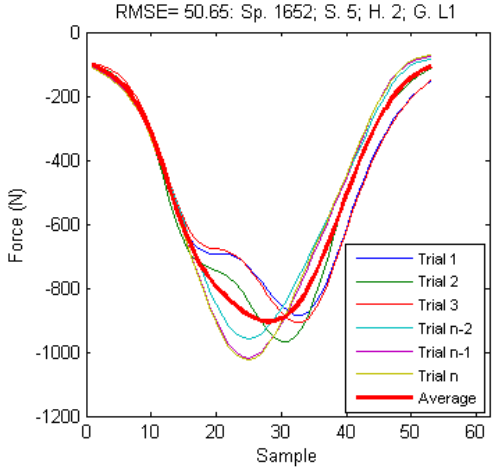

(d) Sample curve of reproducibility RMSE = 50.65

Figure 2.13: Sample curves of repeatability RMSE

an oversight in the programming of the processing code prevented us from determining the RMSE values for the second level of repeatability, but the third level of repeatability RMSE values were accessible by calculating the RMSE of the first three trials and the last three trials of specimens 1643, 1652 and 1653. The values found for this third level of repeatability are summarized in Table 2.3. The average of these RMSE values was found to be 49.73N, which is why a representative 3rd level repeatability RMSE curve in Figure 2.13d depicts an RMSE value of 50.65N.

2.4 DISCUSSION

2.4.1 System Performance

The quantitative capabilities of this impactor satisfied the initial design goals. All impacts durations were less than 0.5ms suggesting suitability for vibrational response research, and the force ranges attained were sufficient for both repeated subfracture and fracture testing. Furthermore, the device satisfied our qualitative criteria of inexpensive cost, ease of mobility and spatially conservative.

The customized device also performed well compared to the capabilities of previous impactor designs. Specifically, the impact velocities attained (0.36 to 1.89 m/s subfracture, 2.88-3.36m/s fracture) were directly comparable, as all impactors discussed in Section 1.3 confirmed velocities ranging from 0.1-30m/s with drop towers and guided fall devices accounting for the lower range, 0.1- 10m/s (Rhee et al., 2001; Vander Vorst et al., 2004; Yoganandan et al., 1991, 2004; Gurdjian et al., 1949) and ballistic devices accounting for the upper range. The impact durations induced by our device were in general shorter than those reported for other impactors at 0.56ms-4.2ms compared to the reported impact durations of other non-ballistic devices: 3ms-8ms (Hardy et al., 2007), 7ms (Verschueren et al., 2007), 3-9ms (Vander Vorst et al., 2004), and 8ms (Yoganandan et al., 2004). Our device even produced impact durations shorter than Hodgson's 1967 ballistic device (2-24ms) and was comparable to the impact durations of more

modern ballistic devices (2.5ms, Raymond et al. (2009)).

Qualitatively, the subfracture protocol was fairly successful, with only a few problems arising in the initial setup. One of these problems was that the strain gauges were found to burn out with prolonged connection. Reducing the excitation voltage of each gauge solved this issue as it was determined that although the gauges were correctly wired for use on most engineering materials, bone is less conductive than other materials and the stagnant heat was contributing to the burnout.

Issues also arose with some of the electrical connections linking the instruments to the data acquisition system. Because the strain gauges are fragile and experimental preparation involved significant positioning of the specimen, the decision to wire the strain gauge leads with short light wires ending in a pin was made. This method would allow the specimen to be moved without long heavy lead wires getting caught, pulled and damaging the gauges. However, with a pin and plug connection to the data acquisition system, it was found that any jostling of the wires resulted in large shifts and jogs in the strain gauges signals. After refining the protocol to include anchoring each connection to an immoveable surface the problem was reduced, however I still had to be extremely diligent in checking for faulty gauge signals and I had to redo several trials to get acceptable data. Future tests should consider different connection methods from the pin and plug system we used.

The neck-like support used to constrain the specimen worked quite well. At no time did a specimen impinge with the dental cemented pot, and the realistic nodding motion was adequate enough to maintain the specimen at a specific orientation and also minimized constraints on the skull motion. Specifically, the flexible support provided by the rubber washers mimicked the relative range of motion of an in vivo neck. It is noted that this range of motion is not complete leading to some limitations in studying the inertial effects. However these effects are assumed to be negligible considering the 1-2ms time scale of the impact and the fact that the inertial effects have been found to occur only after 3-5 ms (Verschueren et al., 2007). Therefore minimal limitations arise from simply estimating support stiffness and specific range of motion

of our simulated neck support. This also minimizes the effect of another noticed difficulty. As repeated impacts were performed, the rubber grommet spacers were compressed and found to shift relative to each other, reducing the stiffness of the nodding constraint. Although this issue in the context of support is minimized, this shifting can result in subtle reorientation of the skull causing differences in impact sites between trials. The effects of this will be addressed as part of the repeatability discussion. Failure of the occipital bone in the vicinity of the bolts was also avoided. Neither fractures due to stress concentrations nor fractures due to impingement of the metal washers on the bone occurred.

The velocity sensor did not function particularly well as it was very inconsistent particularly at high velocities where it would fail to record a time. When it did manage to record a speed, the values were reasonable for the cranial impact sites where velocities were higher, with only a 10% difference from the theoretical free fall value which was calculated using the following equation.

$$v = \sqrt{2gH} \tag{2.1}$$

where

v is the velocity of the projectile

g is the acceleration due to gravity, $9.81 \frac{m}{s^2}$

H is the height between the initial projectile position and the specimen

This however was not consistent for the lower facial sites, where the deviation increased to 25-40% of the analytical calculation. This deviation can be the result of friction in the tube, as well as of a wobble motion on the projectile in the tube. Also, the value with which the theoretical free-fall speed was calculated is based on the distance between the initial projectile height and the specimen, whereas the velocity sensor was positioned above the specimen about 1-2 cm. This 1-2 centimeters accounts for a greater percentage of the overall height on the lower drops accounting for a much larger difference between the calculated value and the recorded one. When this is taken into account, the higher drops decrease to a deviation of about 5% of the

theoretical value, where the lower drops decrease to a deviation of only about 15-25% of the theoretical value.

All sites were accessible for impact; however, it was difficult to position the specimen and anchor it in an appropriate place. Because the bracket anchor holes had to be directly aligned with one of the holes in the base matrix, translational alterations once the specimen was oriented with the desired site exposed could result in oblique impacts. Although several iterations of aligning and translational repositioning for anchoring ensued, it was difficult to achieve a directly normal strike for every site. With a ball peen end-effector, this was not found to affect the results of the subfracture testing, however more care and diligence in positioning may be important for determining fracture criterion in future fracture testing. Furthermore, on the facial sites where space was limited, a double strike was found to occur for some trials. This happened when the impactor contacted two different areas of the face. For example at site 2, the inferior orbit was close enough to the nasal bones that in some cases, an initial impact would occur on the nasal bone by the edge of the impactor before fully striking the 2nd site.

2.4.2 The Fracture Protocol

The fracture protocol was done primarily to validate our device and experimental setup against articles previously published on facial fracture. First of all, the fracture forces resulting from our study were similar to the fracture force ranges of established facial fracture studies. Specifically, our values between 631N-1548N are similar to both early facial impact studies: 1600N-2800N (Hodgson, 1967) and more recent studies: 1515N-2304N (Viano et al., 2004). Admittedly, our values are relatively smaller in comparison; however this can be accounted for by the difference in specimen preparation. Both reported studies researched on embalmed (Hodgson, 1967) and fresh-frozen (Viano et al., 2004) specimens with soft tissues that were well hydrated, whereas the specimens used in this study were dried and denuded and known to have a reduced force to fracture (Reilly and Burstein, 1974).

The preparation of our specimens may also account for the drastically reduced deflection

to fracture values compared to those reported in other studies. Specifically, Yoganandan et al. (1995), Delye et al. (2007), and Raymond et al. (2009) all found comparable deflection to fracture values between 4-8mm and all used fleshed, unembalmed post mortem human specimens. Our values of 0.66-0.97mm of deflection to fracture align more accurately when you consider that dried bone is more brittle (Reilly and Burstein, 1974). Another aspect that may account for differences in this value is the impact site. The reported values of Yoganandan et al. (1995), Delye et al. (2007) and Raymond et al. (2009) were cranial bones, either the frontal, or parietal bones. The facial bones are known to be weaker, and, in the case of the zygoma, the zygomatic arch or supports may buckle potentially leading to fracture failure before significant deformation could occur (Bhatt et al., 2011).

2.4.3 Repeatability and Reproducibility

The repeatability values obtained are the result of several sources of error in our system. Inherently, the accelerometer precision can contribute to error of up to 5% for the force and impact energy measurements of specimen 1622, and 2% for the measurements of the other specimens, however this will not affect the repeatability of the impact duration. The QDAC gain accuracy was determined to be negligible, accounting for only 0.1% error. The remaining sources of error are due to experimental setup, procedure and post processing.

The difficulty in maintaining identical skull positioning hit to hit probably accounted for the majority of error observed. The specimen was susceptible to shifting thus altering the initial impact condition. This shifting was the result of a number of reasons including the pot sliding in the bracket or the skull shifting on the carriage bolt when the rubber grommits got squished or displaced. In an attempt to alleviate this, a laser pointer was used to mark the position of the specimen before each hit, however this introduced a new inconsistency. Specifically, the operator realigning the laser marker may have different standards of precision. Specimen 1643 sites 4 and 5 as well as specimen 1652 site 2 was tested twice with and without diligence in positioning the head with respect to the laser allowing us to comment on the effect

of laser use. Figure 2.14 indicates that the deviation of sites with significant laser diligence were smaller than those obtained by the initial test for nearly all repeatability levels and impact characteristics suggesting that care in intermitting positioning can have a drastic effect. This however is not supported by the RMSE values, as the two conditions result in an inconclusive effect (see Figure 2.15).

Post processing can be attributed to the larger standard deviations in the impact duration deviations. The automated peak width code identified peaks by marking the distance between two threshold values which were defined as the point where the curve reached 10% of the overall peak height. To locate these points, the code first identified all points lying above this threshold and then found the two particular values that corresponded with the first and last elements of a peak (see Appendix C. Errors in the execution of this code occurred when noise or drift jumped above the 10% threshold misidentifying the true event start or finish. In some cases, this could cause deviations of up to 20% in the impact duration repeatability, however extreme cases were double checked manually and rectified. Despite our best efforts, larger deviations (such as the maximal deviations of the impact duration in Figure 2.9) may be due to similar errors that were not double checked.

The material and structural properties of the specimen were expected to affect the repeatability of the testing, however this was not fully confirmed with testing. For example, specimen 1625 and 1652 were observed to have very porous bone while sanding locations for gauge application, and therefore it was expected that micro breaks in the trabeculae would affect the overall repeatability of these specimens. However, the deviations in peak force and impact energy as well as the RMSE values of these specimens were comparable to those of the remaining specimens (see Figures 2.9, 2.10, 2.11, and Table 2.2). Nevertheless, there was a distinct increase in deviation of the impact duration (see Figures 2.9c, 2.10c, 2.11c) for these specimens which suggests that weaker material properties inconsistently alter the impact duration of each strike.

The impact site also did not appear to significantly affect repeatability of strikes. Impacts

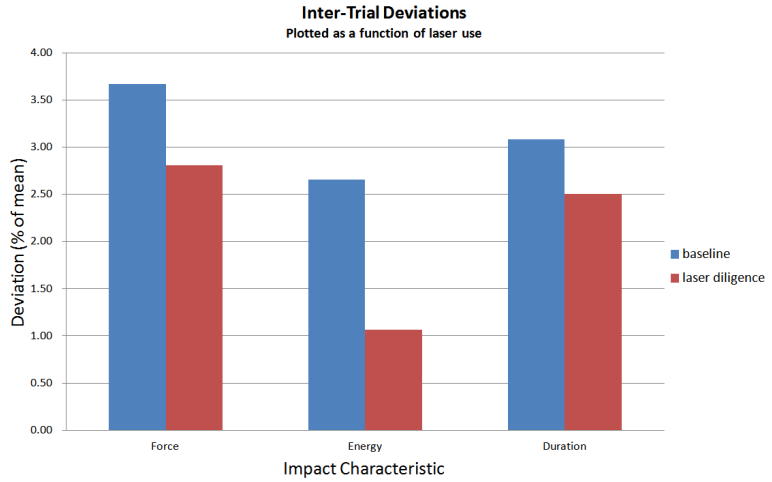

(a) First level repeatability comparison of laser use. Deviation values are the mean deviation values of all specimens and sites of a particular impact characteristic.

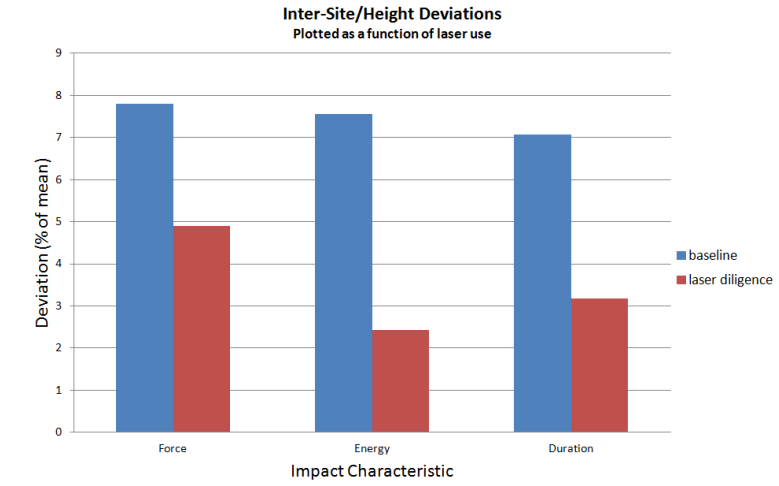

(b) Second level repeatability

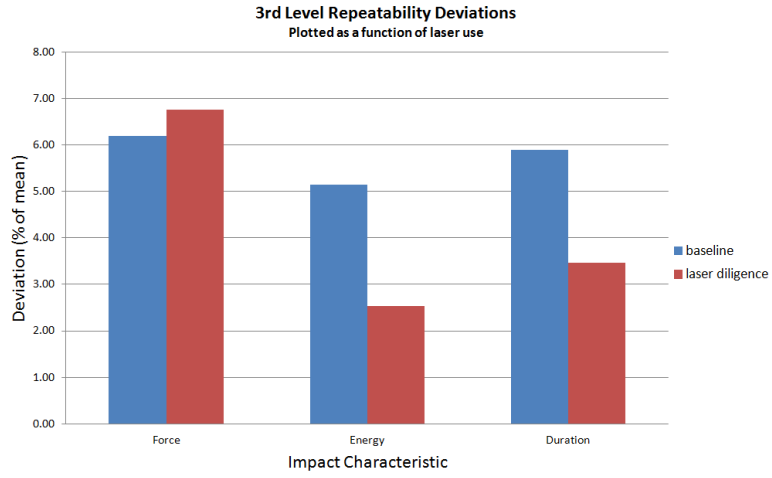

(c) Third level repeatability

Figure 2.14: Laser use comparison of deviation values. Deviation values are the mean deviation values of all specimens and sites with two trials completed (with and without diligent use of laser; Sp. 1643 S.4 and S.5 and Sp. 1652 S.2) of a particular impact characteristic.

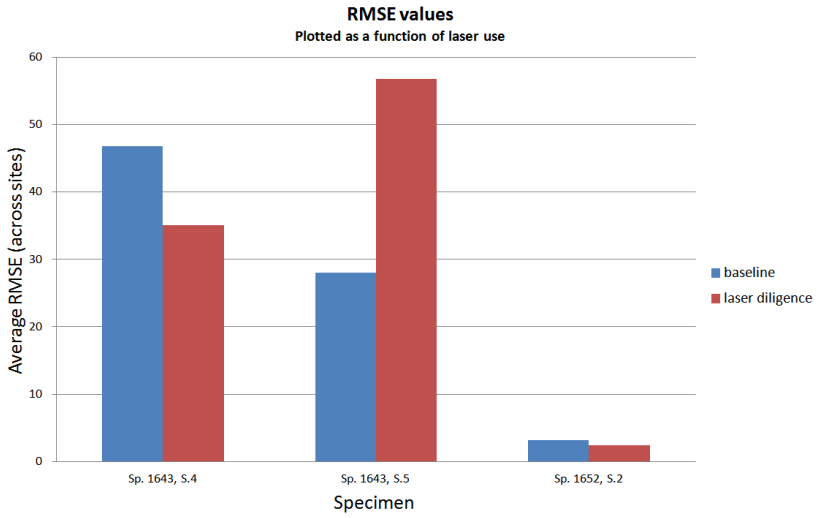

Figure 2.15: The average RMSE values of both heights for each condition (Sp. 1643 site 4 and site 5 and Sp. 1652 site 2) with and without laser use

to facial and cranial sites were comparable, however the facial sites were apparently more susceptible to faulty impacts such as the double peaked strikes, most likely due to the number of protrusions around a limited spatial area that might impinge on different areas of the impactor surface (for example, the nasal bone impinging on the projectile before the strike at the intended site). Specifically, four of the six events with bad trials (see Figure 2.9) were facial sites, and a fifth is site 3 which can include protrusions such as the brow bone validating this argument. Furthermore, although it is not supported by the deviations nor the RMSE values, testing observation seemed to suggest that shifting of the skull on the carriage bolts was found to occur more often on the facial sites because of the tilted orientation of skull. This may be supported weakly by the third level repeatability results. For example, 70% of all deviations between the first three trials and the last three trials over 15% were found among facial sites and all were found among sites 1, 2 and 3 (Figure 2.11). This suggests that at some point during testing a large cumulative deviation occurred, most likely accounted for by subtle differences in initial impact conditions throughout the repeated impacts due to shifting.

Finally some inconsistencies in repeatability may be accounted for by inconsistent friction losses in the tubed track, however this is most likely minimal for freefall condition considering the lack of effect height seems to have on repeatability (see Figure 2.12). Most likely inconsistent friction losses occurred with differences in the initial release of the projectile. For example, inconsistent pin removal may cause the projectile may be nudged upon release causing the initial begin falling with a wobbling motion. This wobbling motion would both inconsistently increase the friction of the edges of the projectile on the walls of the tube, and would also alter the initial impact condition accounting for an undetermined component of the overall deviation.

2.5 CONCLUSION

Overall, the impact apparatus designed was sufficient for the purposes for which it was designed. It produced quick impacts (less than 4.2ms) as well as forces capable of facial fracture

conditions. Furthermore, it was reasonably repeatable and reproducible in subfracture ranges.

The overall design of the apparatus could be improved by more reliable electrical connections, rubber grommits with a tighter fit to reduce inter-grommit shifting, and an improved velocity sensor. Although the customized bracket was very effective, reduced setup time and more consistent normal impacts may be possible if a sliding track anchoring system or an increase in the number of anchoring holes in the apparatus base matrix were implemented, so that subtler shifts in lateral translation would be possible for anchoring the specimen.

To improve the repeatability of the apparatus, maintaining a consistent initial impact condition is vital. Specifically, diligent realigning of the specimen to the laser marks was found to improve repeatability, and a second laser may provide an increased improvement by covering all degrees of freedom. An automated release mechanism may promote consistency of the initial drop and lubrication of the tube may reduce friction effects of the track.

The results from the fracture protocol were admittedly crude; however they did provide some insight to fracture response comparable to previously published material. To further validate the apparatus in this context, fresh-frozen specimens may be used, or fracture impacts to cranial sites may be attempted.

Bibliography

Byomesh Bhatt, Jason Green, Kieron McVeigh, Andrew Monaghan, and Stephen Dover. Contemporary management of orbitozygomatic complex trauma. *Trauma*, 14(2):99–107, 2011.

E S Gurdjian, John E Webster, and Herbert R Lissner. Studies on skull fracture with particular reference to engineering factors. *American Journal of Surgery*, 78:736–742, 1949.

Bo Hakansson, Anders Brandt, and Peder Carlsson. Resonance frequencies of the human skull in vivo. *Journal of the Acoustical Society of America*, 1994.

David Hampson. Facial injury: A review of biomechanical studies and test procedures for facial injury and assessment. *Journal of Biomechanics*, 1995.

Warren Hardy, Matthew Mason, Craig Foster, Chirag Shah, James Kopacz, King Yang, and Albert King. A study of the response of the human cadaver head to impact. *Stapp Car Crash Journal*, 2007.

Voight R. Hodgson. Tolerance of the facial bones to impact. *American Journal of Anatomy*, 1967.

T Khalil and D Viano. Experimental analysis of the vibrational characteristics of the human skull. *Journal of Sound and Vibration*, 1979.

David Raymond, Chris Van Ee, Gregory Crawford, and Cynthia Bir. Tolerance of the skull to blunt ballistic temporo-parietal impact. *Journal of Biomechanics*, 2009.

D T Reilly and A H Burstein. The mechanical properties of cortical bone. *Journal of Bone and Joint Surgery America*, 1974.

John S Rhee, Lisa Posey, Narayan Yoganandan, and Frank Pintar. Experimental trauma to the malar eminence: Fracture biomechanics and injury patterns. *Otolaryngology - Head and Neck Surgery*, 125:351–355, 2001.

Michael Vander Vorst, Philemon Chan, Jiangyue Zhang, Narayan Yoganandan, and Frank Pintar. A new biomechanically-based criterion for lateral skukll fracture. *Annual Proceedings/Advancement of Automotive Medicine*, 48:181–195, 2004.

P Verschueren, H Delye, B Depreitere, C Van Lierde, B Haex, D Berckmans, I Verpoest, J Goffin, J Vander Sloten, and G Van Der Perre. A new test set-up for skull fracture characterisation. *Journal of Biomechanics*, 40:3389–3396, 2007.

David C Viano, Cynthia Bir, Tim Waliko, and Don Sherman. Ballistic impact to the forehead, zygoma and mandible: Comparison of human and frangible dummy face biomechanics. *The Journal of Trauma: Injury, Infection and Critical Care*, 2004.

R Willinger, L Taleb, and C Kopp. Modal and temporal analysis of head mathematical models. *Journal of Neurotrauma*, 1995.

Narayan Yoganandan, Anthony Sances, Frank Pintar, Dennis Maiman, David Hemmy, Sandford Larson, and Victor Haughton. Traumatic facial injuries with steering wheel loading. *The Journal of Trauma*, 31:699–710, 1991.

Narayan Yoganandan, Frank Pintar, Anthony Sances Jr., Patrick Walsh, Channing Ewing, Daniel Thomas, and Richard Snyder. Biomechanics of skull fracture. *Journal of Neurotrauma*, 1995.

Narayan Yoganandan, Jiangyue Zhang, and Frank Pintar. Force and acceleration corridors from lateral head impact. *Traffic Injury Prevention*, 5:368–373, 2004.

Chapter 3

Factors Affecting the Frequency Domain Response of a Skull to Impact

3.1 INTRODUCTION

With head injuries accounting for significant mortality, disability and socioeconomic costs around the world (O'Riordain et al., 2003; Brands, 2002) head impact biomechanics and brain injury mechanisms have received considerable attention in recent years. However, a large majority of this research has been done addressing the temporal biomechanics of the head to impact, namely the kinematics and kinetics. Specifically, acceleration (both linear and angular) has been widely considered as a prominent injury mechanism focussed on by nearly all notable brain injury research studied as of the 1950s (McLean and Anderson, 1997). However despite this extensive body of literature, conclusions of these studies remain contradictory and vague, leading to a crude understanding of brain injury mechanisms today (McLean and Anderson, 1997).

In recent years a few researchers have taken a different approach by studying the vibrational response of the head upon impact. These studies do not only provide alternate hypotheses of head injury mechanisms, but they also provide critical information on the dynamic characteris-

tics of the head and skull necessary to validate analytical and finite element models. Building off of the pioneering work of Békésy (1948), Franke (1956) and Stalnaker et al. (1971) the current state of knowledge of the vibrational response of the head to impact is based primarily on studies by Khalil et al. and Viano et al. (1979), Hakansson et al, (1994) and Willinger et al. (1995). These studies discuss the observed vibrational responses of both dry cadaver skulls and in vivo subjects. Khalil et al. found 11 and 6 resonant frequencies respectively for two individual cadaver specimens upon impact, with no comparison of the values of these frequencies or the modal response between the two skulls. The Hakansson et al. study of induced vibration through bone conducted hearing aids in in vivo subjects came to similar conclusions but with the resonant values recorded being generally lower than the Khalil et al. study, consistent with the added mass of soft tissue. Applying concepts of vibration to the context of head injury mechanisms, Willinger et al. measured the mechanical impedance of a live subject and discovered a resonant frequency at a value significantly lower than the other studies at 150Hz (compared to Khalil et al., 1385Hz and Hakansson et al., 828Hz). Willinger et al. focussed his examination on the implications of this decoupling resonant frequency (discussed with more detail in Section 1.4.3) and made little consideration to the effects of higher vibrational modes such as those reported by Khalil et al. or Hakansson et al.

The current study examines the vibrational responses of six in vitro skulls to impact, using a drop-weight tower impactor. Specifically, this study measures the natural frequencies and associated powers of the skulls and how they are affected by impact location, impact energy (drop height) and specimen properties. I will also attempt to determine gauge specific consistency between trials of variable conditions. Finally I will also validate the experimental setup with a discussion on how our findings compare with the established vibrational studies previously mentioned.

A final section of this chapter will analyze the frequency response of a few specimens post facial fracture. Because roughly a third of head impact injuries are concomitant with facial fractures (Keenan et al., 1999) an attempt to quantify the changes within a specimen

due to structural trauma may be helpful in future research on the development of head injury mechanisms.

3.2 MATERIALS AND METHODS

3.2.1 Specimen Preparation

Six fresh frozen cadaveric heads were used for this study (mean age: 80+- 12 years, 2 female, 4 males). CT scans were made of each specimen prior to preparation. Soft tissue was removed first with surgical denuding and the remaining soft tissue was removed by Dermestidae beetles (from a colony at the University of Guelph). Once only the bony anatomy remained, the specimens were degreased, disinfected and ready for instrumentation.

The strain gauges used to measure the specimens' response to impact were adhered to the specimens at placement sites selected to maximize craniofacial coverage. They were adhered according to a preparating protocol consisting of sanding, cleaning and the application of a bonding agent to ensure secure bonding of the gauge on bone (detailed gauging protocol in Appendix B). Triaxial strain gauges were used where space permitted; otherwise uniaxial gauges were used (Omega Engineering Inc. Montreal, QC, Canada). Five of the six specimens were configured with 11 triaxial gauges and 6 uniaxial gauges, and the other specimen (1622) was outfit with 9 triaxial gauges and 8 uniaxial gauges. The gauge placement sites of these specimens are illustrated in Figure 2.4 in chapter 2.

3.2.2 Specimen Fixation, Experimental Setup and Testing Protocol

The vertical drop mass tower described and validated in Chapter 2 was used with a 0.173kg mass weight to induce short duration (1-5ms), localized impacts on the specimen fixed below the drop chute.

The specimen was fixed according to the protocols discussed in Section 2.2.3 in Chapter 2,

and once the specimen was secured in the bracket and oriented appropriately under the impact zone, the testing protocol was started with a sampling rate of 50 000Hz. This consisted of first marking a laser mark on the specimen surface to ensure consistent impacts and beginning with subfracture impact loadings on five different saggital sites (illustrated in Figure 2.5). All skulls were impacted at the parietal bone (Site 5), the frontal bone (Site 4), the superior brow (Site 3), the inferior orbit (Site 2) and the malar eminence (Site 1). Specimen 1625 was impacted on the right side, but all other specimens were impacted on the left.

The body of data I aimed to collect involved six impacts worth of data (three trials at two different heights) from each strain gauge for each impact site. This was accomplished by first collecting three trial strikes at one height and site combination. Then the height was increased for a further three trials. Due to the high sampling rate, data recordings for all 17 gauges and the accelerometer simultaneously was not possible, so the procedure was completed while recording from as many gauges as possible. Then the protocol was repeated until six impacts from each gauge was collected. The specimen was then reoriented to a different impact site and the process was repeated. Refer to the tree diagram in Figure 2.6 in chapter 2 for a visual description of this procedure. Between each strike the laser marking was realigned with the marking on the specimen to ensure consistent impacts and the accelerometer data was collected for each impact. The exact procedure followed for each specimen is provided in Appendix A.

3.2.3 Post Processing

Custom-written software (Matlab™, The Mathworks Natick, MA, USA) converted the raw voltage data from the gauges and the accelerometer into impact force and strain data (see Appendix C). The strain data was then further processed with a customized discrete fourier transformation (DFT) code to obtain frequency domain behaviour of each impact. This process along with a representative sample of the strain gauge data and associated frequency spectra is illustrated in Figure 3.1. Each individual impact trial was analyzed manually to extract both the frequency values of each impact and the magnitude of that frequency component (the power).

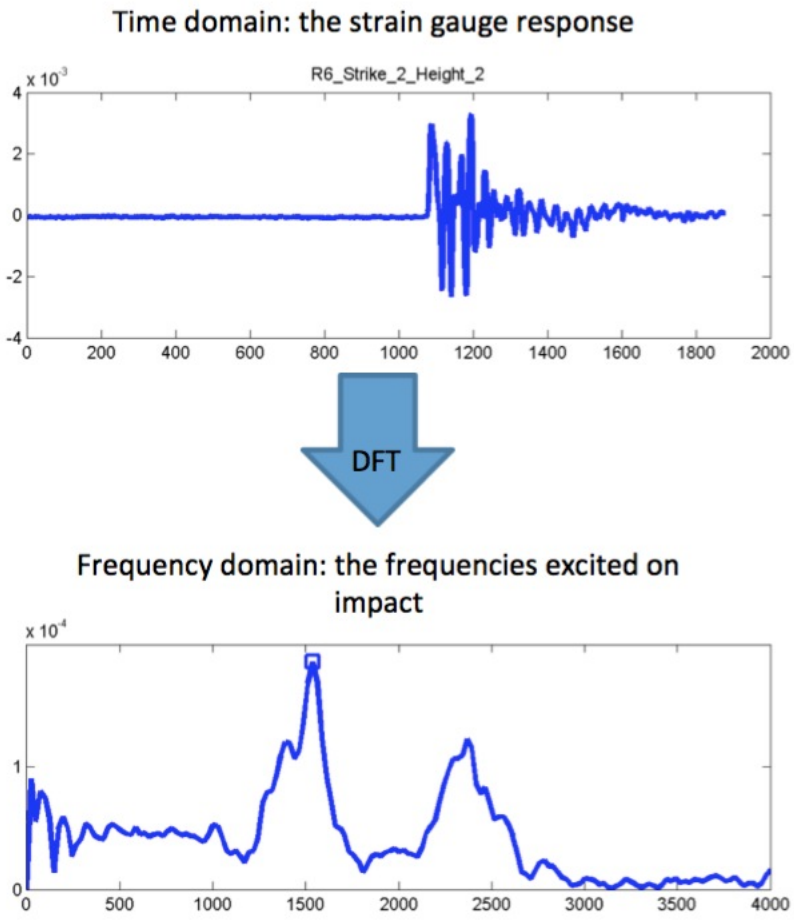

Figure 3.1: Strain gauge data in the temporal (top) and frequency (bottom) domain. A DFT was used to tranform the former to the latter.

The identification of all natural frequencies of a specimen from the combined strain gauge data was complicated by the fact that, depending on their location, different strain gauges may detect none, one or multiple non-consecutive resonant frequencies. Therefore, the resonant frequencies of all heights and sites were aggregated for each specimen and analysed with a cluster analysis and 2-way analysis of variance (ANOVA) tests to identify the resonant frequencies of each specimen as well as to compare the effect of heights and sites on the frequencies found. The cluster analysis used is an agglomerative hierarchical technique (Lance and Williams, 1967) which identifies groups of data based on a Euclidean distance proximity matrix and an average between groups linkage criteria. This method allowed us to determine the approximate number of resonant frequencies for each specimen, as well as classify each data-point as part of a distinct resonant frequency. Section 1.5.3 explains cluster analysis techniques in more detail and Figure 3.2 illustrates the effect of this technique for specimen 1652. The cluster analysis was necessary for the following steps in our procedure

Firstly, it was used to compare the sequence of resonant frequencies of each skull. A 1-way ANOVA was used to test the effect of this final variable of specimen on the frequency response of the human skull.

Secondly, with resonant frequency ranges identified for each specimen, the frequencies excited by each gauge to evaluate the gauge specific repeatability were re-examined. Each numerical frequency value excited in a gauge was binned as a resonant frequency according to the ranges identified by the cluster analysis and was then compared to other trials of the same gauge. A binary condition was assigned to each gauge to describe matching frequencies between trials, heights and impact sites. 1 recorded a match and 0 recorded a mismatch. In this way, the consistency of each gauge at exposing particular frequencies with changing impact conditions was evaluated. This also allowed the evaluation of our cluster analysis technique and modify cluster groups if necessary. Specifically if two or more recorded frequencies at a single gauge belonged in the range of only one frequency according to the cluster analysis, the cluster analysis was modified to split that bin to distinguish between the two separate frequencies

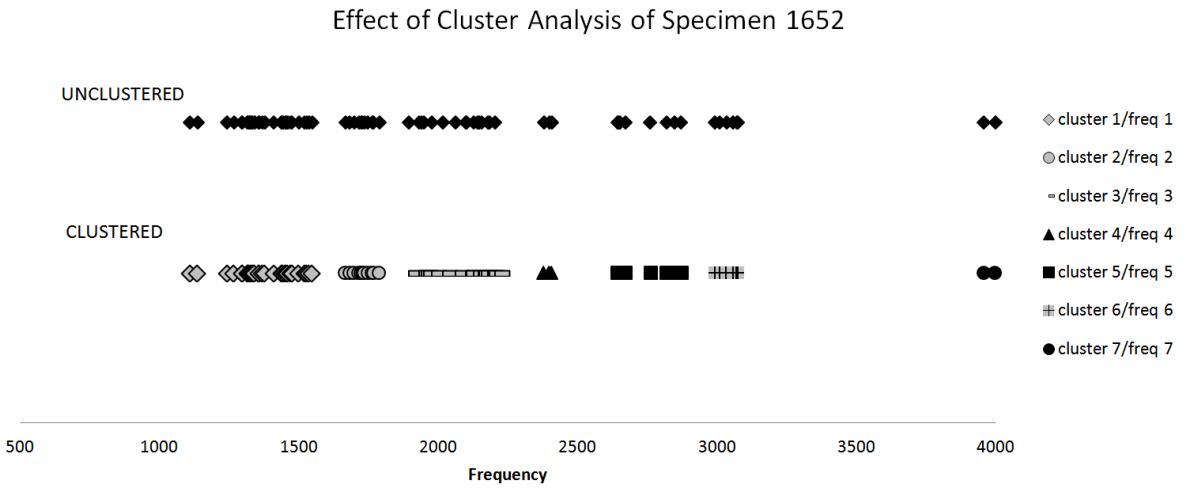

Figure 3.2: Effect of cluster analysis for specimen 1652. Each data point represents a frequency value extracted from one of the gauge frequency spectra. The cluster analysis algorithmically determines groups in the linear data, clumping all similar frequency values in the same cluster. Each cluster is then identified as a different resonant frequency, with each data point of that cluster representing a sample exposing that frequency.

identified by the gauge.

The effect of height, site and specimen on the powers of each resonant frequency was analyzed by comparing the ratios of these powers for each frequency. To do this, the power of each resonant frequency evident in each trial was recorded. As it was typical for a single gauge to record only a few of the possible resonant frequencies (as per the cluster analysis) a 0 power was assigned to the cases were a particular resonant frequency was not exposed by the gauge for a particular trial. This allowed us to take a weighted average of each resonant frequency and calculate it as a ratio of all resonant frequencies possible. A ratio of each resonant frequency was calculated for the total of all hight/site combinations, as well as for the total of all sites for a particular height, and of all heights for a particular site. The power ratio was also taken for individual height/site combinations and compared to establish the effect of height, site and specimen on the power ratio of the frequency spectra.

3.2.4 Post-fracture Analysis

Once the entire subfracture protocol was completed, specimens 1643, 1652 and 1653 were fractured at the malar eminance using the procedure described in Section 2.2.3. Then, a modified subfracture protocol was perfomed on the fractured specimens to obtain data comparable to the pre-fracture data. Specifically, only impact site 3 was impacted for these post fracture tests and only information from gauges that remained intact following the fracture was obtained. Furthermore, data pertaining to only one drop height was collected for specimens 1652 and 1653 as the vibration of the impact was found to increase the severity of the fracture.

The data was then processed in the same way as the pre-fractured data (described in Section 3.2.3) and the natural frequencies exposed by these impacts were identified. A cluster analysis was performed on the post-fracture data as well as on the isolated impact site 3 pre-fracture data and compared to establish whether any similarities existed. An examination of the frequencies excited at each individual gauge was also done to confirm the cluster analysis as well as to establish repeatability of the gauges at exposing consistent resonant frequencies in the post

fractured cases. The power ratios of each frequency was also calculated for the post-fracture data in the same way it was calculated for the pre-fracture data, however, because only one site was tested, no comparison between sites will be expected and a comparison between heights will only be discussed for specimen 1652.

3.3 RESULTS

3.3.1 Frequencies Excited

Of the six specimens tested, five produced meaningful data. Specimen 1625 exhibited longer impact durations, that is likely attributable to its porous, weak bone material properties. This resulted in sparse frequency data and was omitted in this study. Similarly, impacts to the facial bones at sites 1 and 2 of the remaining five specimens were also on average longer than 2ms so only impacts of sites 3, 4 and 5 will be considered.

Between zero to three identified frequencies were found per strike per gauge for a total data set of between 77 and 166 frequency values per specimen. The two-way ANOVA done to analyze the effect of height and site on the frequency values obtained was found to have p-values greater than 0.05 for all specimens (Table 3.1). This insignificant conclusion confirmed our hypothesis that the resonant frequencies for each skull were independent of impact location or impact energy (drop height).

The initial cluster analysis identified six resonant frequencies for specimens 1641 and 1653, and seven resonant frequencies for specimens 1622, 1643 and 1652. However, upon examination of the individual frequency spectra for each gauge/strike combination a known discrepancy was found for three of the specimens. Specifically, gauges recorded two distinct frequencies clustered within a single group twice for specimens 1622 and 1641 prompting the original first and third frequencies to be divided to accommodate the distinct frequencies. The first cluster of specimen 1643 was found to be too large with one gauge identifying three distinct frequencies clustered into the original first frequency.

Table 3.1: ANOVA table of frequency response. No values are smaller than 0.05 suggesting that impact height and impact site are insignificant factors in the resonant frequencies found for each specimen at a significance level of 0.05.

Specimen	Source	p-value
1622		
	Site	.178
	Height	.765
	Interaction	.938
1641		
	Site	**.062**
	Height	.924
	Interaction	.960
1643		
	Site	.284
	Height	.604
	Interaction	.953
1652		
	Site	.563
	Height	.972
	Interaction	.999
1653		
	Site	**.074**
	Height	.594
	Interaction	.912

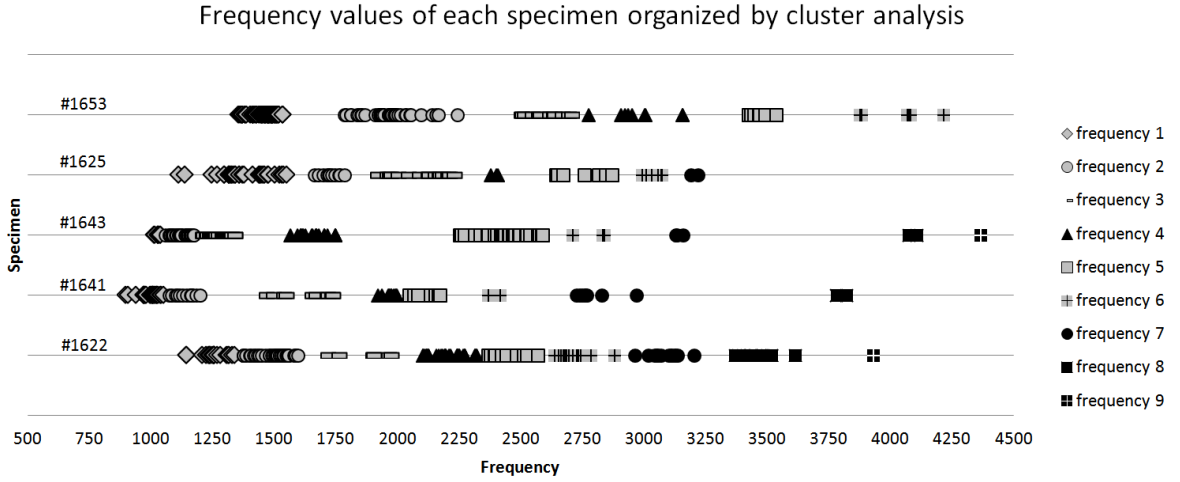

Figure 3.3: Cluster analysis results showing ranges of each resonant frequency identified. As in 3.2, each data point represents a sample extracted from the frequency spectra of one of the gauges, and each cluster represents the resonant frequency that those particular samples expose. Note how each specimen has a different collection of data resulting in very different clusterings.

Table 3.2: the data count, mean (Hz) and standard deviation (Hz) of each resonant frequency cluster found for each specimen

Specimen	Frequency Number	Data Count	Frequency Value (mean)	Standard Deviation
1622				
	1	21	1252	51.53
	2	52	1504	58.03
	3	6	1842	106.79
	4	33	2204	68.37
	5	12	2455	68.65
	6	15	2716	60.89
	7	14	3083	59.24
	8	11	3462	70.5
	9	1	3931	0
1641				
	1	24	991	38.57
	2	15	1141	37.91
	3	10	1599	102.85
	4	11	1967	24.23
	5	8	2113	48.51
	6	2	2393	34.88
	7	8	2788	79.55
	8	2	3801	28.52
1643				
	1	8	1024	8.99
	2	30	1122	31.71
	3	38	1245	38.61
	4	20	1658	55.00
	5	32	2433	99.77
	6	3	2794	72.77
	7	7	3237	127.13
	8	2	4090	23.33
	9	1	4366	0
1652				
	1	33	1374	105.99
	2	11	1727	37.19
	3	16	2067	103.25
	4	3	2393	14.79
	5	8	2736	96.86
	6	6	3038	33.54
	7	2	3976	28.99
1653				
	1	55	1451	48.74
	2	47	1964	95.77
	3	12	2569	72.04
	4	9	2977	120.82
	5	10	3457	34.84
	6	6	4032	131.62

Thus the modified cluster analysis revealed between six and nine resonant frequencies in each specimen. Specifically, six resonant frequencies were identified for specimen 1653, seven for specimen 1652, eight for specimen 1641 and nine for specimens 1622 and 1643. The results of this analysis are illustrated in Figure 3.3 and show the assignments of each frequency value to a particular cluster. The mean and standard deviation of each frequency cluster are tabulated in Table 3.2 and represent the resonant frequencies of each specimen.

The results of the 1-way ANOVA on frequencies between skulls yielded significant differences in frequency values for the first eight resonant frequencies ($p<0.001$). The ninth resonant frequency only had one data value for each of two specimens so no p-value was calculated; however the values differed by 435Hz.

3.3.2 Binary Examination of Individual Gauges

In addition to verifying the cluster analysis, the binary examination of each gauge revealed that frequencies identified by each gauge between trials were very consistent, between 93.5% and 98.7% match. The consistency was found to decrease when comparing frequencies exposed by each gauge as a function of height and site, with all specimens exhibiting between 70.2% and 83.3% match except specimen 1622 which had a frequency match of only 36.0% between heights. This binomial analysis also revealed that the natural frequencies revealed at each gauge differed between location of impact with only between 0% and 16.6% match between sites.

3.3.3 Power Ratios

The power ratio results are compiled in Tables 3.3, 3.4, 3.5, 3.6, 3.7 and Figures 3.4, 3.5, 3.6, 3.7, 3.8.

To summarize, the frequency ratios of specimens 1622, 1641, 1652 and 1653 remain relatively consistent between heights with the maximum deviation being 8.9% (frequency 4), 1.7%

Table 3.3: Power ratios of specimen 1622. H represents the different height levels that the impactor was dropped from, and S represents the different sites onto which the impactor struck.

	frq 1	frq 2	frq 3	frq 4	frq 5	frq 6	frq 7	frq 8	frq 9
Total	0.1560	0.4936	0.0109	0.1213	0.0802	0.0590	0.0466	0.0313	0.0010
H1	0.1634	0.4680	0.0134	0.1752	0.0428	0.0522	0.0480	0.0346	0.0024
H2	0.1508	0.5107	0.0092	0.0860	0.1049	0.0635	0.0457	0.0292	0
S3	0.2045	0.2919	0.0441	0.2221	0.0565	0.0415	0.0465	0.0929	0
S4	0.1120	0.5987	0.0023	0.0551	0.1000	0.0550	0.0567	0.0188	0.0015
S5	0.2617	0.3199	0.0095	0.2559	0.0343	0.0891	0.0121	0.0174	0
S3H1	0.2457	0.3342	0.0272	0.2140	0.0132	0	0.0780	0.0877	0
S3 H2	0.1722	0.2586	0.0574	0.2286	0.0905	0.0740	0.0218	0.0970	0
S4 H1	0.1092	0.5462	0.0059	0.1417	0.0596	0.0607	0.0486	0.0244	0.0039
S4 H2	0.1139	0.6320	0	0	0.1257	0.0514	0.0618	0.0152	0
S5 H1	0.2630	0.3386	0.0249	0.2515	0.0157	0.0786	0.0142	0.0136	0
S5 H2	0.2588	0.3092	0	0.2593	0.0460	0.0959	0.0109	0.0199	0

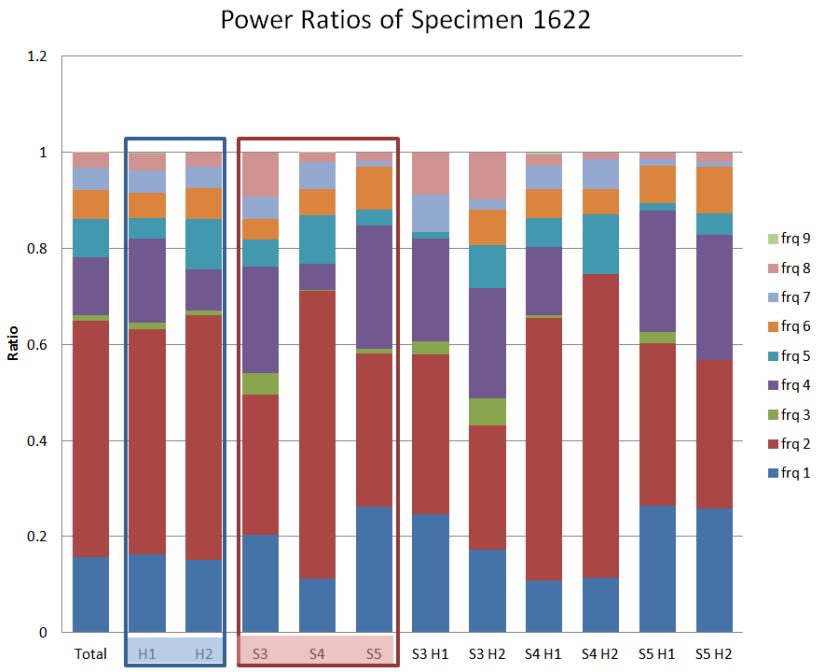

Figure 3.4: Frequency power ratios of specimen 1622

Table 3.4: Power ratios of specimen 1641. H represents the different height levels that the impactor was dropped from, and S represents the different sites onto which the impactor struck

	frq 1	frq 2	frq 3	frq 4	frq 5	frq 6	frq 7	frq 8
Total	0.5683	0.2364	0.0464	0.0688	0.0304	0.0077	0.0364	0.0055
H1	0.6110	0.2201	0.0316	0.0749	0.0205	0.0074	0.0300	0.0044
H2	0.5939	0.2306	0.0382	0.0666	0.0317	0.0051	0.0297	0.0042
S4	0.4218	0.2892	0.0840	0.0762	0.0251	0.0186	0.0719	0.0133
S5	0.6724	0.1990	0.0196	0.0636	0.0342	0	0.0112	0
S4 H1	0.4568	0.2618	0.0819	0.0787	0.0247	0.0193	0.0655	0.0115
S4 H2	0.3933	0.3115	0.0857	0.0742	0.0254	0.0180	0.0772	0.0148
S5 H1	0.7081	0.1938	0	0.0725	0.0179	0	0.0077	0
S5 H2	0.6358	0.2043	0.0398	0.0544	0.0509	0	0.0147	0

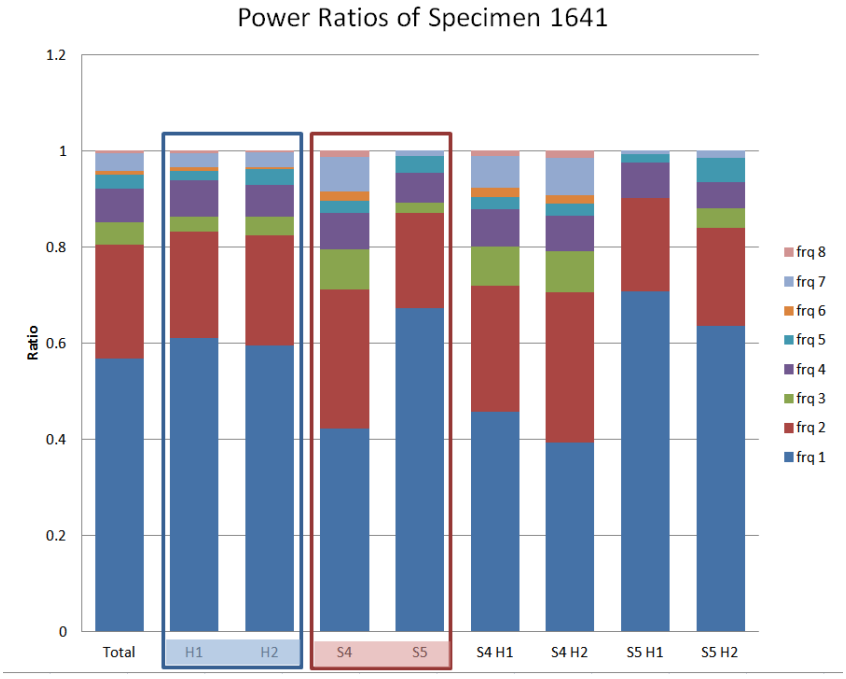

Figure 3.5: Frequency power ratios of specimen 1641

Table 3.5: Power ratios of specimen 1643. H represents the different height levels that the impactor was dropped from, and S represents the different sites onto which the impactor struck

	frq 1	frq 2	frq 3	frq 4	frq 5	frq 6	frq 7	frq 8	frq 9
Total	0.0059	0.0046	0.7528	0.0029	0.2330	0.0004	0.0003	0.0001	0
H1	0.0026	0.0020	0.7589	0.0013	0.2349	0.0002	0.0001	0	0
H2	0.2238	0.1800	0.3460	0.1111	0.1018	0.0182	0.0130	0.0047	0.0015
S3	0.1218	0.6492	0	0.1529	0.0681	0	0.0081	0	0
S4	0	0.0023	0.7599	0.0024	0.2350	0.0004	0	0	0
S5	0.7815	0.0425	0.0880	0	0.0297	0	0.0409	0.0143	0.0031
S3 H1	0.1367	0.6728	0	0.1168	0.0548	0	0.0189	0	0
S3 H2	0.1106	0.6315	0	0.1800	0.0780	0	0	0	0
S4 H1	0	0.0010	0.7619	0.0011	0.2358	0.0002	0	0	0
S4 H2	0	0.1426	0.5325	0.1543	0.1391	0.0315	0	0	0
S5 H1	0.9207	0	0.0175	0	0.0127	0	0.0368	0.0122	0
S5 H2	0.6993	0.0676	0.1296	0	0.0398	0	0.0433	0.0155	0.0049

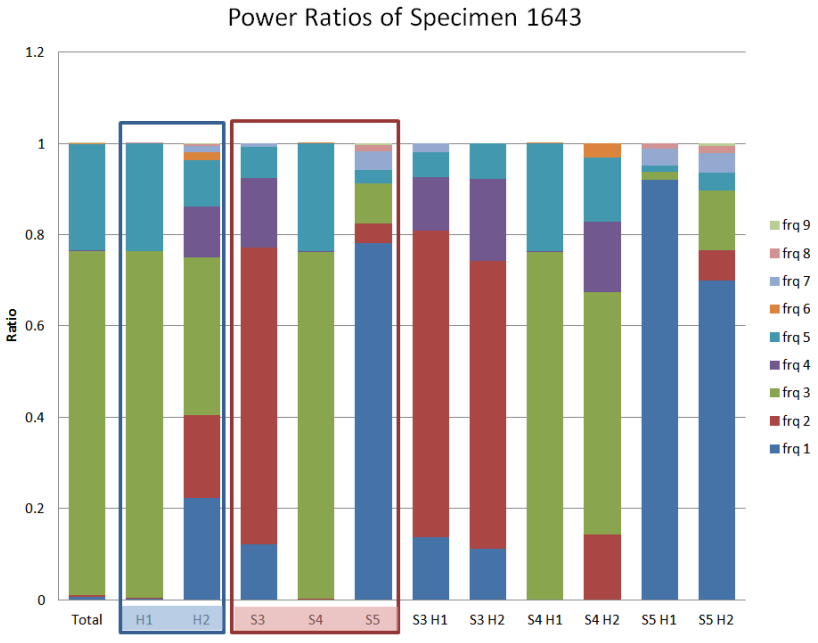

Figure 3.6: Frequency power ratios of specimen 1643

Table 3.6: Power ratios of specimen 1652. H represents the different height levels that the impactor was dropped from, and S represents the different sites onto which the impactor struck

	frq 1	frq 2	frq 3	frq 4	frq 5	frq 6	frq 7
Total	0.6214	0.1336	0.1123	0.0080	0.0803	0.0342	0.0102
H1	0.6099	0.1467	0.1072	0.0136	0.0790	0.0320	0.0117
H2	0.6301	0.1236	0.1161	0.0038	0.0813	0.0359	0.0091
S3	0.7520	0	0.1282	0	0.0644	0.0553	0
S4	0.4536	0.3757	0.1075	0.0133	0.0158	0.0341	0
S5	0.5692	0.1194	0.0908	0.0160	0.1679	0	0.0367
S3 H1	0.7709	0	0.1187	0	0.0575	0.0530	0
S3 H2	0.7371	0	0.1358	0	0.0699	0.0572	0
S4 H1	0.3798	0.4463	0.1167	0.0130	0.0148	0.0294	0
S4 H2	0.5047	0.3269	0.1012	0.0136	0.0164	0.0373	0
S5 H1	0.5509	0.1205	0.0798	0.0363	0.1713	0	0.0411
S5 H2	0.5836	0.1186	0.0994	0	0.1652	0	0.0332

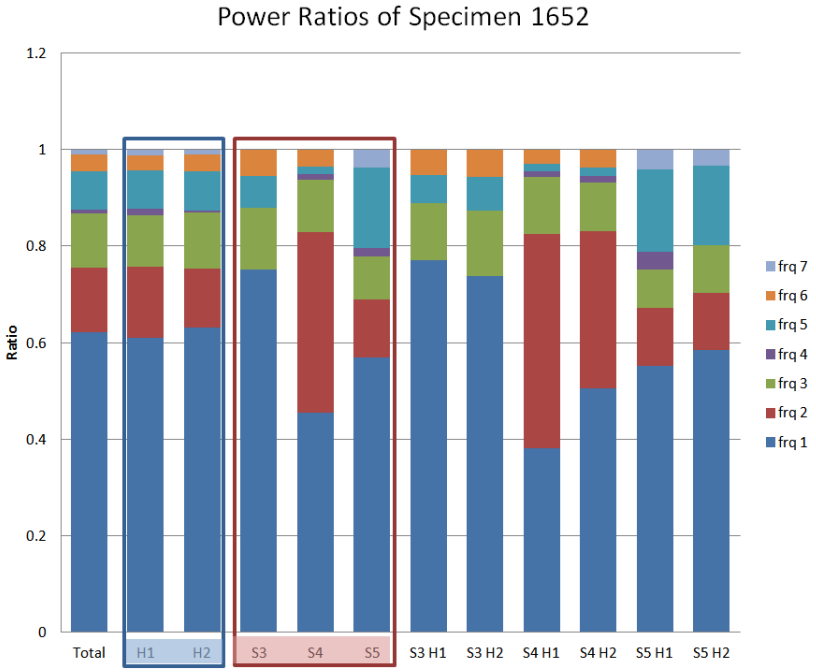

Figure 3.7: Frequency power ratios of specimen 1652

Table 3.7: Power ratios of specimen 1653. H represents the different height levels that the impactor was dropped from, and S represents the different sites onto which the impactor struck

	frq 1	frq 2	frq 3	frq 4	frq 5	frq 6
Total	0.4710	0.3776	0.0568	0.0338	0.0437	0.0171
H1	0.4795	0.3815	0.0621	0.0204	0.0471	0.0094
H2	0.4642	0.3745	0.0527	0.0444	0.0410	0.0231
S3	0.1742	0.8258	0	0	0	0
S4	0.4643	0.4127	0.0283	0.0164	0.0783	0
S5	0.6125	0.1298	0.1210	0.0727	0.0161	0.0480
S3 H1	0.1725	0.8275	0	0	0	0
S3 H2	0.1753	0.8247	0	0	0	0
S4 H1	0.4372	0.4345	0.0278	0.0195	0.0810	0
S4 H2	0.4862	0.3951	0.0287	0.0139	0.0761	0
S5 H1	0.6598	0.1310	0.1335	0.0297	0.0200	0.0259
S5 H2	0.5740	0.1288	0.1109	0.1076	0.0129	0.0659

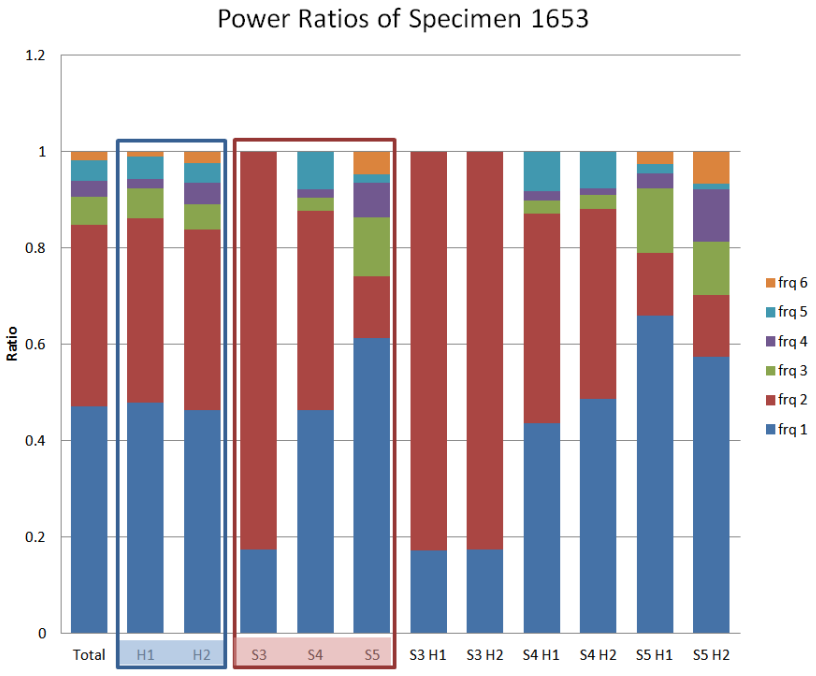

Figure 3.8: Frequency power ratios of specimen 1653

(frequency 1), 2.3% (frequency 2) and 2.4% (frequency 4) respectively. This is also evident among specific impact sites; the difference in power ratio between heights of individual sites range from a minimal deviation of 0.06% (specimen 1652, Site 4, frequency 4) to a maximum power ratio difference of 14.1% (Specimen 1622, Site 4, frequency 4). Specimen 1643 on the other hand had deviations of up to 41% between heights for frequency 3, however deviations between heights for the other frequencies were found to be more comparable between 0.14% (frequency 9) and 22.1% (frequency 1). The power ratio difference between heights of individual impact sites for this specimen is also more comparable with maximal deviations of 6.3% (Site 3, frequency4), 22.9% (Site 4, frequency 3) and 22.1% (Site 5, frequency 1). The frequency ratios between sites are overall less consistent that those between heights. This is most evident in Figures 3.4 through 3.8 as the frequency bands differ in length between sites (outlined in red) more than they do when comparing the bands between heights (outlined in blue).

3.3.4 Post-fracture Analysis

The cluster analysis of isolated site 3 pre fracture data for specimens 1643, 1652 and 1653 exposed seven, four and two resonant frequencies respectively. This was confirmed to be associated with the general pre-fracture data because the individual gauge analysis of specimens 1643, 1652 and 1653 suggests that only seven (frequencies 1,2,3,4,5,6,7), four (frequencies 1,3,5,6) and two (frequencies 1,2) resonant frequencies were exposed by site 3 impacts for each specimens 1643, 1652 and 1653 respectively.

With the isolated site 3 pre-fracture cluster analysis confirmed, it was compared with the cluster analysis done on the post fracture data. Figure 3.9 shows the two cluster groups of each specimen side by side, and it is evident that the resonant frequencies between pre and post fracture are not comparable. Table 3.8 exhibits this difference by providing the descriptive statistics for each cluster both pre and post fracture.

Examination of the individual gauge data from the post-fracture data revealed that gauges

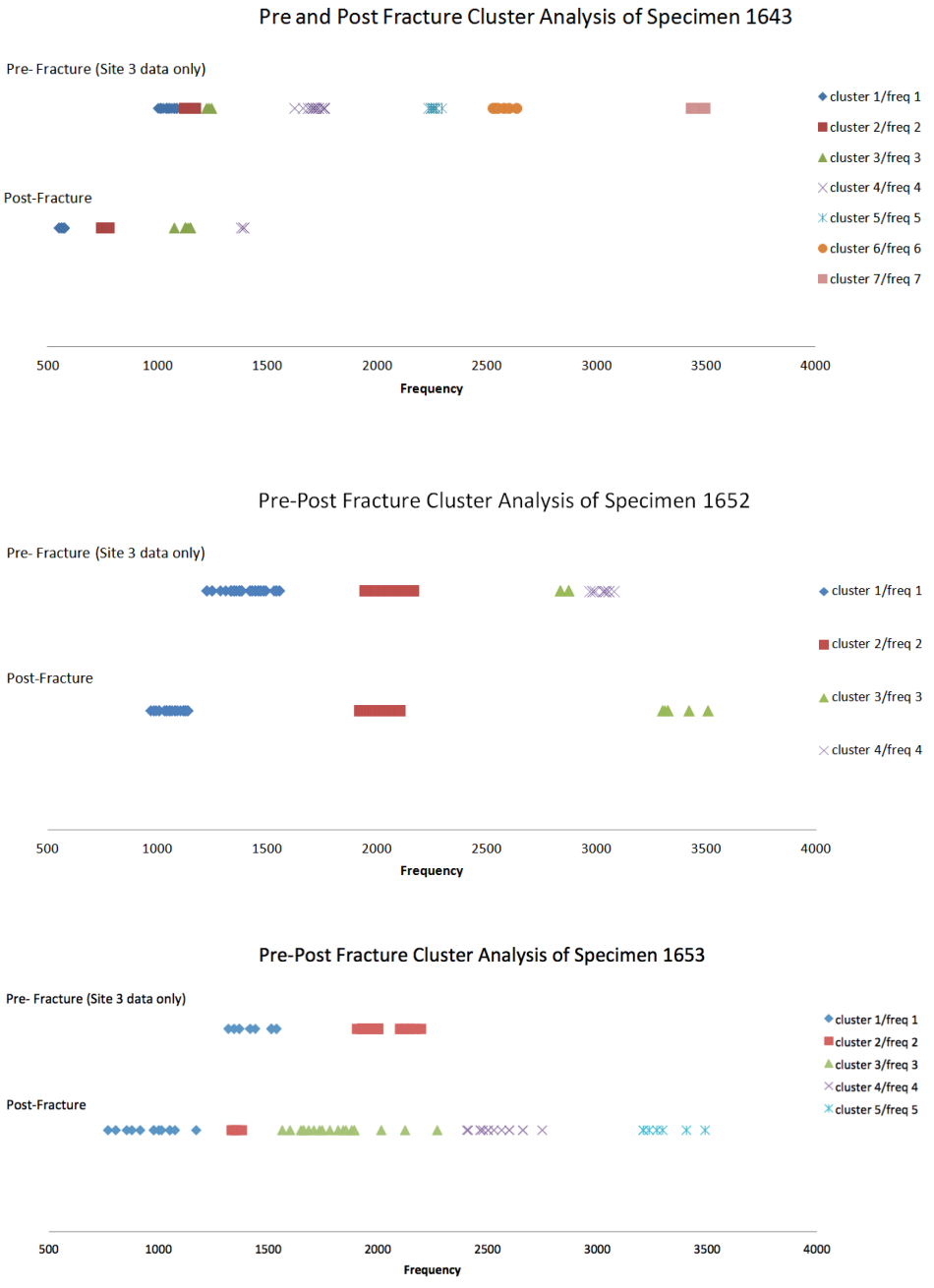

Figure 3.9: Pre and post cluster analysis results of specimens 1643, 1652 and 1653

Table 3.8: Pre and post fracture resonant frequency ranges obtained from the cluster analysis. The pre fracture columns describe only the frequencies exposed upon impacts to site 3, and these are compared to the general frequency ranges calculated in Table 3.2 (comparison column).

Specimen		Pre Fracture				Post Fracture		
	frequency	count	mean	stdev	comparison	count	mean	stdev
1643								
	1	25	1046	26.9	1024 (1)	21	553	35.01
	2	23	1139	12.95	1122 (2)	9	774	12.37
	3	3	1233	12	1245 (3)	12	1192	119.57
	4	18	1719	37	1658 (4)	3	1388	7.51
	5	12	2258	15.71				
	6	6	2572	41.42	2433 (5)			
	7	3	3454	32.32	3237(7)			
1652								
	1	48	1400	87.06	1374 (1)	24	1062	51.92
	2	18	2077	72.23	2067 (3)	18	1999	61.08
	3	6	2857	19.11	2736 (5)	6	3361	82.23
	4	12	3021	34.68	3038 (6)			
1653								
	1	12	1449	82.99	1451 (1)	13	964	115.08
	2	45	1986	73.55	1964 (2)	4	1352	20.49
	3					19	1809	180.69
	4					15	2537	99.35
	5					8	3355	178.69

Table 3.9: Post fracture power ratios of each specimen.

1643		463-573	744-781	1074-1147	1379-1392	
	Total	0.624	0.226	0.122	0.027	
1652		960-1135	1917-2100	3296-3503		
	Total	0.720	0.236	0.044		
	H1	0.715	0.239	0.047		
	H2	0.724	0.233	0.042		
1653		805-1172	1331-1379	1563-2271	2405-2747	3210-3723
	Total	0.400	0.077	0.332	0.147	0.044

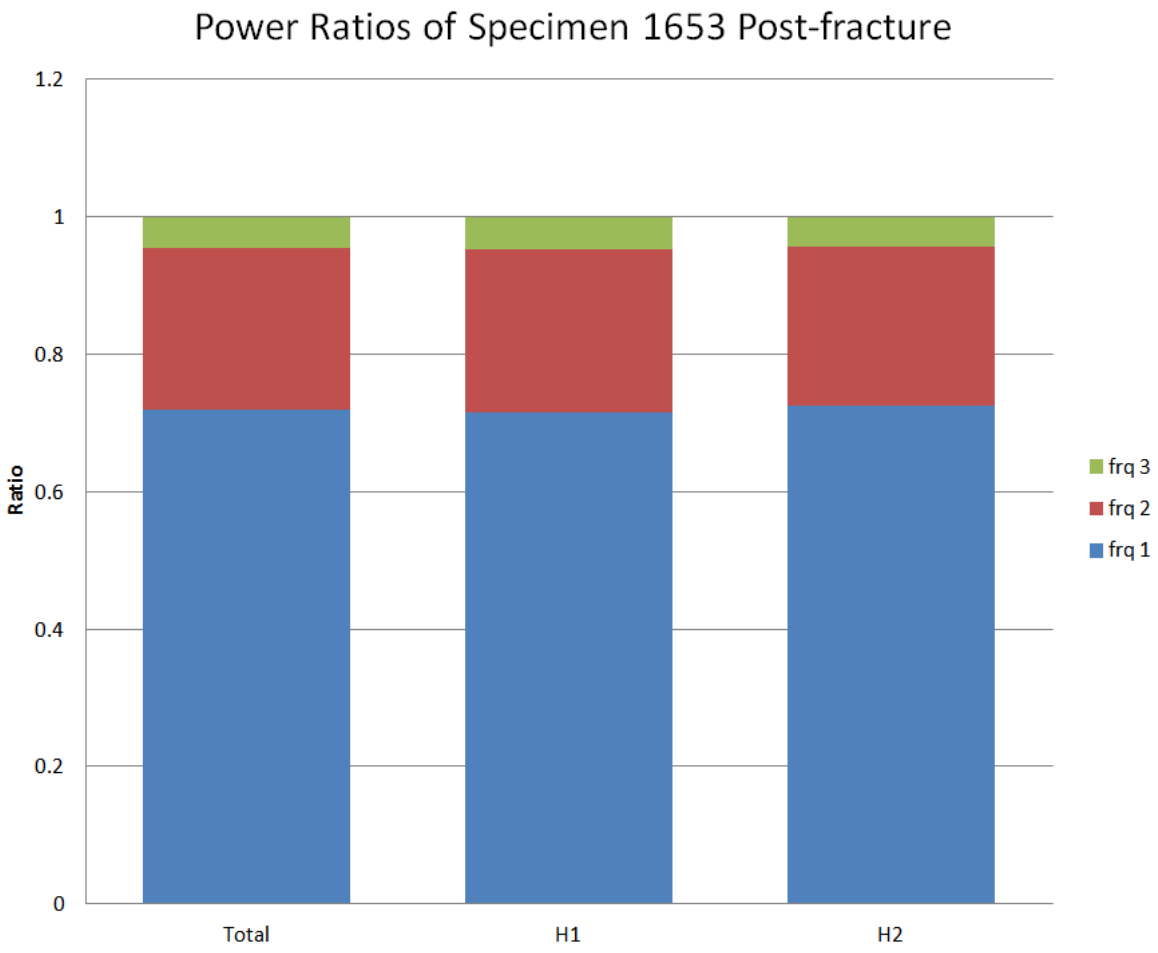

Figure 3.10: The power ratios of post-fractured specimen 1652.

would expose the same frequencies 100% of the time trial to trial for specimens 1643 and 1652 and 80% of the time for specimen 1653. Because only one site was tested post fracture there are no results on the consistency of the gauges on a site to site basis. Furthermore, only specimen 1652 was tested with varied heights and the gauges were found to expose the same frequencies 100% of the time, which comments on the post-fracture height to height repeatability of each individual gauge.

Finally, the power ratios of the post fracture data are tabulated in Table 3.9. For specimen 1652 the ratios are plotted in Figure 3.10 to facilitate comparison between the two heights tested post-fracture.

3.4 DISCUSSION

The results acquired in this study provide insight as to the vibrational response of the human skull. Specifically, it explores the resonant frequencies and associated powers that are excited upon impact, as well as the effect of impact location and impact energy on the expression of these frequencies.

3.4.1 Resonant Frequencies Excited

Discussing first the frequency values collected in this study, our results were found to be similar to the research of both Khalil et al. (1979) and Hakansson et al. (1994) despite differences in methodology and context. Khalil et al. studied two dry skull specimens and found eleven and six resonant frequencies between 20-5000Hz and Hakansson et al. studied six in vivo human subjects and found 14-19 resonant frequencies between 500 and 7500Hz with 8-11 of these resonant frequencies in the 500-4500Hz range (Hakansson et al., 1994). The results of this study corroborate these with 6-9 found resonant frequencies between 500-4500Hz, however they are notable lower, particularly in comparison to the resonant frequencies found by Hakansson et al. This may be attributed to the methodology employed by Hakansson et al.

Specifically, his study was done by incrementally increasing the vibration of a titanium hearing aid vibrator bone impact and noting the response of an accelerometer on the contralateral implant (Hakansson et al., 1994) which has the advantage of clearly distinguishing between resonant frequencies that may be too close together to be observed as separate peaks in the frequency spectrum, or as separate bins in the cluster analysis. Furthermore, the Hakansson et al. study researched live subjects and the increased mass of the soft tissue, bone moisture and heavy instrumentation (55g for the vibrator attachment on the driving implant and 5g for the accelerometer on the contralateral implant) may have damped some of the higher resonant frequencies to the lower values inside the range picked up in the current study.

This damping may also suggest why the first resonant frequency found in Hakansson et al. is lower than those found in both the Khalil and current study. The six subjects in the Hakansson et al. study were found to have their first resonant frequency between 828Hz and 1164Hz whereas the Khalil et al. study found the first resonant frequencies to be 1385Hz and 1641Hz. The current study had first resonant frequencies similar to Khalil et al. with values between 990Hz and 1452Hz.

Despite these minor discrepancies, all studies have concluded that each specimen has a unique number of resonant frequencies with variable values. The ANOVA results in the current study suggest drastically significant p-values of less than 5.83E-8 for the effect of specimen on the first eight resonant frequencies which is also supported in the discussions of both the Khalil et al. and the Hankansson et al. study.

Furthermore, the Hakansson et al. paper suggests that the spacing between the ascending resonant frequencies of each specimen differ. This is also confirmed by the current study and is illustrated in Figure 3.11 by the inconsistent spacing between the zigzagging dashed lines grouping the resonant frequencies found for each specimen.

This uniqueness of excited frequencies between specimens does not extend to the cranial impact location or to the impact energy of strikes on a single specimen. The two-way ANOVA performed in the current study resulted in very large p-values (noted in Table 3.1) which sug-

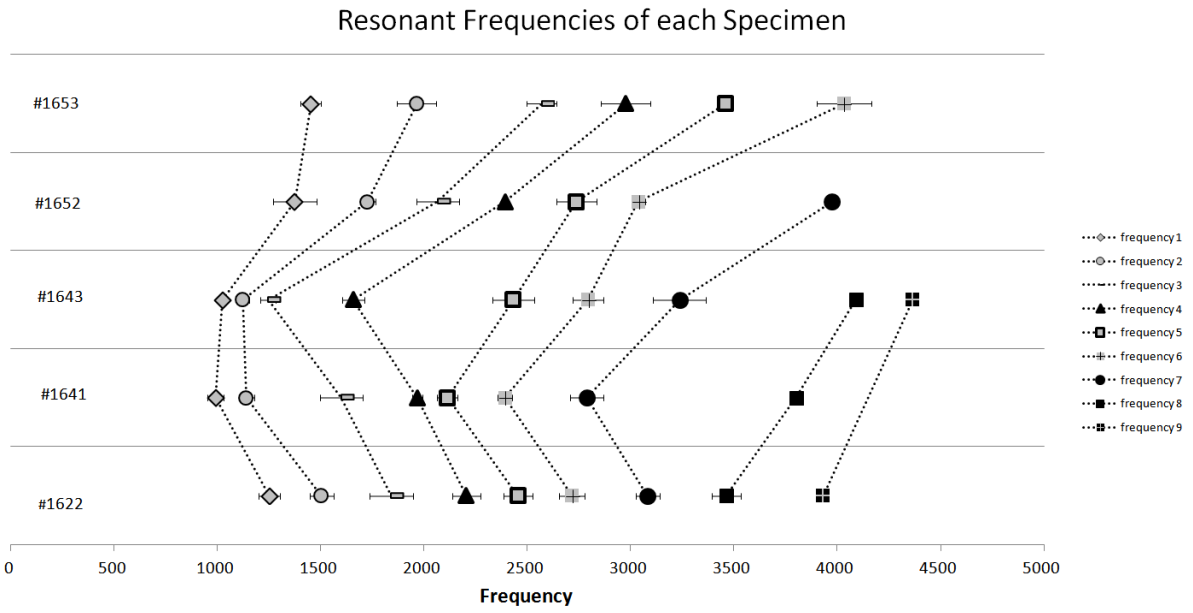

Figure 3.11: Comparison of the resonant frequencies observed between specimens. Note how not only do the values change drastically between specimens, but the spacing between each frequency band differs as well.

gests insignificant effects of site and drop height. Consistent excited resonant frequencies with four different impact locations was also concluded in the Khalil et al. study despite the fact that he did not perform statistical tests to confirm his observations (Khalil and Viano, 1979). From a structural perspective, this result is important as it suggests that geometry and dynamic characteristics of each individual specimen dictates the frequencies excited as opposed to the particular characteristics of each impact.

3.4.2 Binary Examination of Individual Gauges: Repeatability and Evaluation of the Cluster Analysis Technique

The initial objective in examining each individual gauge was to evaluate the effectiveness of the cluster analysis. A disadvantage of the cluster analysis technique was highlighted by the binary examination of individual gauges. Specifically, the cluster analysis is biased towards creating clusters with similar spacings, which was noticed with the gauge examinations of specimen 1622, 1641 and 1643, prompting the modification to include two additional clusters and split clusters initially assumed to be combined. However considering that only five of the 33 created clusters (across all specimens) exhibited this discrepancy, I generally conclude the cluster analysis to be an adequate technique, especially considering that the results of this study compared quite agreeably to conclusions of past literature.

Furthermore, although the decision to use an average between groups linkage criteria was carefully made, an alternate linkage criteria may further reduce the bias towards similarly spaced clusters. For example, by using average between group linkages, proximity matrices between groups as the average of the distances between all members of two groups were recreated. This method is preferable to methods such as nearest neighbour linkage and furthest neighbour linkage which are prone to more serious biases of chain linking and space dilution respectively (see Section 1.5.3) (Blashfield, 1976) however a weighted average linkage method, such as the centroid method may rectify this bias. Specifically, the centroid method may increase the distance between new members and an existing cluster enough to maintain space

conservancy of the average linkage method, but also distinguish between separate frequencies. The centroid method was not used in the current study because I wanted to retain the effect of disparate members of the cluster groups equally as a relatively large range between resonant frequencies was expected. Furthermore, I wanted avoid the opposite problem of creating two clusters out of data belonging in reality to a single resonant frequency (Lance and Williams, 1967). However, in light of the results and the discrepancies found, this method may ultimately improve our clustering technique in the context of defining resonant frequency ranges.

When assessing the consistency of each gauge to exhibit a particular frequency between trials, heights and sites, another minor shortcoming of the cluster analysis was exposed. Occasionally, the frequency value obtained by the same gauge between trial/height/site were similar enough to assume consistency, but were identified as an extreme maximum value of one cluster, and an extreme minimum value of a consecutive cluster. This does not affect the results much, as the general response of each specimen will not be more accurately captured by ensuring these frequencies are aligned in the same cluster; however it will affect the following results in the discussion on the repeatability and reproducibility of each gauge by decreasing the consistency of a gauge.

Considering trial to trial repeatability, this binary examination confirms the repeatability of our system in the frequency range for consistent impact conditions. Gauges exposed the same resonant frequencies trial to trial 94% (specimen 1643) to 99% (specimen 1622) of the time.

In Section 3.4.1 we established that the collection of frequencies excited for each specimen do not differ significantly between heights or sites. To build on this, observations of the recordings of individual gauges give us insight as to whether these excited frequencies are originating from the same cranio-facial locations. With 70.2%-83.3% height to height match of individual gauges for the majority of specimens (all except 1622) it is reasonable to expect reproducibility of frequencies excited on the individual gauge level between differing drop heights. This is an especially reasonable assessment considering most of the discrepancies in height to height matching occurred when the frequency values of each height occurred at the extreme high and

low ends of consecutive frequency ranges, as it was discussed above. Furthermore, several cases were also marked as a mismatch when an additional frequency was noted in the second drop height. This is also a reasonable discrepancy, as an increase in impact energy may increase the amplitude of mode shape exposing frequencies previously unnoticed as indistinguishable from the noise. When accounting for both of these discrepancies drop height to drop height match of individual gauges is between 87.5% and 100% (all specimens except 1622). Even the consistency of specimen 1622 increased from 36.1% height to height match to 73.1% when these factors were accounted for. The relatively low matching percentages for this specimen is most likely accounted for by experimental and procedural inconsistencies, as it was the first specimen tested.

However, this cannot be said for frequencies excited per gauge as a function of impact site. In essence, this means that although a similar collection of frequencies are being excited (as per the ANOVA analysis) they are being recorded by different gauges with different impact locations. For example, in specimen 1643 the 5th frequency was recorded by four gauges while testing both site 3 and site 5. Though, for impact site 3 the frequency was recorded in gauges at L8, R4, R5 and R9, whereas it was recorded in gauges at L4, L9, R5 and R6 for testing at impact site 5 (see Figure 3.12).

3.4.3 Power Ratio Analysis

The impact site to impact site inconsistency observed in the examination of individual gauges reflects the results in Section 3.3.3 of large deviations of the power ratios of each frequency between differing impact sites, and it is reasonable to speculate that the explanation for both observations are similar. Specifically, we can account for the discrepancies by considering vibration theory and modal analysis. Operating deflection shapes (ODSs) are the shapes created by the motion of two or more points on a structure, and they are often employed in the study of vibrational response, as they are easily and directly measured upon excitation (impact, sinusoidal force input, etc) (Schwarz and Richardson, 1999). In this context, they can be confused

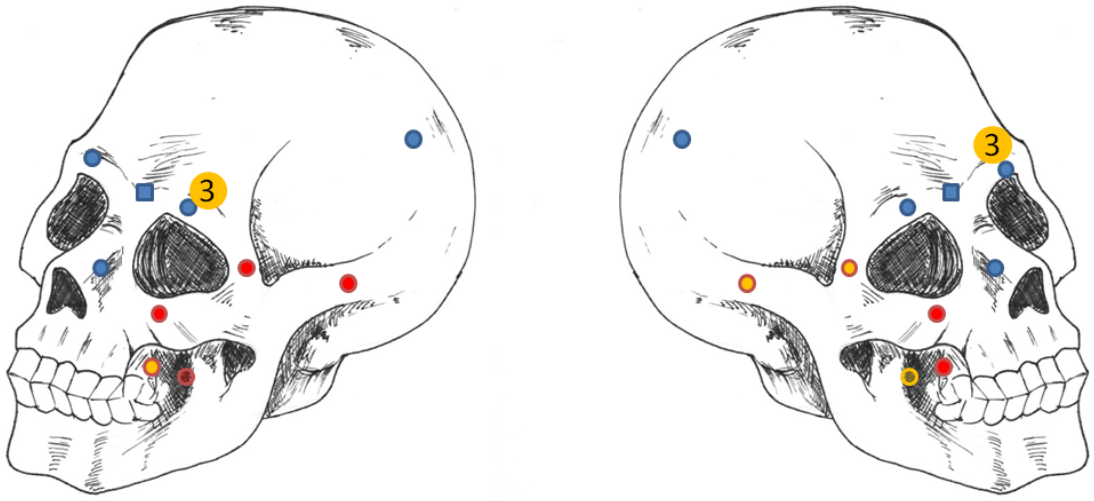

(a) Impacts at site 3

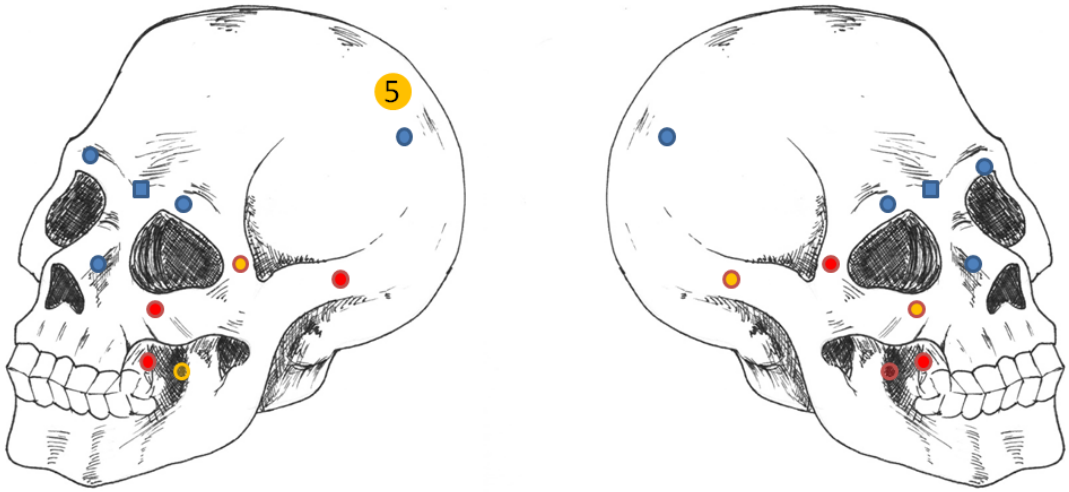

(b) Impacts at site 5

Figure 3.12: Gauges coloured yellow are the gauges exposing the 5th frequency of specimen 1643 upon impacts at sites 3 and 5. In this figure, the transparent marker on the maxilla represents the gauge applied to the pterygoid plate, which was shown here because it was a gauge that exposed this frequency.

with mode shapes because ODSs essentially measure the real-life deformation of a structure undergoing resonant vibration, and can be used with fourier transformations to estimate the former. However, it is important to note that mode shapes and ODSs are not identical; firstly because they account for the deformation due to forces or loads applied to the structure, and most significantly because they also reflect the sum of individual mode shapes of each resonant frequency excited (Richardson, 1997). By measuring the strain upon impact we are actually measuring the ODS of the craniofacial skeleton which unlike the mode shapes will change with changing conditions such as impact site. For example, if the impulsive excitation force strikes a nodal line of a particular mode shape, the mode shape will not contribute to the ODS of the skull, and that particular mode shape's frequency will not be recorded by the strain gauge (Richardson, 1997). In the context of power ratios, altering the proximity of an impact to a modal node line will alter the power to which that mode shape (and thus that frequency) is expressed in the ODS measured. In the frequency domain, this translates to a decrease in the peak size of that frequency, overall reducing its power ratio relative to all other frequencies excited.

This theory can also be applied to the discussion on the power ratio changes between heights. Although the general height to height power ratios are fairly consistent (Figure 3.4 through 3.8, blue outline), the following explanation might account for the discrepancies found in the height to height data specific to individual impact sites (Figure 3.4 through 3.8, bars not outlined). An increase in impact energy will increase the amplitudes of all vibrating mode shapes. Therefore, these discrepancies can arise when the impact energy is increased at an impact location near a node line of a mode, the frequency belonging to that mode shape may acquire enough increase in amplitude to distinguish it from the noise. Although an increase in energy will increase the amplitude of all frequencies, this gain is not proportional. Mode shapes excited by an impact near its pole will be amplified more than mode shapes excited by an impact near one of its node lines. This may also account for some of the discrepancies in the power ratios between heights. This is interesting to consider, however, as it was mentioned

above, the majority of the specimens did not show significant discrepancies in their general height to height power ratios suggesting that these effects are quite minimal.

In fact, only specimen 1643 showed any drastic discrepancies of power ratios between drop heights, and even larger power ratio deviations between impact sites relative to the other specimens (Figure 3.4 through 3.8). This may be attributed to shortcomings of the cluster analysis performed on this particular specimen. Initially, the cluster analysis identified 7 resonant frequency, but the gauge examination cross check revealed that one gauge spectrum identified three distinct resonant peaks all falling within the first cluster created by the cluster analysis. As per protocol, this cluster was separated into 3 separate clusters to account for the distinct peaks. Although, misreading of the spectrum may have altered the interpretation of the vibrational response of this particular specimen, Figure 3.13 compares the power ratios of specimens 1643 before and after modifications to the cluster analysis, and we can see that there are still discrepancies unaccounted for. These discrepancies occur mostly with additional frequencies revealed upon impacts with increased drop heights, suggesting that the primary reason for the inconsistencies of specimen 1653 is due to the theories discussed above.

3.4.4 Post-fracture Analysis

The most significant observation of the post fracture testing confirmed that the vibrational response of a single specimen is altered with fracture. This was to be expected in the same way a bell is expected to ring with a different sound after damage, however, the response would be expectantly inconsistent as we assumed that the fractures would be unstable, propogating unexpectedly with subsequent impacts.This was found to be unsupported considering the gauges exposed the same frequencies trial to trial 100% (specimens 1643, 1652) and 80% (specimen 1653) of the time, which is even more consistent than the prefractured data. However, this repeatability may be increased due to a decrease in trials performed as only one site and one height (for specimens 1643 and 1653) was tested. Also, less gauges were tested because the fracture caused damage to some of the gauges which further decreased the number of trials

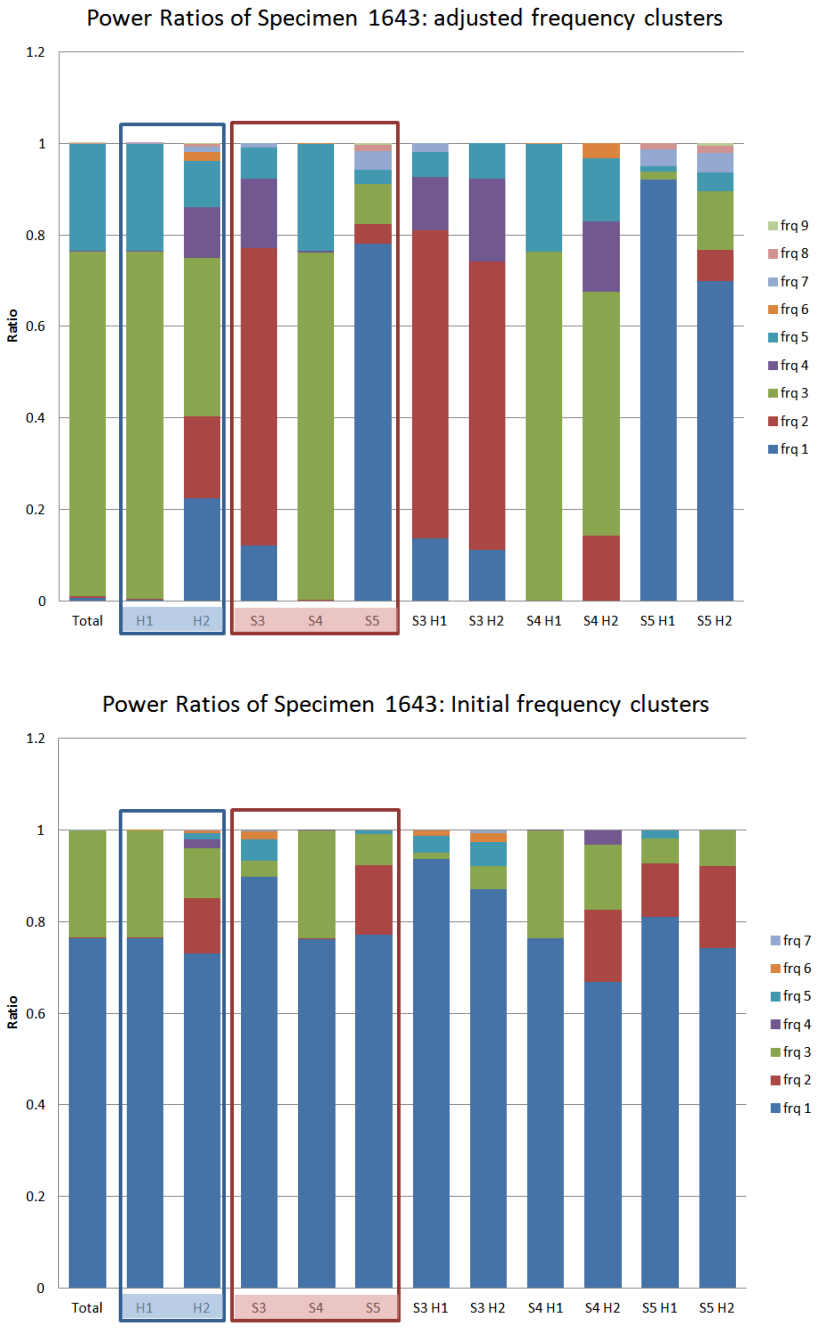

Figure 3.13: Comparison of the power ratios of adjusted and initial clusters for specimen 1643

with which we could evaluate gauge repeatability.

Because the frequencies between the pre and post fractured specimens were incomparable, it is inconsequential to discuss how the power ratios of the pre and post fractured specimens compare, and so the power ratios obtained for specimens 1643 and 1653 are noted for informations sake only. However specimen 1652 was tested at two heights and revealed that the power ratios remained very consistent between heights, with a maximum difference of 0.001.

Overall the post-fracture analysis didn't reveal much, mainly because limited testing was performed. In retrospect, this analysis would be significantly improved if the entire protocol was completed on the post-fractured specimen, so that comparisons between impact sites and drop heights could be made. At the very least, the analysis could have been drastically improved by testing at site 4 instead of site 3 as this impact location excited the most resonant frequencies during pre-fracture testing. Furthermore, considering we were erroneous in our assessment of the stability of the fracture, testing at two different drop heights could have been completed without significant changes to the frequency response during post-fracture testing.

3.5 CONCLUSION

The results presented in this study are extensive due to the wide range of vibrational characteristics investigated. Specifically, we have concluded the following:

- the resonant frequencies excited upon impact of a human skull is unique between specimens, but consistent for varying impact locations and impact energies.

- the power ratios of these frequencies per specimen are consistent for varying impact energies, but differ between impact locations.

- A single gauge will expose the same frequencies both trial to trial as well as with differing impact energies, however the exposed frequencies of a single gauge will differ with varying impact locations.

- Fracture alters the vibrational response of a specimen, but a fractured specimen appears to maintain consistency between varying impact energies.

To the author's knowledge, other studies that have researched the dynamic effects of the skull have looked only into the resonant frequencies excited. Fortunately, these studies seem to support the first conclusion drawn in this research, validating the experimental methods and post processing involved. Furthermore, internal validation confirmed the applicability of a cluster analysis to identify the resonant frequencies, suggesting that the this study can help grow a body of literature that can be used for further study of head injury and skull fracture mechanic research.

Specifically, this study builds upon the research presented in past literature by discussing the power ratios of each resonant frequency, as well as the effect of fracture on the frequency response. This is information important to fully define the biomechanical properties of the human skull and to provide insight as to how the CFS responds to impact as a whole. With added clinical investigation, these observations may contribute to the development of injury mechanisms that properly account for factors in blunt trauma such as impact location, impact energy, specimen geometry and occurrence of fracture.

The biomechanics described by the vibrational response can also contribute to the growing field of head impact research by providing a means with which to validate finite element models for use in computational experiments. These computational experiments in turn can assist with further investigations of the human cranium in a number of contexts including clinical examinations and head injury mechanisms, allowing for rapid and thorough investigations into the many research questions still unanswered in this field.

Bibliography

Roger K Blashfield. Mixture model tests of cluster analysis: Accuracy of four agglomerative hierarchical methods. *Psychological Bulletin*, 1976.

D Brands. Predicting brain mechanics during closed head impact: Numerical and constitutive aspects, 2002.

Bo Hakansson, Anders Brandt, and Peder Carlsson. Resonance frequencies of the human skull in vivo. *Journal of the Acoustical Society of America*, 1994.

Heather T Keenan, Susan J Brundage, Diane C Thompson, Ronald V Maier, and Freerick P Rivara. Does the face protect the brain? a case control study of traumatic brain injury and facial fractures. *Archives of Surgery*, 1999.

T Khalil and D Viano. Experimental analysis of the vibrational characteristics of the human skull. *Journal of Sound and Vibration*, 1979.

G N Lance and W T Williams. A general theory of classificatory sorting strategies: Hierarchical systems. *The Computer Journal*, 1967.

A J McLean and Robert WG Anderson. *Head Injury: Pathophysiology and Management of Severe Closed Injury*, chapter 2 Biomechanics of Closed Head Injury, pages 25–37. Chapman and Hall Medical, New York, NY, 1 edition, 1997.

K O'Riordain, P M Thomas, J P Phillips, and M D Gilchrist. Reconstruction of real world

head injury accidents resulting from falls using multibody dynamics. *Clinical Biomechanics*, 2003.

Mark H Richardson. Is it a mode shape or an operating deflection shape? *Sound and Vibration*, 1997.

Brian J Schwarz and Mark H Richardson. Introduction to operating deflection shapes. In *CSI Reliability Week*, 1999.

Chapter 4

Conclusion

4.1 SUMMARY

Research addressing head impact biomechanics can provide valuable information necessary for the development of head injury mechanisms and safety tolerance criterions. The main objectives of this study were to design and develop a head impact apparatus and experimental protocol capable of producing repeatable short-duration impacts as well as to determine the effect of different specimens, impact sites and impact energies on the frequency response of the skull upon impact. We were successful in meeting our objectives and also exposed several conclusions addressing the hypotheses discussed in Section 1.6.

Specifically, Chapter 2 found that the apparatus designed successfully produced impacts under 5ms in duration with impact forces of 117-2035N, exceeding the desired range of 0.5-1500kN. The apparatus design as well as the experimental protocol was found to be relatively repeatable with consistent impact conditions. To the author's knowledge, no head impact apparatuses have reported repeatability values, as a great majority of head impact testing is unconcerned with repeatable, subfracture testing. Therefore although our values are not comparable to anything concrete, Section 2.4.3 discusses the various factors contributing to the deviations between strikes and ways to rectify these if increased repeatability is required. For our pur-

poses, the repeatability was acceptable for the vibration study in the subsequent chapter, thus supporting our second hypothesis and meeting our first objective: to design and develop a head impact apparatus and experimental protocol capable of producing repeatable short duration impacts with a large range of energy inputs on variable impact sites of a human cadaver skull.

Chapter 3 was concerned with addressing hypotheses 3, 4 and 5, the speculated effects of specimen, height, site and fracture on the vibrational response of the skull. ANOVA tests on the frequency data collected supported hypothesis 3 in that there was little difference in the frequency data between impact sites or impact energies of a single specimen, however there was large differences in the frequency values between specimens. However, the power ratio analysis revealed that a change of impact site can change the relative contribution of each frequency component in the overall vibrational response, causing us to reject this specific stipulation of hypothesis 3. Once the frequency ranges were known from the cluster analysis, the individual gauge analysis confirmed a repeatable frequency response between impacts with consistent conditions (trial to trial repeatability). We were also able to observe that different gauges exposed different frequencies and that individual gauges exposed the same frequencies with different impact energies, but different frequencies with different impact sites. These results supported hypothesis 4, and the results discussing the effect of fracture on the vibrational response in Section 3.4.4 confirmed hypothesis 5. We were even able to briefly comment that although fracture altered the vibrational response of the specimen, changes in impact energy of a fractured specimen maintained a consistent vibrational response.

Overall, we reached our objectives and observed ample data to discuss the hypotheses presented in this document.

4.2 STRENGTHS AND LIMITATIONS

There have been several apparatuses designed for head impact research, with various strengths and limitations associated with each design (see Section 1.3). The apparatus designed for

the current study compares most directly with drop tower designs, with general strengths of simplicity and consistent input energy (such as that arising from the source of gravity). This specific design has the added benefit of being spacially conservative and mobile, so testing can be performed in several different laboratory settings. Also, considering most apparatuses described in past literature were designed to produce fracture inducing impacts, this impactor is one of the few apparatuses focussed on delivering repeatable subfracture impacts. The modular drop mass design also allows the impact duration and impact force to be modified as needed for a variety of testing objectives. Like other drop tower designs, our apparatus had limitations in determining the localized impact deflection, as no instrumentation was employed to measure this directly. Furthermore, although the repeatability of our design was acceptable for our use, there are definitely factors that can be addressed to improve this. Specifically, improving on the electrical connections will reduce the number of faulty strikes, and a stiffer neck support may reduce slippage between grommits and maintain an identical specimen orientation strike to strike.

To the authors knowledge, the experimental protocol employed for the vibrational response study of this project is unique. It is the only study known to use strain gauge instrumentation in biomechanical vibration studies of the skull, which has allowed us to sample the response at several locations of the skull simultaneously while avoiding high accelerometer costs. Furthermore, although significant post-processing was required to reduce the data, the frequency spectra plotted allowed us to comment on the power ratio of individual resonant frequencies, an aspect of the vibrational response that has not been discussed in past skull impact studies. Of course, the findings presented in this research are limited to their description of dried, denuded specimens. Also, because of system noise and transient effects, a lot of the low frequency response was drowned out in the frequency spectra by the initial attenuation peak suggesting our results are somewhat limited to frequencies above 600-700Hz. It is because of these effects that we were unable to comment on any findings comparable to those reported in Willinger et al. 1995 where he describes a significant ”decoupling” resonant frequency at 150Hz (Willinger

et al., 1995). Refined filtering of the data signal could reduce the attenuation signal of the frequency spectrum, allowing for a description of a larger frequency bandwidth.

4.3 FUTURE WORK

Building off the work presented in this document are a few projects already started. Specifically, pilot testing has begun with helmets, in an attempt to obtain the vibrational response of a human skull protected by a helmet. The specimens used in this study were also embalmed specimens, with the majority of soft tissue intact and brain matter present. This project addresses another level of the current research; an attempt at classifying the vibrational response with a more realistic specimen, either a fresh-frozen or embalmed specimen with brain matter, or brain matter analogue. The study of specimens with soft tissue and brain analogues would likely change the vibrational response in a number of ways. These include reducing the resonant frequencies with the increased mass of tissue, decreasing the bandwidth of found resonants due to an increase in impact duration when striking soft tissue, as well as increased damping of the vibrational signals due to the absorption of energy into the soft tissue. These are merely hypotheses based on the current state of knowledge in head impact biomechanics, and an established study focussing on these questions will be a welcome addition to the overall body of literature.

There is also considerable work being done to study the human skull computationally. The results of this project will be used to validate various finite element models which can be used to study various impact responses, and biomechanical details without the need for extensive laboratory resources or human specimens.

Bibliography

R Willinger, L Taleb, and C Kopp. Modal and temporal analysis of head mathematical models. *Journal of Neurotrauma*, 1995.

Appendices

Appendix A

Detailed Subfracture Protocol

OVERVIEW: This appendix provides detailed testing protocol information for each specimen

All specimen had their respective gauges tested at specific sites (S) 1-5. These gauges are referenced by a label corresponding to the gauge number (described in Figures 2.4a and 2.4b as well as the side it is placed. For example, a gauge on the left zygomatic arch is labelled 5L. As a note gauge 3M is placed on the medial axis and is not associated with a left (L) or right (R) side. These gauges were grouped in configurations (C) that varied from site to site. A few of the specimens were tested for reproducibility where the initial configuration of each site was retested after all configurations were tested. The testing of each configuration was done at two heights (H) to a minimum of three trials (T) per height.

A.1 Specimen 1622

Specimen 1622 was gauged according to Figure 2.4a and impacted at the same 5 sites described in Section 2.2.3.

All sites except site 2 were tested with following configurations:

C1 1R

C2 1L

C3 2R

C4 2L

C5 3M

C6 4R, 5R, 6R

C7 7R
C8 7L
C9 8R
C10 8L
C11 4L, 5L, 6L
C12 9R, 9L

For site 5, configurations C1-C3, C6, and C9-C12 were tested at two heights of 303mm and 154mm. The other configurations (C4-C5, C7-C8) were tested at three heights of 303mm, 154mm and 90mm, however only the heights consistent with the rest of the configurations were used for analysis. Three trial strikes were taken of all configure-height combinations.

All configurations for site 4 were tested with three trials at two heights of 154mm and 90mm.

Site 3 configurations were tested with three trials at two heights of 157mm and 94mm.

Configurations of site 1 were tested at the same heights as site 3.

During testing of site 2, we caused fracture at the impact site, so we attempted to complete the protocol on the contralateral side. Thus testing at a site on the right inferior orbit consisted of the following configurations:

C1 1R
C2 1L
C3 2R
C4 2L
C5 3M
C6 4R, 5R, 6R
C7 7R
C8 7L
C9 8R
C10 4L, 5L
C11 9R

The gauges not included in any of these configurations were damaged by the fracture. These configurations were only tested at a low height of 94mm, to decrease the risk of further damaging a compromised skull by testing at a higher height.

A.2 Specimen 1625

Specimen 1625 was gauged according to Figure 2.4b and impacted contralaterally (on the right side) to the site locations of specimen 1622.

The first site tested was site 4. Due to technical difficulties, testing of this site included retests of a few gauges, as it is noted in the following configurations. If a gauge was retested, analysis was done on the retests of the gauge and the earlier configurations that contained the initial tests were used only if other gauges in the configuration were not retested.

C1 R1, L2
C2 L1, R2
C3 M3, R8
C4 R6, L8
C5 R4, R5, L6, R9
C6 L4, L5, R7, L9
C7 L7
C8 M3, R6
C9 M3
C10 R6
C11 R4, R5, L7, R9

Each configuration was tested at heights of 120mm and 181mm except C4 which was only tested at 181mm.

The configurations were as follows for sites 3 and 5:

Site 3:

C1 R1, L2
C2 L1, R2
C3 L7, R8
C4 R7, L8
C5 R4, R5, L6, R9
C6 L4, L5, R6, L9

Site 5:

C1 R1
C2 L2, R4, R5, R9
C3 L1, R2
C4 L6, R8
C5 L4, L5, R6, L9
C6 R7, L8
C7 L7

Note that M3 was not tested at these sites, as it was damaged during the site change. The heights tested for sites 3 and 5 respectively were 127mm, 173mm and 118mm and 214mm.

Site 2 was not tested because specimen 1622 was too small to properly place the gauges as well as leave enough open space for the two impact sites of 1 and 2. Thus only facial site tested was site 1. Unfortunately, after testing only two configurations the bone at site 1 was found to crumble with a pitted fracture so testing was stopped at that site and resumed on a comparable

site 1 on the contralateral (left) side. The heights tested on the right side prefracture were 75mm and 123mm and the two configurations captured were C1: R1, L2 and C2: R2. Site 1 left configurations were as follows:

C1 R1, L2
C2 L1, R2
C3 L6, R8
C4 M3, L7
C5 R4, R5, L8, R9
C6 L4, L5, R7, L9

Gauge M3 was replaced and R6 was damaged for this site. Configurations C1 and C2 were tested with 3 trials at a height of 55mm and with 1 trial at a height of 81mm. The rest of the configurations (C3 through C6) were only tested with 3 trials at a height of 100mm.

A.3 Specimen 1641

Specimen 1641 was gauged at the sites described in Figure 2.4b however gauge R7 was damaged before testing began and is thus not included in any of the gauge configurations. The specimen was tested at all five sites described in Section 2.2.3.

Sites 4 and 5 were tested at heights of 125mm and 172mm and site 3 was tested as close as possible to identical conditions with heights of 126mm and 173mm with the following configurations. Site 4:

C1 R1, L2
C2 L1, R2
C3 M3, R7
C4 R6
C5 R4, R5, R9, L4, L5, L9
C6 L6, R8
C7 L8

Site 5:

C1 L1, R4, R5, R9
C2 L4, L5, L9, R6
C3 L6, R8
C4 M3, L8
C5 R2, L7
C6 R1, L2

Site 3:

C1 L6 L7 **C3** R4, R5, R9, L8 **C5** R1, L2

C2 L4, L5, L9, R6 **C4** M3, R8 **C6** L1, R2

Sites 1 and 2 were tested at heights of 46mm, 71mm and 43mm, 67mm respectively with configurations that omit the damaged gauges L6, R7 and L7.

Site 2:

C1 R4, R5, R9, L8 **C3** M3, R8 **C5** L1, R2

C2 L4, L5, L9, R6 **C4** R1, L2

Site 1:

C1 L4, L5, L9, R8 **C3** M3, R4, R9 **C5** L1, R2

C2 R6, L8 **C4** R1, L2

Note that R5 was also damaged upon testing site 1.

A.4 Specimen 1643

Specimen 1643 was gauged at the sites described in Figure 2.4b, and tested at all 5 sites described in Section 2.2.3. Sites 4 and 5 were tested at identical heights of 125mm and 172mm and site 3 was tested at 132mm and 179mm because we had difficulties attaining identical impact heights. The configurations tested for these sites were as follows: Site 5:

C1 L2, M3 **C4** R7, L7 **C7** R2

C2 R1, L1 **C5** R6, L6

C3 L4, L5, L9, L8 **C6** R8, R4, R5, R9

Site 4:

C1 L1, L2
C2 L8, L4, L5, L9
C3 L6, L7
C4 M3, R7
C5 R4, R5, R9, R8
C6 R6, R2
C7 R1

Site 3:

C1 L2, L7
C2 L1, R1
C3 M3, L6
C4 L4, L5, L9, L8
C5 R2, R7
C6 R4, R5, R9, R8
C7 R6

Sites 1 and 2 were tested at two heights of 39mm and 61mm with the following configurations.

Site 1:

C1 L4, L5, L8, L9
C2 L1, L2
C3 R4, R5, R9, R8
C4 R1, R2
C5 R6, R7
C6 L6, L7
C7 M3

Site 2:

C1 L4, L5, L6, L9
C2 L2, L8
C3 L7, M3
C4 R2, R7
C5 R4, R5, R8, R9
C6 R1, L1
C7 R6

Specimen 1643 was actually tested at sites 4 and 5 twice, however the configurations and heights were identical to those described for the first round of testing, so the configurations will not be repeated here.

A.5 Specimens 1652 and 1653

Protocol was established upon testing specimen 1652 and 1653 and they were tested with the same configurations and heights. Both specimen were gauged at the sites described in Figure 2.4b, and we tested at all 5 sites as described in Section 2.2.3. Sites 3, 4 and 5 were tested at identical heights of 125mm and 172mm, and sites 1 and 2 were tested at sites 38mm and 61mm. The configurations tested for these sites were as follows:

Site 5:

C1 L2, L1
C2 L4, L5, L9, L8
C3 L6, L7
C4 R6, R7
C5 R8, R4, R5, R9
C6 R1, R2
C7 M3

Site 4:

C1 L2, M3
C2 R6, R7
C3 L6, L7
C4 L4, L5, L9, L8
C5 R4, R5, R9, R8
C6 R1, L1
C7 R2

Site 3:

C1 L2, L7
C2 L1, L6
C3 L4, L5, L9, L8
C4 M3, R1
C5 R4, R5, R9, R8
C6 R6, R7
C7 R2

Site 2:

C1 L4, L5, L6, L9
C2 L7, L8
C3 L1, L2
C4 R1, R2
C5 R4, R5, R8, R9
C6 R6, R7
C7 M3

Site 1:

C1 L4, L5, L8, L9

C2 L1, L2

C3 R4, R5, R9, R8

C4 R1, R2

C5 R6, R7

C6 L6, L7

C7 M3

The only difference between the two specimens was that Site 2 was repeated for specimen 1652, however the same gauge configurations were tested so they will not be reiterated.

Appendix B

Gauging Protocol

OVERVIEW: This appendix describes the protocol for gauging on bone, the wiring of gauge bridges as well as the calculations associated with strain measurements

B.1 Strain Gauge Placement on Bone

1. Clean and smooth area on bone

   (a) Remove all soft tissue present on the bone site usinga scalpel.

   (b) Use 220 sand paper to get rid of all residual soft tissue at the bone site.

   (c) Clean site with 99% alcohol using a q-tip. Make sure q-tip is rolled as you clean to ensure you don't use the same side twice.

   (d) Use a 320 sand paper to scuff the skull throroughly.

   (e) Clean site with 99% alcohol using a q-tip. Make sure q-tip is rolled as you clean to ensure you don't use the same side twice.

   (f) Use 400 sand paper to scuff skull thoroughly.

   (g) Clean site with 99% alcohol using a q-tip. Make sure q-tip is rolled as you clean to ensure you don't use the same side twice.

(h) Use 600 sand paper to scuff the skull throughly.

(i) Use the neutralizer solution to clean the site with a q-tip. Make sure the q-tip is rolled as you clean to ensure you don't use the same side twice.

(j) Use a piece of tape to dab the bone site, removing any residual dust.

2. Put glue on bone site to create a smooth surface for gauge application

(a) Use the neutralizer solution to clean the site with a q-tip. Make sure the q-tip is rolled as you clean to ensure you don't use the same side twice.

(b) Take a piece of scotch tape and hold one end of it on the bone site with your index finger.

(c) Take out the caralyst and wipe the brush on the bottle edge so that it is no longer dripping. Spread remaining catalyst on the sticky surface of the tape.

(d) Put glue (1-2 drops depending on gauge size) on the bone site, using your thumb to slide over tape, smearing glue underneath and eliminating air bubbles.

(e) Keep pressure on teh tape for 1-2 minutes to let the glue dry.

(f) Remove the tape, pulling at an angle of 180 degrees to avoid removing any glue from the bone surface.

(g) Use 600 sand paper to scuff the area.

(h) Use the neutralizer solution to clean the site with a q-tip. Make sure the q-tip is rolled as you clean to ensure you don't use the same side twice.

(i) Use a piece of tape to dab the bone site, removing any residual dust.

3. Apply gauge to the bone surface

(a) Take out the gauge (avoid touching the silver plates). Put the gauge down on a flat surface with the shiney, bulbous connectors on teh gauge surface pointing upwards. This is the top of the gauge.

(b) Align the guage lead ires with terminal pads on the flat surface. Use the scotch tape to pick up the gauge and the terminal pads together.

(c) Remove the gauge from the flat surface by removing the tape at an angle of no more than 90 degrees to ensure that the gauge and terminal pads remained stuck to the tape.

(d) Stick an edge of the tape to the bone site with your index finger. Add the catalyst in the same manner as step 2 to the tape, gauge, terminals strips and lead wires.

(e) Add glue (1-2 drops) to the bone site. Push the tape with your thumb smearing glue underneath the entire tape surface and eliminating any air bubbles. Hold for 2 minutes to ensure glue drying.

(f) Roll the tape back off the terminal pads at 180 degrees to expose the terminal pads and lead wires. Leave the gauge covered by the tape to protect it during soldering.

(g) Solder lead wires to terminal strips and connect any extra length lead wires at this solder point as well.

(h) Test connection to ensure no short-circuiting occurred during soldering

(i) Put an isolating agent (such as polyeurethane or silicone mixture) on teh terminal strips, solder joints and exposed wires to insulate connections and added adhesion.

(j) Remove tape from gauge surface by removing tape at a 180 degree angle to ensure gauge remains securely anchored.

B.2 Strain Gauge Bridge Circuits

Specimens 1625 through 1653 were tested with the bridge circuit illustrated in figure B.1a. Specimen 1622 was wired differently because we accidentally wired the extra 120 ohm resistor in the wrong location. This bridge is significantly more unbalanced and is illustrated in figure B.1b.

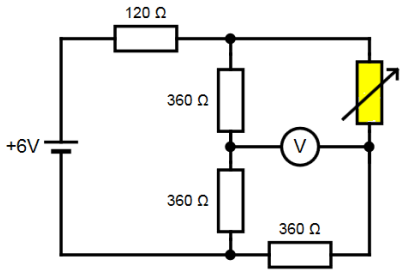

(a) Strain gauge bridge circuit for specimens 1625 through 1653. Gauge is yellow variable resistor

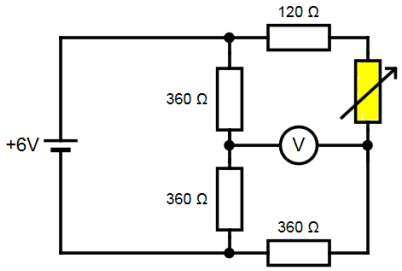

(b) Strain gauge bridge circuit for specimen1622. Gauge is yellow variable resistor

B.3 Strain Calculations

The bridges described in the previous section are all inherently unbalanced (particularly that of specimen 1622). However, this should not affect the results because we are interested only in the relative strain changes during the response of the specimen to impact. Thus, the following calculations are specific for use in unbalanced bridges.

$$V_r = V_{unstrained}/V_{in} \tag{B.1}$$

$$\epsilon = \frac{-4 * V_r}{GF(1 + 2 * V_r)} \tag{B.2}$$

where

$V_{unstrained}$ is the unstrained output voltage

V_{in} is the gauge excitation voltage. For specimen 1622 this value is 6V, for the remaining

specimens, this value was taken to be 6V minus the 1.5V voltage drop due to the 120 ohm resistor, to a value of 4.5V.

GF is the gauge factor of the strain gauge

Appendix C

Matlab Codes

OVERVIEW: This appendix outlines the Matlab codes used in post processing of the data.

C.1 Preliminary Code

C.1.1 reader.m

```
% This script creates a structure using data files it reads in the same
% directory. The structure is initialized using a configuration file
% created by the user. The data structure is formatted as follows:

% s.site = impact_site
% s.heights = heights impactor was dropped from in mm

% s.gauges.[Gauge] = Accesses a particular strain gauge (e.g.
% Site4.gauges.R1, Site4.gauges.M3, etc.)

% s.gauges.[Gauge].Type = 'R' = rosette, 'U' = uniaxial

% s.gauges.[Gauge].Key = Lists the column number in the data file
```

```
14 % corresponding to strain data from a uniaxial gauge, or from arms ...
       A, B,
15 % and C, respectively, of a rosette gauge.
16
17 % s.gauges.[Gauge].h(m) = structure containing strain data from ...
       [Gauge] at
18 % a particular drop height m, where m is an ordinal number ...
       corresponding to
19 % the drop heights used ordered from lowest to highest. For example, if
20 % drops were made at 100 mm and 200 mm, h(1) corresponds to drops ...
       from 100
21 % mm and h(2) to drops from 200 mm.
22
23 % s.gauges.[Gauge].h(m).height = number value for height of drop in mm
24
25 % s.gauges.h(m).strike(k).filename = filename holding the data for
26 % that particular gauge, height, and strike number (k).
27
28 % s.gauges.h(m).strike(k).inds = The start and end indices that identify
29 % the start and end of impact for strike k. The window is defined as the
30 % data points between the initial impact and the first subsequent ...
       impact of
31 % the impactor, using peaks in the impactor accelerometer data to ...
       identify
32 % these events.
33 %% Initialize paths
34 clear
35 clc
36
37 config_file_path = 'C:\Users\skull\Documents\Thesis\Hugh\Hugh ...
       (1653)Testing\Hugh_Site3.csv';
```

```
38 data_directory_path = 'C:\Users\skull\Documents\Thesis\Hugh\Hugh ...
       (1653)Testing\Site 3 - 16 May 2013\';
39 suffix = '';
40
41 pause on
42
43 jump_amount = 400; %This is used to move past the initial ...
       accelerometer peak, leaving only data after initial impact
44 time_shift_amount = 150; %This is used to ensure the start of the ...
       initial impact is included in the data window
45
46 %% Extract information from data file for impact site
47 file = fopen(config_file_path,'r'); %Open configuration file
48
49 textscan(file,'%*[^\r\n]',1,'delimiter',','); %Skip header
50 impact_site = textscan(file,'%d',1); %Read impact site number
51
52 textscan(file,'%*[^\r\n]',1); %Skip header
53 heights = textscan(file,'%f','delimiter',','); %Read height values
54
55 textscan(file,'%*[^\r]',1); %Skip header
56 GaugeInfo = textscan(file,'%s %s %d %d %d','CollectOutput',1,...
57     'delimiter',','); %Collect gauge type, label and channel info
58
59 fclose(file);
60
61 %% Turn cell arrays into regular arrays
62 impact_site = impact_site{1};
63 heights = heights{1};
64 GaugeName = GaugeInfo{1}(:,1);
65 GaugeType = GaugeInfo{1}(:,2);
66 GaugeKey = GaugeInfo{2};
```

```
67 %% Enter site info
68 s.site = impact_site;
69 s.heights = heights;
70
71
72 %% Loop to initialize structure
73 for i = (1:numel(GaugeName)) % Loop though all gauge names
74     gaugelabel = GaugeName{i}; % Get gauge name as string
75     s.gauges.(genvarname(gaugelabel)) = struct('Type', GaugeType(i),...
76         'Key', GaugeKey(i,1:find(GaugeKey(i,:),1,'last')));
77     for j = (1:numel(heights))
78         s.gauges.(genvarname(gaugelabel)).h(j) = struct('height', ...
               heights(j),...
79              'strike', ([]));
80     end
81 end
82
83 %% Collect filenames of all .txt files in a single
84 filenames = dir(strcat(data_directory_path, '*.txt'));
85 filenames = struct2cell(filenames);
86 filenames = filenames(1,:);
87
88 % Quick for loop to elminate any log .txt files, as they do not include
89 % data, only a log from the data acquisition session.
90 temp = {};
91 for i = (1:numel(filenames))
92     if isempty(findstr('log', filenames{i}))
93         temp = [temp filenames(i)];
94     end
95 end
96 filenames = temp;
97
```

```
98  %% Enter filename corresponding to each gauge/strike into structure
99  for i = (1:numel(filenames))
100 %for i = (1:3);
101     filename = filenames{i}; %Get filename
102     filename_and_path = strcat(data_directory_path, filename); %Add ...
            data path to filename
103     msg = sprintf('Processing %s (file %d of %d)', filename, i, ...
            max(size(filenames))); %Make message showing progress
104     disp(msg) %Display progress
105
106     tag = textscan(filename, '%s','delimiter','_'); %Separate parts ...
            of filename
107     tag = tag{1}; %This puts all the
108     tag(end) = []; %Eliminates last entry
109
110     site = tag{1}; %Identify impact site
111     height = sscanf(tag{2},'%d%*s'); %Identify drop height
112     height_index = find(heights==height); %Identify drop height index
113     data = dlmread(filename_and_path); %acquire data
114     data = data(:,1); %look at just accelerometer data
115     inds1 = find(data == min(data)); %initial impact is at global ...
            minimum
116     inds2 = find(data(inds1+jump_amount:end) == ...
            min(data(inds1+jump_amount:end))); %end of window corresponds ...
            with global minimum after initial impact, aka when first ...
            bounce occurs
117     inds = [inds1 (inds1+jump_amount+inds2)]; %set inds
118     inds = inds - time_shift_amount; %shift indices back in time a ...
            bit to ensure entirety of first impact is captured
119
120     gauges = tag(3:end); %Gauges are the remaining fields in the tag
```

```
121     for j = (1:numel(gauges)) %Loop through all the gauges and ...
            assign filename and inds
122         gauge = gauges{j};
123         strikenum = ...
                numel(s.gauges.(genvarname(gauge)).h(height_index).strike)+1;
124     %increment strikenum for each gauge involved in this filename
125         s.gauges.(genvarname(gauge)).h(height_index).strike(strikenum)...
126         .inds = inds; %assign to structure
127         s.gauges.(genvarname(gauge)).h(height_index).strike(strikenum)...
128         .filename = filename; %assign to structure
129     end
130
131     %plot the data as it is read to ensure that the impact window is ...
            being
132     %properly bracketed.
133     figure
134     plot(data(inds(1):inds(2)),'LineWidth', 3)
135     hold on
136     plot(data(inds(1):inds(2)+3*time_shift_amount),'r')
137     sprintf('press any key to continue...')
138     pause
139     sprintf('continuing...')
140 end
141
142 %% Save structure
143 Site = strcat('Site', num2str(impact_site), suffix);
144 eval([genvarname(Site) '= s;']);
145 eval(['save ' Site ' ' Site])
```

C.2 Accelerometer Validation Codes

C.2.1 Validation_Accel_Main.m

```
%% Accelerometer Validation File
% The purpose of this program is to assemble a file with the ...
    accelerometer
% repeatability measurements. it is a structure with the following
% elements:

% DATA- the windowed accelerometer data of each gauge/height ...
    combination with each column
% being a strike
% PEAK- the absolute maximum value of each gauge/height combination, ...
    each
% element of the vector represents a strike. In the height section, each
% row represents the gauge and each column represents a strike. The ...
    gauge
% order is based on the configuration file
% DT- contains the indices for the initial and final points of the ...
    impact
% and the impact time in the third column. Each row represents a strike.
% The height section is organized the same as the peak height ...
    section, with
% the impact times of each gauge being represented by the rows and each
% strike of that gauge by the columns
% AREA- is organized the same as peak
% RMS- has 3 substructures, data, avg and rms:
    % DATA has the data of each strike of a gauge height configuration
    % altered so that each strike is aligned at it's respective dti and
```

```
21      % ends at the avg dt of that gauge/height combo. This ensures ...
            that all
22      % strikes contain the same number of elements. The height ...
            section is
23      % the same, however, the data is altered so that every strike at a
24      % specific height has the length of the average dt for that height.
25      % AVG defines the average curve based on each strike (or every ...
            strike
26      % at that height if heights section, that is the average value for
27      % each strike per timepoint
28      % RMS calculates the RMS of each timepoint, that is
29      % sqrt(sum(strike_i(t)- avg(t)))
30
31  %STAT secion is most important: it contains the means, and standard
32  %deviations of each secion, peak, area, dt and rms. It is calculated
33  %according to gauge/height combination, as well as according to all ...
        strikes
34  %done on a particular height. The heights section in this case is ...
        organized
35  %with the corresponding values for each gauge/height combination ordered
36  %according the the configuration file, with the overall average on ...
        the last
37  %line. Note that gauges that were captured along with another have a ...
        zero
38  %because a separate strike was not done and it would skew the standard
39  %deviaton.
40  %% Clean up
41  clear
42  clf
43
44  %% Start clock, turn on pause
45  pause on
```

```
46 tic
47
48 %% Constants
49 Fs = 50000; % Sampling rate
50
51 %% Interrogator Mode Options
52 make_graphs = true;
53 display_graphs = true;
54 save_graphs = false;
55 graph_res = '300';
56 save_data_to_file = false;
57 save_data_to_workspace = false;
58 to_end_of_heights = false;
59 heights_start = 1;
60 heights_end = 2;
61 to_end_of_gauges = false;
62 gauges_start = 1;
63 gauges_end = 17;
64 to_end_of_strikes = true;
65 strikes_start = 1;
66 strikes_end = 3;
67 config_doubles = [3 4 8 9]; %accelerometer signal of some gauges are ...
       duplicated (if gauges were tested at the same time)
68 num_config = 17-config_doubles;
69
70 %% File Paths
71 data_path = 'C:\Users\skull\Documents\Thesis\Hugh\Hugh ...
       (1653)Testing\Site 1 - 24 May 2013\';
72 site_struc_name = 'Site1';
73 site_struc_path = 'C:\Users\skull\Documents\MATLAB\Hugh\';
74 figure_save_path = 'C:\Users\skull\Documents\Thesis\Hugh\Anne\';
75 data_save_path = 'C:\Users\skull\Documents\Thesis\Hugh\Anne\';
```

```
76
77 %% Other Options
78 inds_1_offset = -100;
79 inds_2_offset = 0;
80
81 %% Fetch data structure
82 s = load(strcat(site_struc_path, site_struc_name, '.mat')); %load ...
       the structure created by reader.m
83 s = s.(genvarname(site_struc_name));
84
85 if to_end_of_heights
86     heights_end = max(size(s.heights));
87 end
88
89 data_length = zeros(heights_end-heights_start+1, ...
       gauges_end-gauges_start+1, strikes_end-strikes_start+1);
90
91 for i = (heights_start:heights_end)
92 %% Begin initial loop through heights: for keeping windows of data ...
       the same
93 %% size
94     gauges = fieldnames(s.gauges);
95
96     if to_end_of_gauges
97         gauges_end = max(size(fieldnames(s.gauges)));
98     end
99
100
101
102     for j = (gauges_start:gauges_end)
103 %% Begin initial loop through gauges
104         gauge_name = gauges{j};
```

```
105
106         if to_end_of_strikes
107             strikes_end = max(size(s.gauges.(gauge_name).h(i).strike));
108         end
109             for k = (strikes_start:strikes_end)
110 %% Begin initial loop through strikes
111                 data_filename = strcat(data_path, ...
                        s.gauges.(gauge_name).h(i).strike(k).filename);
112                 inds = s.gauges.(gauge_name).h(i).strike(k).inds;
113                 inds(1) = inds(1) + inds_1_offset;
114                 inds(2) = inds(2) + inds_2_offset;
115                 data = dlmread(data_filename);
116                 data = data(1:end-1, :); %This step makes sure ...
                        columns are same size
117                 data = data(inds(1):inds(2),:); %Cut out window of data
118                 data_length(i,j,k) = length(data);
119                 data_length_check(i,j,k) = length(data);
120                 data_length(data_length == 0) = [];
121             end
122
123     end
124 end
125 for i = (heights_start:heights_end)
126 %% Begin looping through heights
127     gauges = fieldnames(s.gauges);
128
129     name2 = strcat('_Height_',num2str(i));
130     name2 = genvarname(name2);
131      for j = (gauges_start:gauges_end)
132 %% Begin looping through gauges
133         gauge_name = gauges{j};
134         Key = s.gauges.(gauge_name).Key;
```

```
135         name1 = strcat(gauge_name,'_Height_',num2str(i),'Accel');
136         name1 = genvarname(name1);
137
138         if to_end_of_strikes
139             strikes_end = max(size(s.gauges.(gauge_name).h(i).strike));
140         end
141             for k = (strikes_start:strikes_end)
142                 disp(sprintf(strcat(gauge_name, '_Strike_', ...
                        num2str(k), '_Height_', num2str(i))))
143                 data_filename = strcat(data_path, ...
                        s.gauges.(gauge_name).h(i).strike(k).filename);
144                 data = dlmread(data_filename);
145                 inds = s.gauges.(gauge_name).h(i).strike(k).inds;
146                 inds(1) = inds(1) + inds_1_offset;
147                 data = data(1:end-1, :); %This step makes sure ...
                        columns are same size
148                 data = ...
                        data(inds(1):inds(1)+min(min(min(data_length))),1); ...
                        %this step ensures all trials of a gauge are the ...
                        same size
149                 data = data.*(0.714*9.81*1000)./(0.09);
150                 offset = mean(data(1:25));
151                 data = data-offset;
152             %% obtain peaks
153             accelval.data.(name1)(:,k) = data;
154             mx = max(accelval.data.(name1)(:,k));
155             mn = min(accelval.data.(name1)(:,k));
156             if abs(mx)≥abs(mn)
157                 accelval.peaks.(name1)(:,k) = mx;
158                 peakloc = find(data == mx);
159                 if ismember(j,config_doubles) == 0
160                     accelval.peaks.(name2)(j,k) = mx;
```

```
161                 end
162             else
163                 accelval.peaks.(name1)(:,k) = mn;
164                 peakloc = find(data == mn);
165                 if ismember(j,config_doubles) == 0 % ensures that if ...
                        one strike hit multiple gauges that the gauge ...
                        multiples are not counted
166                     accelval.peaks.(name2)(j,k) = mn;
167                 end
168             end
169             %% Obtain area under curve
170             [dti dtf] = peakinit_int(data);
171             accelval.dt.(name1)(k,1) = dti;
172             accelval.dt.(name1)(k,2) = dtf;
173             accelval.dt.(name1)(k,3) = (dtf-dti)/50;  %obtains ...
                    impact time of strike
174
175             X = [dti:1:dtf]'./100000;
176
177             accelval.area.(name1)(k) = trapz(X,data(dti:dtf));
178             dt_temp1(j,k,i) = (dtf-dti)/50; %to kick out for use in ...
                    the gauge validation file
179             if ismember(j,config_doubles) == 0;
180                 accelval.dt.(name2)(j,k) = (dtf-dti)/50;
181                 accelval.area.(name2)(j,k) = trapz(X,data(dti:dtf));
182             end
183             end
184
185             if size(accelval.peaks.(name2),1) == 1
186                accelval.peaks.(name2)(2,:) = [0 0 0];
187             end
188
```

```
189             %obtaining the trial to trial statistics
190             accelval.stat.peak.(name1)(1) = ...
                   mean(accelval.peaks.(name1));
191             accelval.stat.peak.(name1)(2) = ...
                   std(accelval.peaks.(name1),0);
192             accelval.stat.peak.(name1)(3) = ...
                   std(accelval.peaks.(name1),0)*100/mean(accelval.peaks...
193             .(name1));
194
195             accelval.stat.area.(name1)(1) = mean(accelval.area.(name1));
196             accelval.stat.area.(name1)(2) = ...
                   std(accelval.area.(name1),0);
197             accelval.stat.area.(name1)(3) = ...
                   std(accelval.area.(name1),0)*100/mean(accelval.area...
198             .(name1));
199
200             accelval.stat.dt.(name1)(1) = ...
                   mean(accelval.dt.(name1)(:,3));
201             accelval.stat.dt.(name1)(2) = ...
                   std(accelval.dt.(name1)(:,3),0);
202             accelval.stat.dt.(name1)(3) = ...
                   std(accelval.dt.(name1)(:,3),0)*100/mean(accelval.dt...
203             .(name1)(:,3));
204
205             figure %figure plotted to check code's process
206             plot(accelval.data.(name1)(:,1))
207             title(strcat(gauge_name,'\_Height\_', int2str(i)));
208             hold on
209             plot(accelval.data.(name1)(:,2),'c')
210             plot(accelval.data.(name1)(:,3),'g')
211 %             plot(accelval.data.(name1)(:,4),'r') used depending on ...
    how many k values there are (3 or 6)
```

```
212 %             plot(accelval.data.(name1)(:,5),'m')
213 %             plot(accelval.data.(name1)(:,6),'y')
214             yL = get(gca, 'YLim');
215             line([accelval.dt.(name1)(1,1) ...
                    accelval.dt.(name1)(1,1)], yL, 'Color','r');
216             line([accelval.dt.(name1)(1,2) ...
                    accelval.dt.(name1)(1,2)], yL, 'Color','r');
217             line([accelval.dt.(name1)(2,1) ...
                    accelval.dt.(name1)(2,1)], yL, 'Color','m');
218             line([accelval.dt.(name1)(2,2) ...
                    accelval.dt.(name1)(2,2)], yL, 'Color','m');
219             line([accelval.dt.(name1)(3,1) ...
                    accelval.dt.(name1)(3,1)], yL, 'Color','y');
220             line([accelval.dt.(name1)(3,2) ...
                    accelval.dt.(name1)(3,2)], yL, 'Color','y');
221 %             line([accelval.dt.(name1)(4,1) ...
    accelval.dt.(name1)(4,1)], yL);
222 %             line([accelval.dt.(name1)(4,2) ...
    accelval.dt.(name1)(4,2)], yL);
223 %             line([accelval.dt.(name1)(5,1) ...
    accelval.dt.(name1)(5,1)], yL, 'Color','c');
224 %             line([accelval.dt.(name1)(5,2) ...
    accelval.dt.(name1)(5,2)], yL, 'Color','c');
225 %             line([accelval.dt.(name1)(6,1) ...
    accelval.dt.(name1)(6,1)], yL, 'Color','g');
226 %             line([accelval.dt.(name1)(6,2) ...
    accelval.dt.(name1)(6,2)], yL, 'Color','g');
227             hold off
228
229       end
230             %obtaining the "by height" statistics of each section
231             temp = mean(accelval.peaks.(name2),2);
```

```
232             n = length(temp);
233             temp2 = std(accelval.peaks.(name2),0,2);
234             temp3 = accelval.peaks.(name2);
235             temp3(temp3 == 0) = [];
236             accelval.stat.peak.(name2)(1:n,1) = temp;
237             accelval.stat.peak.(name2)(1:n,2) = temp2;
238             accelval.stat.peak.(name2)(1:n,3) = temp2.*100./temp;
239             accelval.stat.peak.(name2)(n+1,1) = mean(temp3);
240             accelval.stat.peak.(name2)(n+1,2) = std(temp3);
241             accelval.stat.peak.(name2)(n+1,3) = ...
                    std(temp3)*100/mean(temp3);
242
243             temp = mean(accelval.area.(name2),2);
244             n = length(temp);
245             temp2 = std(accelval.area.(name2),0,2);
246             temp3 = accelval.area.(name2);
247             temp3(temp3 == 0) = [];
248             accelval.stat.area.(name2)(1:n,1) = temp;
249             accelval.stat.area.(name2)(1:n,2) = temp2;
250             accelval.stat.area.(name2)(1:n,3) = temp2.*100./temp;
251             accelval.stat.area.(name2)(n+1,1) = mean(temp3);
252             accelval.stat.area.(name2)(n+1,2) = std(temp3);
253             accelval.stat.area.(name2)(n+1,3) = ...
                    std(temp3)*100/mean(temp3);
254
255             temp = mean(accelval.dt.(name2),2);
256             n = length(temp);
257             temp2 = std(accelval.dt.(name2),0,2);
258             temp3 = accelval.dt.(name2);
259             temp3(temp3 == 0) = [];
260             accelval.stat.dt.(name2)(1:n,1) = temp;
261             accelval.stat.dt.(name2)(1:n,2) = temp2;
```

```
262             accelval.stat.dt.(name2)(1:n,3) = temp2.*100./temp;
263             accelval.stat.dt.(name2)(n+1,1) = mean(temp3);
264             q3= mean(temp3);
265             accelval.stat.dt.(name2)(n+1,2) = std(temp3);
266             accelval.stat.dt.(name2)(n+1,3) = ...
                    std(temp3)*100/mean(temp3);
267
268             dt_temp2(i) = accelval.stat.dt.(name2)(n+1,1);
269
270             %Calculation of the RMSE values
271             counter = 1;
272             for j = (gauges_start:gauges_end)
273                 gauge_name = gauges{j};
274                 name1 = ...
                        strcat(gauge_name,'_Height_',num2str(i),'Accel');
275                 name1 = genvarname(name1);
276                 l = j;
277                 if ismember(j, config_doubles) == 0;
278                     l = l-counter;
279                     counter = counter+1;
280                 end
281
282                 if to_end_of_strikes
283             strikes_end = max(size(s.gauges.(gauge_name).h(i).strike));
284                 end
285
286                 for k = (strikes_start:strikes_end) %this loop makes ...
                        all trials the same length as an average
287                     p = round(accelval.dt.(name1)(k,1));
288                     q1 = round(accelval.stat.dt.(name1)(1)*50);
289                     q2 = round(q3*50);
```

```
290                     accelval.rms.data.(name1)(:,k) = ...
                            accelval.data.(name1)(p:p+q1,k);
291                  if ismember(j,config_doubles) == 0;
292                    accelval.rms.data.(name2)(:,k,j) = ...
                           accelval.data.(name1)(p:p+q2,k);
293                  end
294                  end
295
296                  temp = ...
                        sum(accelval.rms.data.(name2),3)./sum(accelval.rms...
297              .data.(name2)~=0,3);
298                  accelval.rms.avg.(name2) = mean(temp,2); %calculates ...
                        the average of each trial of a single height for ...
                        each timepoint
299
300                  accelval.rms.avg.(name1) = ...
                        mean(accelval.rms.data.(name1),2); %calculates ...
                        the average of each trial of a single trial for ...
                        each timepoint
301
302                  figure
303                  plot(accelval.rms.data.(name1))
304                  title(strcat(gauge_name,'\_Height\_', int2str(i)));
305                  hold on
306                  plot(accelval.rms.avg.(name1),'r','Linewidth',3)
307                  hold off
308
309              [m,n] = size(accelval.rms.data.(name1));
310
311              for k = 1:m
312                  for l = 1:n
```

```
313                     sums(k,l) = ...
                            (accelval.rms.data.(name1)(k,l)-accelval.rms.avg...
314                         .(name1)(k))^2;
315                     end
316                 end
317
318                 if m>length(accelval.rms.avg.(name2))
319                     A = ...
                            accelval.rms.data.(name1)(1:length(accelval.rms.avg...
320                         .(name2)),:);
321                     for k = 1:length(accelval.rms.avg.(name2))
322                         for l = 1:n
323                             sums2(k,l) = (A(k,l)- ...
                                    accelval.rms.avg.(name2)(k))^2;
324                         end
325                     end
326                 elseif m<length(accelval.rms.avg.(name2))
327                     A = accelval.rms.avg.(name2)(1:m);
328                     for k = 1:m
329                         for l = 1:n
330                             sums2(k,l) = (accelval.rms.data.(name1)(k,l) ...
                                    - A(k))^2;
331                         end
332                     end
333                 elseif m == length(accelval.rms.avg.(name2))
334                     for k= 1:m
335                         for l= 1:n
336                             sums2(k,l) = (accelval.rms.data.(name1)(k,l) ...
                                    - accelval.rms.avg.(name2)(k))^2;
337                         end
338                     end
339                 end
```

```
340
341             accelval.rms.rms.(name1) = sqrt(sum(sums,2))/sqrt(n);
342
343             accelval.rms.rms.(name2) = ...
                    sqrt(sum(sums2,2))/sart(n*(gauges_start-gauges_end);
344
345             accelval.stat.rms.(name1)(1) = ...
                    mean(accelval.rms.rms.(name1));
346             accelval.stat.rms.(name1)(2) = ...
                    max(accelval.rms.rms.(name1));
347
348             if j ~=config_doubles
349             accelval.stat.rms.(name2)(j,1) = ...
                    mean(accelval.rms.rms.(name1));
350             accelval.stat.rms.(name2)(j,2) = ...
                    max(accelval.rms.rms.(name1));
351             end
352             end
353             accelval.stat.rms.(name2)(j+1,1) = ...
                    mean(accelval.rms.rms.(name2));
354             accelval.stat.rms.(name2)(j+1,2) = ...
                    max(accelval.rms.rms.(name2));
355 end
356
357 name = strcat(site_struc_name,'_accelval');
358 eval([genvarname(name) '= accelval;']);
359 eval(['save ' name ' ' name])
360
361 % clear
362
363 t = toc;
364 sprintf(strcat('Time: ', num2str(t)))
```

C.2.2 peakinit_int.m

```
function [dti dtf] = peakinit_int(var, peak_size)
%finds the start, and finish and dt of a peak, var needs to be windowed
%before inputting

ind = find(var == min(var)); %find the peak, in the accelerometer ...
    signals, this is a minimum
thresh = 0.10*var(ind(1)); %defines the threshold as when 10% of the ...
    peak is reached
peak = find(thresh > var); %finds all the values that are above the ...
    threshold (> because we are working with negative numbers)
x = find(diff(peak)> peak_size); %calculates the difference between ...
    each value of peak, if the difference between two sub threshold ...
    values is greater than peak_size, then it's location is marked in x
if numel(x) == 0 %if x has no population, then all values of peak ...
    are below the threshold or all values consist of the peak
     dti = peak(1);
     dtf = peak(end);
elseif numel(x) == 1 % then the peak began at the indicated element ...
    of peak and ends at the next element of peak
     dti = peak(1);
     dtf = peak(x(1));
else %if more than one, find where the diff is the largest and ...
    consider the peak to be there. This will be double checked ...
    through figures in the main code.
     m= find(x == max(x))
     dti = peak(x(m));
     dtf = peak(x(m)+1);
end

```

```
21 dt = (dtf-dti)/50000;
22 end
```

C.3 DFT and Strain Calculation Codes

C.3.1 DFT_Analysis.m

This code will both transform the voltage data into strain data as well as perform the discrete fourier transform of this data.

```
1  %% Header
2  % The purpose of this program is to plot strain data from successive ...
       impact
3  % trials for one impact height, strain gauge, and gauge channel, to
4  % visually determine if there is a difference in the strain output ...
       for each
5  % trial.
6
7  %% Clean up
8  clear
9  clf
10
11 %% Start clock, turn on pause
12 pause on
13 tic
14
15 %% Constants
16 Fs = 50000; % Sampling rate
17
18 %% Interrogator Mode Options
19 make_graphs = true;
```

```
20 display_graphs = true;
21 save_graphs = false;
22 graph_res = '300';
23 save_data_to_file = true;
24 save_data_to_workspace = true;
25 to_end_of_heights = true;
26 heights_start = 1;
27 heights_end = 1;
28 to_end_of_gauges = true;
29 gauges_start = 1;
30 gauges_end = 10;
31 to_end_of_strikes = true;
32 strikes_start = 1;
33 strikes_end = 2;
34
35 %% File Paths
36 data_path = 'C:\Users\skull\Documents\Thesis\Hugh\Hugh ...
       (1653)Testing\crumple - 27 May 2013\multivar qdac data\';
37 site_struc_name = 'Site1';
38 site_struc_path = 'C:\Users\skull\Documents\MATLAB\Hugh\';
39 figure_save_path = 'C:\Users\skull\Documents\Thesis\Hugh\Anne\';
40 data_save_path = 'C:\Users\skull\Documents\Thesis\Hugh\Anne\';
41 %% Other Options
42 window_type = 'rectwin';
43 inds_1_offset = -1000;
44 inds_2_offset = 0;
45
46 %% Fetch data structure
47 s = load(strcat(site_struc_path, site_struc_name, '.mat'));
48 s = s.(genvarname(site_struc_name));
49
50 if to_end_of_heights
```

```
51      heights_end = max(size(s.heights));
52  end
53
54  for i = (heights_start:heights_end)
55  %% Begin looping through heights
56      %sprintf('cycling heights')
57      gauges = fieldnames(s.gauges);
58
59      if to_end_of_gauges
60          %fprintf(fout,strcat(gauge_name));
61          gauges_end = max(size(fieldnames(s.gauges)));
62      end
63
64      for j = (gauges_start:gauges_end)
65  %% Begin looping through gauges
66          %sprintf('cycling gauges')
67          gauge_name = gauges{j};
68          Key = s.gauges.(gauge_name).Key;
69          %num_channels = max(size(Key));
70          if to_end_of_strikes
71              %fprintf(fout,strcat(gauge_name));
72              strikes_end = max(size(s.gauges.(gauge_name).h(i).strike));
73          end
74
75          if ¬((isempty(s.gauges.(gauge_name).h(i).strike)) || ...
                isempty(Key))
76              res_freqs = [];
77              rel_mags = [];
78              for k = (strikes_start:strikes_end)
79  %% Begin looping through strikes
80                  %hold off
81                  disp(sprintf(strcat(gauge_name, '_Strike_', ...
```

```
                num2str(k), '_Height_', num2str(i))))
82              %sprintf('cycling strikes')
83              data_filename = strcat(data_path, ...
                    s.gauges.(gauge_name).h(i).strike(k).filename);
84              inds = s.gauges.(gauge_name).h(i).strike(k).inds;
85              inds(1) = inds(1) + inds_1_offset;
86              inds(2) = inds(2) + inds_2_offset;
87              %data = load(data_filename);
88              %data = data(inds(1):inds(2),2:end); %Note data goes ...
                    from 2:end to exclude accelerometer data
89              data = dlmread(data_filename);
90              data = data(1:end-1, :); %This step makes sure ...
                    columns are same size
91              data = data(inds(1):inds(2),:); %Cut out window of data
92              window = eval(strcat(window_type, ...
                    '(size(data,1))')); %Set window type for fourier ...
                    transform
93              for m = (1:size(data,2)) %Subtract mean and window data
94                  data(:,m) = data(:,m) - mean(data(:,m));
95                  data(:,m) = data(:,m).*window;
96              end
97
98      %% Collect time-domain data and calculate principal strains for rosettes
99              if (s.gauges.(gauge_name).Type == 'U')
100                 data = data(:, Key);
101             elseif (s.gauges.(gauge_name).Type == 'R')
102                 %num_channels = size(Key, 2);
103                 data_temp = [data(:,Key(1)) data(:,Key(2)) ...
                        data(:,Key(3))]; %data_temp used to plot ...
                        individual channels
104                 data = Principal_Strain(data(:,Key(1)), ...
                        data(:,Key(2)), data(:,Key(3)));
```

```
105                 end
106
107 %% Plot time-domain
108                 if make_graphs
109                     visibility = 'off';
110                     if display_graphs
111                         visibility = 'on';
112                     end
113                     fig = figure('Visible',visibility);
114                     time = linspace(0,(numel(data)-1)/50000, ...
                            numel(data));
115                     time = time'; %make column
116                     subplot(2, 1, 1);
117                     plot(time, data, 'LineWidth', 3)
118                     title(strcat(site_struc_name, '\_', gauge_name, ...
                            '\_Strike\_', num2str(k), '\_Height\_', ...
                            num2str(i)))
119                     if (s.gauges.(gauge_name).Type == 'R')
120                         hold on
121                         plot(time, data_temp(:,1), 'r')
122                         plot(time, data_temp(:,2), 'g')
123                         plot(time, data_temp(:,3), 'c')
124                     end
125                 end
126
127 %% Calculate frequency-domain data
128                 [spec, f] = DFT(Fs, data);
129                 if (s.gauges.(gauge_name).Type == 'R')
130                     [spec_ch1] = DFT(Fs, data_temp(:, 1));
131                     [spec_ch2] = DFT(Fs, data_temp(:, 2));
132                     [spec_ch3] = DFT(Fs, data_temp(:, 3));
133                 end
```

```
134
135 %% Plot Frequency Domain
136                 if make_graphs
137                     subplot(2, 1, 2); plot(f, spec/abs(max(spec)), ...
                            'b', 'LineWidth', 3)
138                     %subplot(2, 1, 2); plot(f, 10*log10(spec), 'b', ...
                            'LineWidth', 3)
139                     hold on
140                     if (s.gauges.(gauge_name).Type == 'R')
141                         plot(f, spec_ch1/abs(max(spec)), 'r')
142                         plot(f, spec_ch2/abs(max(spec)), 'g')
143                         plot(f, spec_ch3/abs(max(spec)), 'c')
144                     end
145                     xlim([0 4000])
146                 end
147
148 %% Save frequency domain data and graphs
149                 if save_graphs && make_graphs
150                     figname = strcat(figure_save_path, ...
                            site_struc_name, '_', gauge_name, '_Height_', ...
                            num2str(i), '_Strike_', num2str(k));
151                     print(fig, '-painters', '-dtiff', '-r300', ...
                            [figname '.tif'])
152                 end
153
154                 if save_data_to_file
155                     filename = strcat(data_save_path, ...
                            site_struc_name, '_', gauge_name, '_Height_', ...
                            num2str(i), '_Strike_', num2str(k));
156                     save(filename, 'f', 'spec')
157                 end
158
```

```
159                 if save_data_to_workspace
160                     if s.gauges.(gauge_name).Type == 'U'
161                         eval([site_struc_name '_' gauge_name ...
                                '_Height_' num2str(i) '_Strike_' ...
                                num2str(k) '_t = [time data];'])
162                         eval([site_struc_name '_' gauge_name ...
                                '_Height_' num2str(i) '_Strike_' ...
                                num2str(k) '_f = [f spec];'])
163 %                         eval([site_struc_name '_' gauge_name ...
    '_Height_' num2str(i) '_Strike_' num2str(k) '_t = data;'])
164 %                         eval([site_struc_name '_' gauge_name ...
    '_Height_' num2str(i) '_Strike_' num2str(k) '_f = spec;'])
165                     else
166                         eval([site_struc_name '_' gauge_name ...
                                '_Height_' num2str(i) '_Strike_' ...
                                num2str(k) '_t = [data data_temp];'])
167                         eval([site_struc_name '_' gauge_name ...
                                '_Height_' num2str(i) '_Strike_' ...
                                num2str(k) '_f = [spec spec_ch1 spec_ch2 ...
                                spec_ch3];'])
168                     end
169                 end
170
171             end
172 %             disp(sprintf('Press any key to continue...'))
173 %             pause
174 %             disp(sprintf('...continuing'))
175         end
176     end
177 %   sprintf('Press any key to continue...')
178 %   pause
179 %   sprintf('...continuing')
```

```
180 end
181
182 t = toc;
183 disp(strcat('Freq resolution = ', num2str(f(2)), 'Hz'))
184 disp(strcat('Runtime: ', num2str(t)))
```

C.3.2 DFT.m

```
1  function [spec,f,Y] = DFT(Fs,y)
2  %This function takes in data recorded over time (time domain)and a
3  %sampling frequency and outputs frequencies and their weightings
4  %(freq domain). The program subtracts the mean from the data set
5  %and pads zeros before and after the data to increase frequency ...
       fidelity.
6
7  %Inputs:
8  %Fs (sampling frequency)
9  %y (input data in time domain)
10
11 %Outputs:
12 %f (frequencies covered in freq domain) and Y (data in frequency domain)
13 %Y (DFT basis function coefficients in complex form)
14 %spec (DFT basis function coefficients without using aliased ...
       frequencies)
15
16 %Subtract mean from data
17 %y = y-mean(y);
18
19 %Identify variables
20 T = 1/Fs; %Time between samples
```

```
%fprintf('Time between samples, T = %f s\n',T)
N = length(y); %Number of data points in time domain
%fprintf('Number of data points, N = length(y) = %i\n',N)
t = (0:N-1)*T; %Time vector, starting at time t0 = 0

if Fs≥N;
%    Nmod = 2^(nextpow2(N));
Nmod = 4096;
else
% Nmod = 2^(nextpow2(N)); %Makes the number of data points a
Nmod = 4096;                          %a power of 2, which makes ...
    algorithm runs faster.
end

%fprintf('Number of data points with padded zeros, Nmod = %i\n',Nmod)
%tic; %Begin timing of FFT
Y = fft(y,Nmod)/N; %Calculate the DFT basis function coefficeints, ...
    divide
                   %by N
%timer = toc; %End timing of FFT
%fprintf('Time to compute DFT, t = %d s\n',timer)

f = Fs/2*linspace(0,1,Nmod/2+1); %Create frequency domain. Only use half
                                 %the band, as higher frequencies are
                                 %folded over.
f = f'; %Make frequency a column vector

%Plot data in time domain.
% figure
% plot(t,y)
% title('Signal')
% xlabel('time')
```

```
% ylabel('magnitude')

% Plot single-sided amplitude spectrum.
% figure
spec = 2*abs(Y(1:Nmod/2+1)); %Create new vector including only first ...
    half
%                            %of the basis functions (+1 to include ...
    the DC
%                            %component).
spec(1) = spec(1)/2; %Divide the DC component by 2, because it isn't ...
    aliased.
% plot(f,spec)
% title('Single-Sided Amplitude Spectrum of y(t)')
% xlabel('Frequency (Hz)')
% ylabel('|Y(f)|')
% XLIM([0 5000])
```

C.3.3 Principal_Strain.m

```
function [e_min e_max theta] = Principal_Strain(g1, g2, g3)

% This function takes in strain information from three-gauge rosette (45
% degrees separating each gauge) and returns the maximum and minimum
% principal strains. It is assumed that gauges g1, g2, and g3 start ...
    at the
% bottom right corner of a square and progress ccw; that is gauge g1 is
% directed along the bottom edge of a square gauge, gauge g3 is directed
% along the vertical edge, and gauge g2 bisects the two.


```

```
11 max_shear = (1/sqrt(2)) * sqrt((g1 - g2).^2 + (g2 - g3).^2);
12 ave_normal = (g1 + g3)/2;
13
14 e_max = ave_normal + max_shear;
15 e_min = ave_normal - max_shear;
16
17 theta = 1/2 * atan2((g1 - 2*g2 + g3),(g1 - g3));
18 theta = -theta * 180/pi;
```

Appendix D

Data Reduction Process

OVERVIEW: This appendix describes the data reduction process, from raw data to presented results. The protocol is descibed in a series of figures, Figures D.1 through D.18

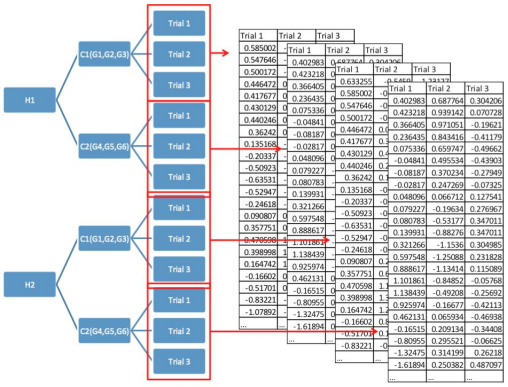

Figure D.1: Raw data of a single site of a single specimen.

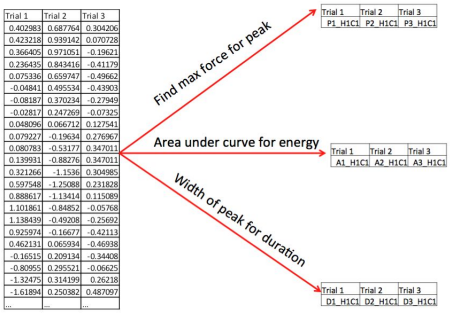

Figure D.2: Parameter of interest reduces this raw data to one value per trial.

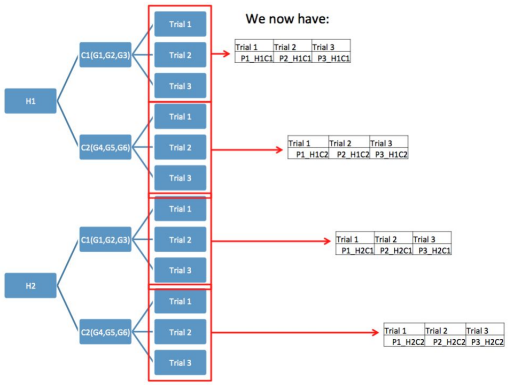

Figure D.3: Proceed with peak value only (same proceedure for other parameters).

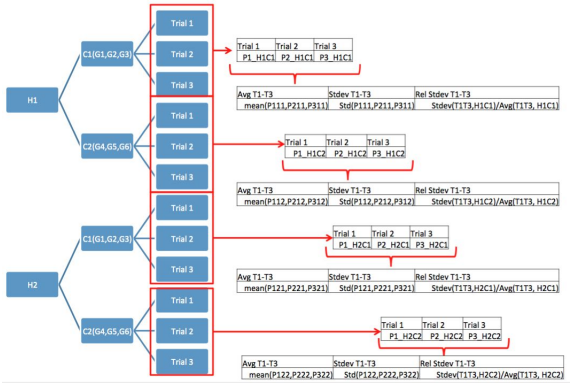

Figure D.4: For the 1st level of repeatability, the Matlab code calculates the average, standard deviations and relative standard deviations of each trial triad.

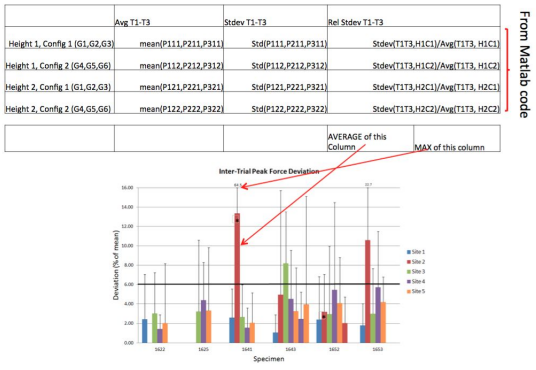

Figure D.5: The values presented involve a bit more manual processing, such as finding the average and maximums of these relative standard deviation values.

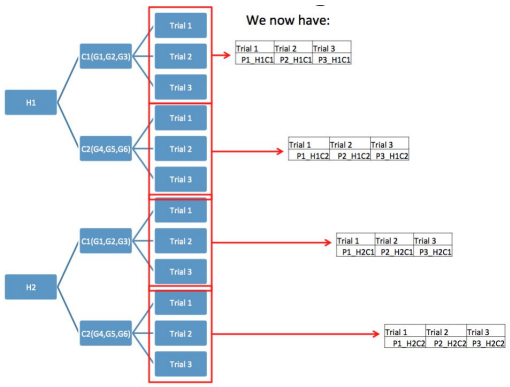

Figure D.6: To show the reduction for the 2nd repeatability level, recall that the Matlab code gave us a single value for each trial.

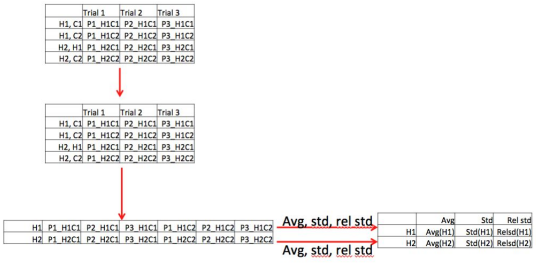

Figure D.7: The Matlab code then processes these values for the 2nd level of repeatability.

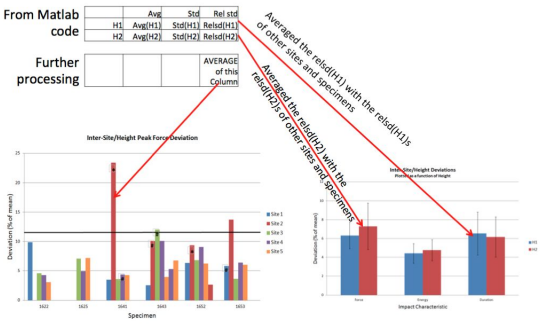

Figure D.8: Again further manual processing involved taking the average relative standard deviation values of the two heights for presentation.

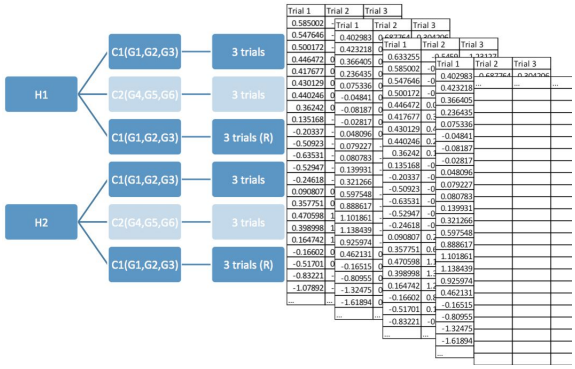

Figure D.9: This is the raw data of a single site of a single specimen, with the reproduced configuration (denoted by R) for the calculation of the 3rd level of repeatability values.

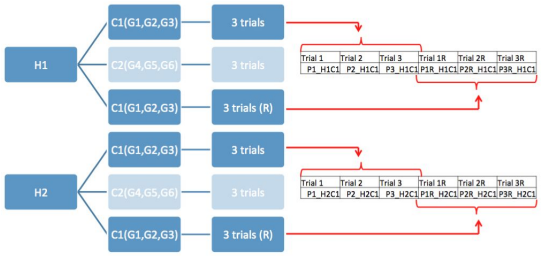

Figure D.10: Again, parameters are calculated and are reorganized like this by the Matlab code.

Figure D.11: The code then takes the average, standard deviation and relative standard deviation of this row for each height.

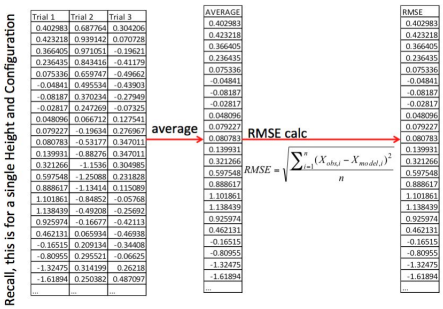

Figure D.12: RMSE was calculated slightely different, as the matlab code took the 3 trials and cut them to the accelerometer peak only. Then the average value of every dataponit was found. Therefore instead of a single parameter, the Matlab code found an RMSE vector.

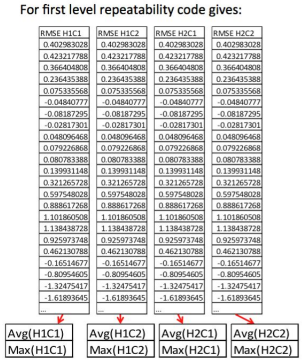

Figure D.13: For the 1st level of RMSE repeatability, the code calculates the average and maximal values of the RMSE vector.

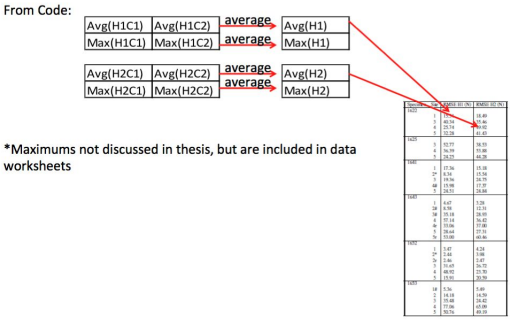

Figure D.14: This was further processed to acheive the mean of the average and the maximum values to reduce the data even further.

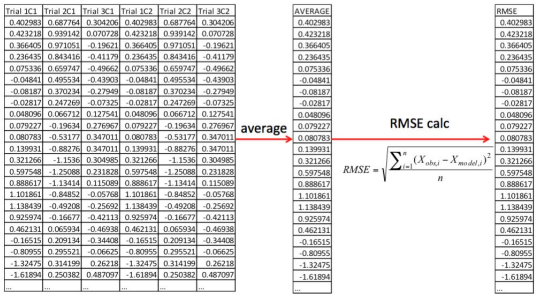

Figure D.15: For the 2nd level of repeatability, all trials of all configurations were averaged, but RMSE calculation was erroneous for this level in the code.

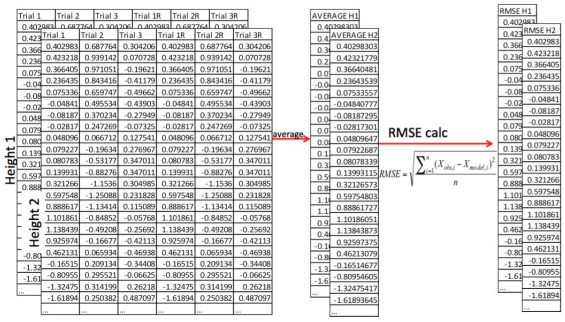

Figure D.16: For 3rd level of repeatability, the 1st and last three trials were averaged for each height.

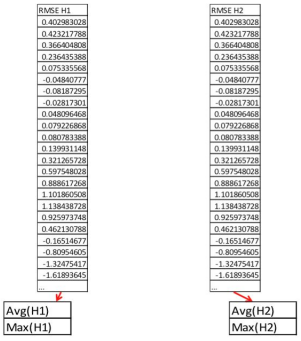

Figure D.17: For the 3rd level repeatability the code gives us the average and maximum RMSE values for each height.

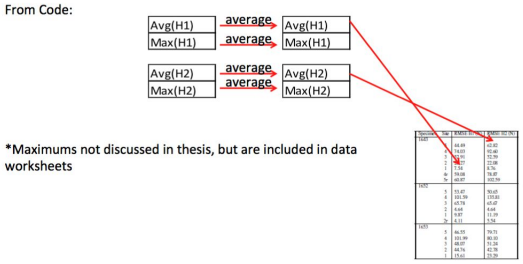

Figure D.18: This average and maximum value was further processed to acheive the reduced data presented.

Appendix E

Detailed Results

E.1 Values Derived from Accelerometer Signal

E.1.1 Summary of Impact Forces

Table E.1: The values presented in the following table describe the mean (in Newtons), standard deviation and relative standard deviation (% of the standard deviation over the mean) of the force values as determined by the accelerometer. The population from which these statistics arise include the three trials from every gauge configuration tested (12 configurations for specimen 1622, 7 configurations for specimens 1625 through 1653) at a particular drop height and impact site combination. Nomenclature used in the table include the terms PF for post fracture values and r for repeated sites with laser diligence.

Specimen	Site	Height 1			Height 2		
1622		*mean*	*std*	*rel. std*	*mean*	*std*	*rel. std*
	5	-1405.4	38.7	2.8	-1893.7	65.0	3.4
	4	-1439.3	95.2	6.6	-2035.3	84.1	4.1
	3	-1416.3	69.0	4.9	-1872.1	79.3	4.2
	2 PF	-570.6	25.6	4.5			
	2	-513.2	51.2	10.0	-584.3	130.6	22.4
	1	-621.9	72.2	11.6	-800.4	65.2	8.1
1625		*mean*	*std*	*rel. std*	*mean*	*std*	*rel. std*
	5	-1266.5	90.3	7.1	-1468.8	105.8	7.2
	4	-1039.9	92.6	8.9	-1258.6	66.0	5.2
	3	-1039.9	92.6	8.9	-1258.6	66.07	5.2
	2	-257.6	34.8	13.5	-320.6	44.7	13.9
	1	-201.6	9.4	4.6	-259.7	18.2	7.0
1641		*mean*	*std*	*rel. std*	*mean*	*std*	*rel. std*
	5	-825.6	30.2	3.7	-986.2	47.7	4.8
	4	-814.9	33.9	4.2	-954.8	43.6	4.6

	3	-760.2	31.0	4.1	-896.4	28.1	3.1
	2	-206.4	6.7	3.3	-307.0	133.8	43.6
	1	-526.9	17.5	3.3	-665.5	24.6	3.7
	3 PF	-472.9	71.0	15.0			
1643		*mean*	*std*	*rel. std*	*mean*	*std*	*rel. std*
	5	-808.6	32.5	4.0	-950.5	37.2	3.9
	5r	-846.5	45.6	5.4	-1053.2	85.7	8.1
	4	-955.6	89.9	9.4	-1149.1	123.6	10.8
	4r	-1026.9	58.2	5.7	-1215.6	59.8	4.9
	3	-511.8	65.6	12.8	-573.8	64.3	11.2
	2	-187.3	16.7	8.9	-233.5	26.3	11.3
	1	-200.3	5.4	2.7	-255.9	6.2	2.4
	3 PF	-472.9	71.0	15.0			
1652		*mean*	*std*	*rel. std*	*mean*	*std*	*rel. std*
	5	-757.9	52.0	6.9	-911.1	50.8	5.6
	4	-900.3	105.4	11.7	-1194.0	76.5	6.4
	3	-978.0	70.8	7.2	-1175.8	74.5	6.3
	2	-121.5	12.6	10.4	-164.6	13.6	8.3
	2r	-117.8	3.5	3.0	-178.1	4.1	2.3
	1	-188.2	11.4	6.0	-255.3	17.0	6.7
	3 PF	-1612.9	190.3	11.8	-1975.7	188.6	9.5
1653		*mean*	*std*	*rel. std*	*mean*	*std*	*rel. std*
	5	-1016.6	59.0	5.8	-1209.4	75.5	6.2
	4	-1117.5	78.4	7.0	-1281.5	74.6	5.8
	3	-731.1	31.3	4.3	-886.0	26.9	3.0
	2	-257.6	34.8	13.5	-320.6	44.7	13.9
	1	-201.6	9.4	4.6	-259.7	18.2	7.0

E.1.2 Summary of Impact Durations

Table E.2: The values presented in the following table describe the mean (in ms), standard deviation and relative standard deviation (% of the standard deviation over the mean) of the impact duration values as determined by the width of the peak in the accelerometer curve. The population from which these statistics arise include the three trials from every gauge configuration tested (12 configurations for specimen 1622, 7 configurations for specimens 1625 through 1653) at a particular drop height and impact site combination. Nomenclature used in the table include the terms PF for post fracture values and r for repeated sites with laser diligence.

Specimen	Site	Height 1			Height 2		
1622		*mean*	*std*	*rel. std*	*mean*	*std*	*rel. std*
	5	0.82	1.81E-05	2.21	0.82	3.69E-05	4.50
	4	0.75	2.46E-05	3.27	0.73	1.29E-05	1.77

	3	0.84	4.07E-05	4.87	0.83	5.05E-05	6.06
	2	2.18	1.73E-04	7.90			
	1	4.25	3.30E-04	7.78	3.96	2.65E-04	6.68
1625		*mean*	*std*	*rel. std*	*mean*	*std*	*rel. std*
	5	0.66	2.68E-02	4.04	0.64	2.18E-02	3.38
	4	0.57	3.61E-02	6.34	0.57	4.67E-02	8.21
	3	0.94	3.19E-02	3.39	0.90	1.13E-02	1.26
	2	3.07	4.29E-01	13.99	3.14	1.39E-01	4.43
	1	2.51	4.74E-01	18.89	2.43	2.97E-01	12.22
	3 PF	1.49	1.03E-01	6.93			
1641		*mean*	*std*	*rel. std*	*mean*	*std*	*rel. std*
	5	0.69	3.14E-02	4.53	0.67	2.55E-02	3.78
	4	0.68	1.67E-02	2.44	0.68	1.20E-02	1.78
	3	0.75	1.97E-02	2.64	0.74	1.73E-02	2.34
	2	1.97	1.99E-01	10.09	1.93	2.31E-01	11.95
	1	1.48	6.48E-02	4.37	1.48	5.07E-02	3.43
1643		*mean*	*std*	*rel. std*	*mean*	*std*	*rel. std*
	5	0.77	1.20E-02	1.55	0.78	1.25E-02	1.60
	5r	0.89	2.31E-02	2.60	0.61	1.91E-02	3.11
	4	0.64	2.12E-02	3.31	0.64	1.55E-02	2.42
	4r	0.62	1.99E-02	3.22	0.61	1.91E-02	3.11
	3	1.15	1.23E-01	10.72	1.18	3.13E-02	2.65
	2	2.41	1.63E-01	6.77	2.39	0.50	20.92
	1	2.42	8.82E-02	3.65	2.60	8.31E-02	3.20
	3 PF	1.49	1.03E-01	6.93	0.76	2.86E-02	3.77
1652		*mean*	*std*	*rel. std*	*mean*	*std*	*rel. std*
	5	1.24	6.95E-02	5.58	1.13	6.48E-02	5.72
	4	0.91	1.30E-01	14.20	0.75	8.44E-02	11.19
	3	0.73	3.64E-02	4.96	0.70	3.01E-02	4.27
	2	2.90	4.40E-01	15.18	2.94	5.41E-01	18.38
	2r	2.98	1.23E-01	4.13	2.57	7.47E-02	2.90
	1	2.46	1.67E-01	6.78	2.27	3.31E-01	14.58
	3 PF	0.78	8.27E-02	10.54	0.76	2.86E-02	3.77
1653		*mean*	*std*	*rel. std*	*mean*	*std*	*rel. std*
	5	0.66	2.68E-02	4.04	0.64	2.18E-02	3.38
	4	0.57	3.61E-02	6.34	0.57	4.67E-02	8.21
	3	0.94	3.19E-02	3.39	0.90	1.13E-02	1.26
	2	3.07	4.29E-01	13.99	3.14	1.39E-01	4.43
	1	2.51	4.74E-01	18.89	2.43	2.97E-01	12.22
	3 PF	1.49	1.03E-01	6.93			

E.1.3 Summary of Impact Energy

Table E.3: The values presented in the following table describe the mean (in kg*m/s), standard deviation and relative standard deviation (% of the standard deviation over the mean) of the impact duration values as determined by the area under the accelerometer curve. The population from which these statistics arise include the three trials from every gauge configuration tested (12 configurations for specimen 1622, 7 configurations for specimens 1625 through 1653) at a particular drop height and impact site combination. Nomenclature used in the table include the terms PF for post fracture values and r for repeated sites with laser diligence.

Specimen	Site	Height 1			Height 2		
1622		*mean*	*std*	*rel. std*	*mean*	*std*	*rel. std*
	5	-0.3722	0.0081	2.17	-0.5049	0.0108	2.15
	4	-0.3395	0.0138	4.07	-0.4755	0.0160	3.37
	3	-0.3551	0.0164	4.62	-0.4786	0.0272	5.69
	2 PF	-0.3510	0.0062	1.77			
	2	-0.0066	0.0003	4.61	-0.0118	0.0046	38.79
	1	-0.4847	0.0505	10.43	-0.6414	0.0581	9.06
1625		*mean*	*std*	*rel. std*	*mean*	*std*	*rel. std*
	5	-0.2241	0.0091	4.07	-0.2604	0.0108	4.15
	4	-0.2072	0.0097	4.66	-0.2412	0.0108	4.47
	3	-0.1982	0.0054	2.74	-0.2372	0.0038	1.61
	2	-0.1566	0.0090	5.72	-0.2132	0.0121	5.68
	1	-0.1384	0.0044	3.19	-0.1747	0.0094	5.38
	3 PF	-0.1774	0.0184	10.39			
1641		*mean*	*std*	*rel. std*	*mean*	*std*	*rel. std*
	5	-0.1906	0.0064	3.35	-0.2218	0.0076	3.41
	4	-0.1907	0.0041	2.13	-0.2228	0.0070	3.13
	3	-0.1942	0.0058	2.97	-0.2264	0.0062	2.75
	2	-0.1197	0.0070	5.86	-0.1487	0.0063	4.26
	1	-0.2370	0.0114	4.83	-0.3070	0.0097	3.17
1643		*mean*	*std*	*rel. std*	*mean*	*std*	*rel. std*
	5	-0.2125	0.0099	4.63	-0.2524	0.0119	4.73
	5r	-0.2449	0.0051	2.06	-0.2871	0.0047	1.62
	4	-0.2006	0.0112	5.57	-0.2431	0.0122	5.00
	4r	-0.2159	0.0092	4.25	-0.2502	0.0089	3.54
	3	-0.1821	0.0313	17.17	-0.2030	0.0174	8.56
	2	-0.1735	0.0118	6.81	-0.2109	0.0449	21.31
	1	-0.1741	0.0050	2.89	-0.2298	0.0053	2.29
	3 PF	-0.1774	0.0184	10.39			
1652		*mean*	*std*	*rel. std*	*mean*	*std*	*rel. std*
	5	-0.2464	0.0072	2.92	-0.2808	0.0060	2.12
	4	-0.2107	0.0038	1.82	-0.2440	0.0035	1.45
	3	-0.2281	0.0068	2.97	-0.2644	0.0063	2.40
	2	-0.1237	0.0119	9.65	-0.1583	0.0249	15.74
	2r	-0.1243	0.0026	2.10	-0.1573	0.0015	0.98
	1	-0.1319	0.0042	3.17	-0.1610	0.0064	3.98

	3 PF	-0.4125	0.0182	4.40	-0.5015	0.0281	5.61
1653		*mean*	*std*	*rel. std*	*mean*	*std*	*rel. std*
	5	-0.2241	0.0091	4.07	-0.2604	0.0108	4.15
	4	-0.2072	0.0097	4.66	-0.2412	0.0108	4.47
	3	-0.1982	0.0054	2.74	-0.2372	0.0038	1.61
	2	-0.1566	0.0090	5.72	-0.2132	0.0121	5.68
	1	-0.1384	0.0044	3.19	-0.1747	0.0094	5.38
	3 PF	-0.1774	0.0184	10.39			

E.2 Relative Standard Deviations at each Repeatability Level

E.2.1 First Level Repeatability, Inter-Trial Repeatability

Table E.4: The values presented in the following table describe the average relative standard deviation and the maximum relative standard deviation between the three trials of each impact condition. An impact condition is defined as a particular height, site and gauge configuration. The deviations are calculated between the impact force, the impact energy and the impact duration. Essentially, the average relative standard deviation values are the averages of columns 5 and 8 of the tables above in section E.1 and the maximum relative standard deviation value is the relative standard deviation between the three trials of the impact condition found to be the largest per impact site (the largest value in the average calculation of the values described in the tables in section E.1). An asterisk indicates a double bounce was present in the trial and a hashtag symbol indicates a faulty trial was present. The relative standard deviations both with and without the faulty trial are represented, with # having it included and #r having it removed from the average calculation and not considered as a maximum deviation. r without a hashtag character indicates a repeated site with laser diligence, and post fracture sites are not included

Specimen	Site	Force		Energy		Duration	
1622		*average*	*max*	*average*	*max*	*average*	*max*
	1	2.45	7.04	1.62	4.63	1.47	4.07
	3	3.03	7.23	1.69	6.69	1.36	4.22
	2	1.42	2.90	1.06	2.90	1.06	1.63
	1	2.03	8.15	1.33	3.61	2.00	13.02
1625		*average*	*max*	*average*	*max*	*average*	*max*
	3	3.22	10.59	2.07	4.34	6.45	20.32
	4	4.41	8.30	2.77	5.97	6.25	20.26
	5	3.34	9.83	2.42	8.44	1.80	3.27
1641		*average*	*max*	*average*	*max*	*average*	*max*
	1	2.58	5.57	2.16	6.00	1.30	3.73
	2*	13.35	64.50	4.58	13.26	8.82	15.85
	3	2.68	5.99	1.42	2.76	1.26	2.78
	4#	7.65	86.60	7.26	86.60	7.64	86.63

	4#r	1.58	3.60	1.16	3.20	1.57	1.73
	5	2.06	5.18	1.81	4.84	2.87	7.56
1643		*average*	*max*	*average*	*max*	*average*	*max*
	1	1.06	2.91	1.43	3.33	1.51	4.02
	2#	4.98	15.69	9.23	75.54	7.84	72.06
	2#r	4.98	15.69	4.13	15.01	2.90	7.06
	3#	8.61	14.19	8.75	48.39	3.96	29.31
	3#r	8.18	13.50	5.70	12.83	2.01	3.45
	4	4.53	9.57	2.09	7.46	1.69	3.03
	4r	2.45	5.22	1.03	2.49	2.20	3.81
	5	3.28	7.71	2.92	10.73	1.25	2.99
	5r	3.95	15.12	0.94	1.85	2.44	4.88
1652		*average*	*max*	*average*	*max*	*average*	*max*
	1	2.38	6.82	1.88	6.45	5.10	22.87
	2	3.20	7.04	2.97	8.65	6.32	16.28
	2r	2.03	4.72	1.22	3.18	2.86	7.61
	3	2.97	9.95	0.89	2.32	2.98	9.10
	4	5.45	14.48	0.94	2.98	5.04	14.86
	5	4.11	8.79	1.61	5.23	3.19	10.37
1653		*average*	*max*	*average*	*max*	*average*	*max*
	1#	2.84	16.31	3.16	13.54	5.90	27.46
	1#r	1.80	4.03	2.36	5.67	4.25	12.47
	2	10.57	22.67	1.77	3.68	5.02	9.16
	3	2.98	7.64	1.52	2.74	2.01	3.69
	4	5.72	11.49	3.49	9.30	5.96	19.32
	5	4.20	6.78	1.92	3.59	2.63	4.54

E.2.2 Second Level Repeatability, Inter-Height Repeatability

Table E.5: The values presented in the first six data columns of the following table describe the relative standard deviation between all trials (three trials per configuration) at a single height. The deviations are calculated between the impact force, the impact energy and the impact duration.The final three columns of this table describe the average relative standard deviation between the two heights. These three columns are plotted in figure 2.10. An asterisk indicates a double bounce was present in the trial and a hashtag symbol indicates a faulty trial was present, however at this level the faulty trial was embedded in the value and not removed from the calculation. r indicates a repeated site with laser diligence, post fracture sites not included.

Specimen	Site	Height 1			Height 2			Average		
1622		*force*	*energy*	*duration*	*force*	*energy*	*duration*	*force*	*energy*	*duration*
	1	11.61	10.43	7.78	8.15	9.06	6.68	9.88	9.74	7.23
	3	4.87	4.62	4.87	4.24	5.69	6.06	4.55	5.15	5.47

	4	4.13	3.37	1.77	4.41	3.32	1.69	4.27	3.35	1.73
	5	2.75	2.17	2.21	3.43	2.15	4.50	3.09	2.16	3.35
1625		*force*	*energy*	*duration*	*force*	*energy*	*duration*	*force*	*energy*	*duration*
	3	8.91	6.85	9.74	5.24	6.04	13.66	7.08	6.44	11.70
	4	4.11	1.53	3.69	5.79	3.07	2.67	4.95	2.30	3.18
	5	7.13	2.05	10.09	7.20	5.09	8.26	7.17	3.57	9.17
1641		*force*	*energy*	*duration*	*force*	*energy*	*duration*	*force*	*energy*	*duration*
	1	3.33	4.83	4.37	3.69	3.17	3.43	3.51	4.00	3.90
	2*	3.27	5.86	10.09	43.57	4.26	11.95	23.42	5.06	11.02
	3	4.07	2.97	2.64	3.14	2.75	2.34	3.61	2.86	2.49
	4#	4.16	2.13	2.44	4.56	3.13	1.78	4.36	2.63	2.11
	5	3.66	3.35	4.53	4.84	3.41	3.78	4.25	3.38	4.16
1643		*force*	*energy*	*duration*	*force*	*energy*	*duration*	*force*	*energy*	*duration*
	1	2.69	2.89	3.65	2.42	2.29	3.20	2.56	2.59	3.43
	2#	8.92	6.81	6.77	11.28	21.31	20.92	10.10	14.06	13.85
	3#	12.81	17.17	10.72	11.21	8.56	2.65	12.01	12.86	6.69
	4	9.41	5.57	3.31	10.75	5.00	2.42	10.08	5.28	2.86
	4r	5.66	4.25	3.22	4.92	3.54	3.11	5.29	3.90	3.17
	5	4.02	4.63	1.55	3.92	4.73	1.60	3.97	4.68	1.57
	5r	5.38	2.06	2.60	8.13	1.62	3.11	6.76	1.84	2.86
1652		*force*	*energy*	*duration*	*force*	*energy*	*duration*	*force*	*energy*	*duration*
	1	6.04	3.17	6.78	6.66	3.98	14.58	6.35	3.57	10.68
	2*	10.41	9.65	15.18	8.27	15.74	18.38	9.34	12.70	16.78
	2r	3.00	2.10	4.13	2.29	0.98	2.90	2.64	1.54	3.51
	3	7.24	2.97	4.96	6.34	2.40	4.27	6.79	2.68	4.62
	4	11.71	1.82	14.20	6.41	1.45	11.19	9.06	1.64	12.69
	5	6.86	2.92	5.58	5.58	2.12	5.72	6.22	2.52	5.65
1653		*force*	*energy*	*duration*	*force*	*energy*	*duration*	*force*	*energy*	*duration*
	1#	4.65	3.19	18.89	7.02	5.38	12.22	5.83	4.29	15.55
	2	13.51	5.72	13.99	13.95	5.68	4.43	13.73	5.70	9.21
	3	4.28	2.74	3.39	3.03	1.61	1.26	3.65	2.17	2.32
	4	7.01	4.66	6.34	5.82	4.47	8.21	6.42	4.57	7.27
	5	5.81	4.07	4.04	6.24	4.15	3.38	6.02	4.11	0.33

E.2.3 Third Level Repeatability, Between First Three and Last Three Strikes

Table E.6: The values presented in the following table describe the relative standard deviation between the first three trials, the last three trials as well as the relative standard deviation of the six trials making up the first and last three trials. This level of repeatability was only tested for specimens 1643, 1652 and 1653 as these specimens were the only tests to include a repeated test of the initial configuration after all configurations of a single height-site comibinations were completed. Thus, with the first and last trials having identical impact conditions, we can comment on the reproducibility of our setup. An asterisk indicates a double bounce was present in the trial and a hashtag symbol indicates a faulty trial was present, however at this level the faulty trial was embedded in the value and not removed from the calculation. r indicates a repeated site with laser diligence, post fracture sites not included.

Specimen	Site	Trials	Height 1			Height 2		
1643			*force*	*energy*	*duration*	*force*	*energy*	*duration*
	1	1st 3	0.80	0.64	0.50	1.85	2.12	1.13
		last 3	0.55	3.52	4.12	0.27	0.02	1.08
		all 6	**1.96**	**4.00**	**5.33**	**2.89**	**2.67**	**2.50**
	2#	1st 3	15.69	15.01	7.06	3.51	0.68	0.48
		last 3	4.34	3.19	1.63	0.52	1.06	0.43
		all 6	**13.03**	**10.93**	**10.53**	**14.26**	**0.82**	**6.29**
	3#	1st 3	3.12	0.56	1.10	8.98	2.52	3.45
		last 3	16.94	5.94	2.99	3.12	3.34	0.96
		all 6	**11.37**	**4.25**	**6.00**	**6.84**	**7.25**	**3.10**
	4	1st 3	3.95	0.76	1.88	3.30	2.45	1.77
		last 3	4.67	0.75	3.13	4.84	0.98	7.37
		all 6	**5.25**	**5.51**	**3.30**	**12.75**	**8.03**	**5.23**
	4r	1st 3	0.98	0.66	3.65	5.22	1.78	1.79
		last 3	3.37	1.09	1.90	5.077	1.44	0.00
		all 6	**4.14**	**6.33**	**3.53**	**5.04**	**3.94**	**4.26**
	5	1st 3	7.71	3.87	0.00	2.10	1.06	1.46
		last 3	2.67	1.79	1.51	1.10	0.96	3.88
		all 6	**5.15**	**4.19**	**1.34**	**1.52**	**2.84**	**2.66**
	5r	1st 3	3.90	0.74	0.00	1.11	1.38	0.00
		last 3	16.30	1.14	2.22	12.23	1.10	3.53
		all 6	**12.40**	**1.45**	**1.88**	**14.76**	**1.90**	**2.37**
1652			*force*	*energy*	*duration*	*force*	*energy*	*duration*
	1	1st 3	1.49	1.92	6.90	3.01	6.45	22.87
		last 3	5.95	1.54	2.96	0.57	0.30	0.60
		all 6	**8.46**	**3.78**	**9.16**	**6.45**	**6.77**	**24.43**
	2*	1st 3	1.08	1.56	1.89	1.00	1.57	4.56
		last3	4.55	1.02	1.75	0.56	0.737	3.42
		all 6	**3.02**	**1.34**	**3.58**	**9.47**	**8.95**	**19.32**
	2r	1st 3	1.16	0.84	2.90	3.09	0.25	4.55
		last3	1.68	0.17	1.067	2.02	1.08	2.12
		all 6	**1.31**	**0.63**	**4.40**	**2.89**	**0.97**	**4.38**
	3	1st 3	0.21	0.38	1.49	2.73	0.91	1.55

		last3	2.06	1.38	1.68	0.43	0.26	1.71
		all 6	**10.98**	**3.84**	**6.65**	**9.99**	**3.29**	**5.84**
	4	1st 3	11.16	2.98	4.90	4.08	0.53	0.00
		last3	5.31	0.86	3.15	2.72	0.81	0.00
		all 6	**17.97**	**1.96**	**18.69**	**10.99**	**0.89**	**17.30**
	5	1st 3	8.08	4.19	7.37	4.61	0.36	4.72
		last 3	3.88	7.20	7.86	3.58	1.92	1.19
		all 6	**5.70**	**5.57**	**8.37**	**5.87**	**2.55**	**8.69**
1653			*force*	*energy*	*duration*	*force*	*energy*	*duration*
	1	1st 3	4.03	3.46	27.46	16.31	13.54	2.86
		last 3	5.63	5.07	1.77	2.50	1.52	8.61
		all 6	**5.33**	**2.56**	**22.75**	**11.85**	**9.13**	**17.66**
	2	1st 3	14.87	2.14	9.16	18.73	3.68	2.75
		last 3	13.03	1.59	6.10	7.22	1.89	2.41
		all 6	**24.10**	**8.61**	**23.67**	**16.14**	**7.60**	**5.95**
	3	1st 3	3.74	2.46	3.37	2.28	0.71	0.00
		last 3	4.47	0.86	2.42	0.57	0.80	1.27
		all6	**3.74**	**3.68**	**3.79**	**4.12**	**1.37**	**0.90**
	4	1st 3	1.91	1.54	7.10	5.97	2.27	3.45
		last 3	3.55	1.53	3.57	4.97	1.30	0.00
		all 6	**4.01**	**6.70**	**5.70**	**5.45**	**5.23**	**2.94**
	5	1st 3	1.60	0.37	0.00	2.83	1.167	3.57
		last 3	1.24	0.38	0.00	2.86	0.52	0.00
		all 6	**2.32**	**0.67**	**1.59**	**5.76**	**1.09**	**6.25**

E.3 DFT results

E.3.1 Frequencies and powers pulled from the frequency spectra of each gauge of each specimen

Table E.7: The frequencies and corresponding poweres of all frequencies pulled from the frequency spectra of specimen 1622. The average values in the last two columns are the values used in the cluster analysis and the ANOVA tests.

Site	Gauge	Height	Strike 1		Strike 2		Strike 3		Average	
3			*frequency*	*power*	*frequency*	*power*	*frequency*	*power*	*frequency*	*power*
	L1	1	0	0	0	0	0	0	0	0
	L1	2	0	0	0	0	0	0	0	0
	L2	1	0	0	0	0	0	0	0	0
	L2	2	0	0	0	0	0	0	0	0
	L4	1	1514	7.67E-05	1563	6.60E-05	1526	9.48E-05	1.53E+03	7.92E-05
	L4	2	1538	9.20E-05	1538	7.05E-05	1538	8.74E-05	1538	8.33E-05
	L4	2	2405	4.27E-05	2429	3.83E-05	2429	4.96E-05	2421	4.35E-05
	L5	1	3491	3.47E-05	3430	3.42E-05	3528	4.33E-05	3483	3.74E-05
	L5	2	3467	6.24E-05	3406	4.24E-05	3491	6.19E-05	3454.67	5.56E-05
	L6	1	1624	3.41E-05	1575	4.98E-05	1563	4.98E-05	1587.33	4.46E-05
	L6	2	3442	5.34E-05	3442	3.63E-05	3418	1.49E-05	3434	3.49E-05
	L7	1	1477	5.36E-05	1453	5.00E-05	1514	5.28E-05	1481.33	5.21E-05
	L7	1	2222	3.45E-05	2222	3.34E-05	2197	2.67E-05	2213.67	3.15E-05
	L7	1	3381	3.06E-05	3381	2.01E-05	3345	2.46E-05	3369	2.51E-05
	L7	2	1453	5.57E-05	1440	5.76E-05	1404	6.16E-05	1432.33	5.83E-05
	L7	2	2100	5.62E-05	2112	5.21E-05	2112	4.68E-05	2108	5.17E-05
	L7	2	3381	3.80E-05	3369	3.24E-05	3394	3.94E-05	3381.33	3.66E-05
	L8	1	0	0	0	0	0	0	0	0
	L8	2	0	0	0	0	0	0	0	0
	L9	1	1233	1.37E-04	1245	1.31E-04	1221	1.30E-04	1233	1.33E-04
	L9	1	2100	5.72E-05	2112	4.29E-05	2087	6.16E-05	2099.67	5.39E-05
	L9	2	1257	1.53E-05	1270	1.59E-05	1270	1.37E-05	1265.67	1.49E-05
	L9	2	2112	8.22E-05	2112	8.60E-05	2112	1.06E-05	2112	5.96E-05
	L9	2	2380	4.92E-05	2417	6.70E-05	2393	6.03E-05	2396.67	5.88E-05
	M3	1	0	0	0	0	0	0	0	0
	M3	2	0	0	0	0	0	0	0	0

R1	1	0	0	0	0	0	0	0	0
R1	2	0	0	0	0	0	0	0	0
R2	1	2173	1.09E-05	2185	1.32E-05	2161	1.47E-05	2173	1.29E-05
R2	1	2490	1.14E-05	2490	1.42E-05	2551	1.51E-05	2510.33	1.36E-05
R2	2	1660	1.42E-05	1697	1.38E-05	1709	1.20E-05	1688.67	1.33E-05
R2	2	2185	1.24E-05	2197	1.64E-05	2197	1.68E-05	2193	1.52E-05
R2	2	2576	1.93E-05	2563	1.42E-05	2563	1.51E-05	2567.33	1.62E-05
R4	1	1514	3.84E-05	1526	4.14E-05	1477	3.07E-05	1505.67	3.68E-05
R4	1	2222	3.23E-05	2246	3.23E-05	2258	2.55E-05	2242	3.01E-05
R4	2	1477	4.56E-05	1514	5.95E-05	1514	5.34E-05	1501.67	5.28E-05
R4	2	2246	3.84E-05	2283	3.63E-05	2283	4.13E-05	2270.67	3.87E-05
R5	1	1233	8.26E-05	1245	7.86E-05	1208	7.66E-05	1228.67	7.92E-05
R5	1	2222	3.42E-05	2246	3.36E-05	2258	3.08E-05	2242	3.29E-05
R5	1	3186	3.33E-05	3210	2.25E-05	3210	2.42E-05	3202	2.67E-05
R5	2	1245	1.22E-04	1257	1.54E-04	1233	1.48E-04	1245	1.41E-04
R5	2	2246	5.81E-05	2283	5.27E-05	2283	6.26E-05	2270.67	5.78E-05
R5	2	2661	4.75E-05	2637	4.82E-05	2661	4.46E-05	2653	4.67E-05
R6	1	1465	5.42E-05	1453	5.72E-05	1477	4.98E-05	1465	5.37E-05
R6	1	2222	6.54E-05	2246	6.04E-05	2258	5.10E-05	2242	5.89E-05
R6	2	1392	8.29E-05	1428	9.57E-05	1392	1.01E-04	1404	9.33E-05
R6	2	2246	7.93E-05	2258	7.18E-05	2283	7.82E-05	2262.33	7.64E-05
R6	2	2673	3.63E-05	2673	4.93E-05	2673	6.51E-05	2673	5.02E-05
R7	1	1538	7.84E-05	1538	7.34E-05	1538	8.06E-05	1538	7.75E-05
R7	1	3088	3.01E-05	3003	3.38E-05	3040	3.57E-05	3043.67	3.32E-05
R7	1	3516	2.51E-05	3516	3.21E-05	3516	2.61E-05	3516	2.78E-05
R7	2	1550	6.05E-05	1538	5.09E-05	1587	4.15E-05	1558.33	5.10E-05
R7	2	1941	3.12E-05	1953	1.56E-05	1941	2.32E-05	1945	2.33E-05
R8	1	1233	4.53E-05	1245	3.53E-05	1282	4.22E-05	1253.33	4.09E-05
R8	1	1868	2.74E-05	1868	2.81E-05	1880	2.83E-05	1872	2.79E-05
R8	1	3101	1.73E-05	3162	2.11E-05	3149	2.29E-05	3137.33	2.04E-05
R8	2	1404	7.18E-05	1245	6.53E-05	1294	7.08E-05	1314.33	6.93E-05

	R8	2	1880	4.51E-05	1868	3.95E-05	1880	3.11E-05	1876	3.85E-05
	R8	2	3125	2.54E-05	3137	3.21E-05	3113	2.81E-05	3125	2.85E-05
	R9	1	0	0	0	0	0	0	0	0
	R9	2	0	0	0	0	0	0	0	0
4			*frequency*	*power*	*frequency*	*power*	*frequency*	*power*	*frequency*	*power*
	L1	1	1465	4.22E-05	1440	3.92E-05	1440	3.91E-05	1448.33	4.02E-05
	L1	1	1733	1.85E-05	1733	2.12E-05	1733	1.97E-05	1733	1.98E-05
	L1	1	3101	1.62E-05	3101	1.44E-05	3125	1.50E-05	3109	1.52E-05
	L1	2	1416	5.41E-05	1416	5.54E-05	1416	5.85E-05	1416	5.60E-05
	L1	2	2734	2.83E-05	2734	3.09E-05	2734	3.12E-05	2734	3.01E-05
	L1	2	3101	2.86E-05	3125	3.09E-05	3101	2.66E-05	3109	2.87E-05
	L2	1	1538	1.68E-05	1587	2.13E-05	1538	1.88E-05	1554.33	1.90E-05
	L2	2	1563	2.80E-05	1538	3.06E-05	1563	2.89E-05	1554.67	2.91E-05
	L4	1	1514	3.31E-04	1514	3.54E-04	1489	3.59E-04	1505.67	3.48E-04
	L4	1	2295	6.46E-05	2319	6.75E-05	2344	6.01E-05	2319.33	6.40E-05
	L4	2	1514	6.03E-04	1514	5.43E-04	1514	5.38E-04	1514	5.61E-04
	L4	2	2466	9.07E-05	2466	1.14E-04	2515	8.62E-05	2482.33	9.71E-05
	L5	1	1538	2.19E-04	1538	2.05E-04	1538	1.79E-04	1538	2.01E-04
	L5	1	2271	7.35E-05	2271	5.41E-05	2271	5.19E-05	2271	5.98E-05
	L5	1	2734	8.81E-05	2734	7.66E-05	2734	8.59E-05	2734	8.35E-05
	L5	2	1514	3.06E-04	1514	3.09E-04	1514	3.22E-04	1514	3.12E-04
	L5	2	2759	1.10E-04	2783	9.84E-05	2808	9.90E-05	2783.33	1.02E-04
	L6	1	1538	1.10E-04	1538	1.15E-04	1538	1.16E-04	1538	1.14E-04
	L6	1	2734	5.66E-05	2759	4.31E-05	2734	5.29E-05	2742.33	5.09E-05
	L6	1	3613	4.68E-05	3540	3.57E-05	3687	3.00E-05	3613.33	3.75E-05
	L6	2	1514	1.83E-04	1514	1.76E-04	1514	1.78E-04	1514	1.79E-04
	L6	2	3516	7.51E-05	3540	9.75E-05	3491	6.84E-05	3515.67	8.03E-05
	L7	1	1489	1.94E-04	1465	1.97E-04	1489	1.84E-04	1481	1.92E-04
	L7	1	3076	5.81E-05	3101	5.37E-05	3052	4.85E-05	3076.33	5.35E-05
	L7	2	1514	3.65E-04	1514	4.00E-04	1514	3.86E-04	1514	3.84E-04
	L7	2	3076	9.57E-05	3076	9.31E-05	3052	9.83E-05	3068	9.57E-05

L8	1	1563	4.51E-05	1538	4.75E-05	1563	5.18E-05	1554.67	4.81E-05
L8	2	1538	9.23E-05	1538	6.10E-05	1538	8.79E-05	1538	8.04E-05
L9	1	1196	2.20E-04	1221	1.76E-04	1245	1.69E-04	1220.67	1.88E-04
L9	1	2295	9.64E-05	2222	1.30E-04	2222	1.11E-04	2246.33	1.13E-04
L9	1	3418	6.54E-05	3345	3.03E-05	3540	3.79E-05	3434.33	4.45E-05
L9	2	1221	2.41E-04	1196	3.03E-04	1196	3.05E-04	1204.33	2.83E-04
L9	2	2368	1.34E-04	2417	2.29E-04	2393	2.15E-04	2392.67	1.93E-04
L9	2	2759	8.71E-05	2734	1.34E-04	2734	9.10E-05	2742.33	1.04E-04
M3	1	2954	1.05E-05	3027	1.39E-05	3003	1.00E-05	2994.67	1.15E-05
M3	2	0	0	0	0	0	0	0	0
R1	1	0	0	0	0	0	0	0	0
R1	2	3931	1.53E-05	3882	1.10E-05	3979	1.28E-05	3930.67	1.31E-05
R2	1	1440	3.62E-05	1440	3.60E-05	1440	3.63E-05	1440	3.62E-05
R2	1	3149	1.93E-05	3101	1.91E-05	3125	1.73E-05	3125	1.85E-05
R2	2	1440	5.25E-05	1416	6.41E-05	1416	4.84E-05	1424	5.50E-05
R2	2	2710	4.22E-05	2710	2.80E-05	2710	3.73E-05	2710	3.59E-05
R2	2	3101	3.64E-05	3101	3.15E-05	3101	3.46E-05	3101	3.42E-05
R4	1	1514	1.88E-04	1538	1.97E-04	1538	2.09E-04	1530	1.98E-04
R4	1	2295	6.44E-05	2368	6.95E-05	2271	7.88E-05	2311.33	7.09E-05
R4	2	1514	3.10E-04	1538	3.58E-04	1514	3.33E-04	1522	3.34E-04
R4	2	2246	9.55E-05	2490	9.63E-05	2368	1.01E-04	2368	9.75E-05
R5	1	1538	1.52E-04	1538	1.62E-04	1538	1.60E-04	1538	1.58E-04
R5	1	2295	1.04E-04	2368	8.71E-05	2271	1.09E-04	2311.33	1.00E-04
R5	1	2661	6.57E-05	2637	6.96E-05	2686	7.42E-05	2661.33	6.98E-05
R5	2	1538	2.07E-04	1514	2.93E-04	1514	2.68E-04	1522	2.56E-04
R5	2	2563	1.24E-04	2490	1.40E-04	2515	1.33E-04	2522.67	1.32E-04
R5	2	3003	5.16E-05	3027	7.04E-05	3027	8.01E-05	3019	6.73E-05
R6	1	1538	1.65E-04	1538	1.86E-04	1538	1.91E-04	1538	1.81E-04
R6	1	2295	1.30E-04	2368	1.23E-04	2295	1.36E-04	2319.33	1.30E-04
R6	2	1514	2.92E-04	1514	3.66E-04	1514	3.44E-04	1514	3.34E-04
R6	2	2271	1.67E-04	2490	1.16E-04	2368	1.54E-04	2376.33	1.46E-04

	R7	1	1538	2.09E-04	1563	2.20E-04	1587	2.15E-04	1562.67	2.15E-04
	R7	1	3076	6.91E-05	3101	6.65E-05	3076	5.89E-05	3084.33	6.48E-05
	R7	2	1538	3.10E-04	1538	3.60E-04	1538	3.51E-04	1538	3.41E-04
	R7	2	3052	8.84E-05	3052	1.03E-04	3052	1.13E-04	3052	1.01E-04
	R8	1	1489	7.75E-05	1489	8.55E-05	1489	1.06E-04	1489	8.97E-05
	R8	1	2271	7.33E-05	2246	5.36E-05	2197	5.00E-05	2238	5.89E-05
	R8	2	1538	1.22E-04	1538	1.41E-04	1538	1.54E-04	1538	1.39E-04
	R9	1	1245	1.77E-04	1245	1.81E-04	1270	1.80E-04	1253.33	1.79E-04
	R9	1	2173	7.49E-05	2148	8.59E-05	2173	8.30E-05	2164.67	8.13E-05
	R9	2	1270	3.09E-04	1221	3.20E-04	1221	3.30E-04	1237.33	3.20E-04
	R9	2	1514	2.94E-04	1514	2.93E-04	1514	2.70E-04	1514	2.86E-04
5			*frequency*	*power*	*frequency*	*power*	*frequency*	*power*	*frequency*	*power*
	L1	1	0	0	0	0	0	0	0	0
	L1	2	0	0	0	0	0	0	0	0
	L2	1	2979	1.14E-05	2954	1.56E-05	2954	1.38E-05	2962.33	1.36E-05
	L2	2	2881	1.57E-05	2881	1.40E-05	2881	2.07E-05	2881	1.68E-05
	L4	1	1538	4.42E-05	1514	4.92E-05	1514	3.23E-05	1522	4.19E-05
	L4	1	1855	2.22E-05	2075	2.55E-05	1880	2.42E-05	1936.67	2.40E-05
	L4	1	3369	1.25E-05	3345	1.94E-05	3491	7.40E-06	3401.67	1.31E-05
	L4	2	0	0	0	0	0	0	0	0
	L5	1	1099	4.56E-05	1196	6.14E-05	1123	4.71E-05	1139.33	5.14E-05
	L5	1	2173	2.11E-05	2222	2.23E-05	2173	3.86E-05	2189.33	2.73E-05
	L5	2	1367	8.21E-05	1367	1.09E-04	1392	1.28E-04	1375.33	1.06E-04
	L5	2	2197	2.81E-05	2124	5.66E-05	2148	3.88E-05	2156.33	4.12E-05
	L5	2	2686	4.99E-05	2710	3.47E-05	2637	3.00E-05	2677.67	3.82E-05
	L6	1	1489	1.57E-05	1440	2.07E-05	1514	1.25E-05	1481	1.63E-05
	L6	1	2515	1.38E-05	2393	1.68E-05	2417	1.47E-05	2441.67	1.51E-05
	L6	2	1245	2.97E-05	1245	3.17E-05	1270	2.98E-05	1253.33	3.04E-05
	L6	2	2686	3.74E-05	2466	2.73E-05	2417	4.12E-05	2523	3.53E-05
	L7	1	1538	7.70E-05	1563	6.16E-05	1563	3.90E-05	1554.67	5.92E-05
	L7	1	2197	4.27E-05	2173	3.83E-05	2197	3.58E-05	2189	3.90E-05

L7	2	1587	3.41E-05	1587	2.63E-05	1587	2.40E-05	1587	2.82E-05
L7	2	2197	6.54E-05	2222	8.37E-05	2197	8.44E-05	2205.33	7.78E-05
L8	1	1123	3.02E-05	1147	2.78E-05	1147	2.28E-05	1139	2.70E-05
L8	1	1465	2.18E-05	1563	1.98E-05	1465	1.95E-05	1497.67	2.04E-05
L8	2	1392	1.14E-04	1416	1.02E-04	1392	1.16E-04	1400	1.11E-04
L8	2	2124	3.64E-05	2100	3.38E-05	2124	3.23E-05	2116	3.42E-05
L9	1	1245	4.19E-05	1221	6.46E-05	1294	9.56E-05	1253.33	6.74E-05
L9	1	2124	6.37E-05	2100	4.51E-05	2124	3.90E-05	2116	4.93E-05
L9	1	2588	3.28E-05	2661	4.53E-05	2661	5.44E-05	2636.67	4.42E-05
L9	2	1392	1.43E-04	1343	1.50E-04	1392	1.65E-04	1375.67	1.53E-04
L9	2	2100	6.63E-05	2100	4.90E-05	2100	7.70E-05	2100	6.41E-05
L9	2	2759	4.85E-05	2710	5.81E-05	2710	6.49E-05	2726.33	5.72E-05
M3	1	0	0	0	0	0	0	0	0
M3	2	0	0	0	0	0	0	0	0
R1	1	0	0	0	0	0	0	0	0
R1	2	0	0	0	0	0	0	0	0
R2	1	0	0	0	0	0	0	0	0
R2	2	0	0	0	0	0	0	0	0
R4	1	1611	2.02E-05	1587	3.43E-05	1587	2.93E-05	1595	2.79E-05
R4	1	2173	1.88E-05	2148	2.06E-05	2246	4.07E-05	2189	2.67E-05
R4	2	1563	2.90E-05	1611	1.68E-05	1587	1.56E-05	1587	2.05E-05
R4	2	2441	4.05E-05	2319	4.36E-05	2417	2.36E-05	2392.33	3.59E-05
R5	1	1416	9.31E-05	1318	4.56E-05	1245	7.05E-05	1326.33	6.97E-05
R5	2	1392	1.31E-04	1343	1.30E-04	1392	9.08E-05	1375.67	1.17E-04
R6	1	1318	2.06E-05	1318	4.68E-05	1270	3.49E-05	1302	3.41E-05
R6	1	2222	3.09E-05	2271	3.11E-05	2246	7.10E-05	2246.33	4.43E-05
R6	2	1416	6.47E-05	1343	5.98E-05	1392	4.25E-05	1383.67	5.56E-05
R6	2	2197	9.87E-05	2197	1.10E-04	2173	4.39E-05	2189	8.40E-05
R7	1	1538	4.65E-05	1538	4.07E-05	1563	4.46E-05	1546.33	4.39E-05
R7	2	1221	3.41E-05	1221	2.91E-05	1270	4.35E-05	1237.33	3.56E-05
R7	2	1489	3.72E-05	1489	4.46E-05	1563	3.84E-05	1513.67	4.01E-05

R8	1	1270	5.71E-05	1270	6.15E-05	1294	5.66E-05	1278	5.84E-05
R8	1	2197	2.83E-05	2222	1.56E-05	2197	2.64E-05	2205.33	2.34E-05
R8	2	1343	7.95E-05	1318	8.43E-05	1343	9.24E-05	1334.67	8.54E-05
R8	2	2222	5.17E-05	2124	3.78E-05	2197	5.12E-05	2181	4.69E-05
R8	2	3442	3.63E-05	3516	2.33E-05	3467	3.27E-05	3475	3.07E-05
R9	1	1587	5.75E-05	1563	4.22E-05	1587	3.99E-05	1579	4.65E-05
R9	1	2124	2.45E-05	2100	3.42E-05	2148	3.73E-05	2124	3.20E-05
R9	1	2710	2.37E-05	2686	2.96E-05	2686	4.10E-05	2694	3.14E-05
R9	2	1245	1.12E-04	1294	8.81E-05	1392	8.93E-05	1310.33	9.64E-05
R9	2	2100	6.42E-05	2148	3.75E-05	2124	5.81E-05	2124	5.32E-05
R9	2	2661	5.90E-05	2686	5.56E-05	2710	4.48E-05	2685.67	5.31E-05

Table E.8: The frequencies and corresponding poweres of all frequencies pulled from the frequency spectra of specimen 1641. The average values in the last two columns are the values used in the cluster analysis and the ANOVA tests.

Site	Gauge	Height	Strike 1		Strike 2		Strike 3		Average	
4			*frequency*	*power*	*frequency*	*power*	*frequency*	*power*	*frequency*	*power*
	L1	1	0	0	0	0	0	0	0	0
	L1	2	0	0	0	0	0	0	0	0
	L2	1	0	0	0	0	0	0	0	0
	L2	2	0	0	0	0	0	0	0	0
	L4	1	2087	4.21E-05	2075	4.76E-05	2087	4.34E-05	2083	4.43E-05
	L4	1	2722	5.92E-05	2710	5.73E-05	2783	5.99E-05	2738	5.88E-05
	L4	1	3809	2.21E-05	3772	1.80E-05	3760	2.20E-05	3780	2.07E-05
	L4	2	2136	4.83E-05	2136	6.30E-05	2124	5.68E-05	2132	5.60E-05
	L4	2	2783	8.14E-05	2734	8.18E-05	2734	7.81E-05	2750	8.04E-05
	L4	2	3809	3.41E-05	3796	3.38E-05	3857	2.98E-05	3821	3.26E-05
	L5	1	1160	1.84E-04	1135	1.86E-04	1135	1.91E-04	1143	1.87E-04
	L5	1	1697	3.99E-05	1746	3.79E-05	1685	4.53E-05	1709	4.10E-05
	L5	1	2783	3.76E-05	2759	3.01E-05	2759	3.54E-05	2767	3.44E-05
	L5	2	1123	2.37E-04	1111	2.36E-04	1111	2.18E-04	1115	2.30E-04
	L5	2	1685	7.52E-05	1672	4.95E-05	1709	4.48E-05	1689	5.65E-05
	L5	2	2698	5.42E-05	2734	5.18E-05	2747	4.73E-05	2726	5.11E-05
	L6	1	0	0	0	0	0	0	0	0
	L6	2	0	0	0	0	0	0	0	0
	L7	1	0	0	0	0	0	0	0	0
	L7	2	0	0	0	0	0	0	0	0
	L8	1	1050	1.35E-04	1025	1.09E-04	1062	1.07E-04	1046	1.17E-04
	L8	1	1624	6.16E-05	1672	4.12E-05	1624	5.04E-05	1640	5.11E-05
	L8	1	2454	3.25E-05	2405	3.28E-05	2393	3.86E-05	2417	3.46E-05
	L8	2	1062	1.20E-04	1086	1.03E-04	1074	1.21E-04	1074	1.14E-04
	L8	2	1599	5.33E-05	1611	6.27E-05	1660	6.80E-05	1623	6.13E-05
	L8	2	2380	3.58E-05	2368	4.10E-05	2356	4.22E-05	2368	3.97E-05

L9	1	1221	2.22E-04	1208	2.22E-04	1172	2.19E-04	1200	2.21E-04
L9	2	1172	2.75E-04	1184	2.69E-04	1196	2.44E-04		
M3	1	0	0	0	0	0	0	0	0
M3	2	0	0	0	0	0	0	0	0
R1	1	0	0	0	0	0	0	0	0
R1	2	0	0	0	0	0	0	0	0
R2	1	1099	5.59E-05	1074	6.58E-05	1074	6.60E-05	1082	6.26E-05
R2	1	2100	3.75E-05	2075	3.64E-05	2075	3.89E-05	2083	3.76E-05
R2	2	1099	8.77E-05	1074	7.75E-05	1123	7.42E-05	1099	7.98E-05
R2	2	2173	4.95E-05	2148	4.75E-05	2173	3.44E-05	2165	4.38E-05
R4	1	1135	1.81E-04	1123	1.88E-04	1123	1.58E-04	1127	1.76E-04
R4	1	1501	6.89E-05	1501	7.73E-05	1526	7.13E-05	1509	7.25E-05
R4	2	1086	2.04E-04	1123	2.01E-04	1111	1.82E-04	1107	1.96E-04
R4	2	1526	1.03E-04	1514	8.01E-05	1514	7.96E-05	1518	8.74E-05
R5	1	0	0	0	0	0	0	0	0
R5	2	0	0	0	0	0	0	0	0
R6	1	964.4	2.41E-05	903.3	2.30E-05	842.3	2.57E-05	903	2.43E-05
R6	1	1868	2.68E-05	1904	2.81E-05	1978	3.93E-05	1917	3.14E-05
R6	1	2734	2.33E-05	2771	2.43E-05	2783	2.61E-05	2763	2.46E-05
R6	2	939.9	3.77E-05	842.3	2.55E-05	903.3	2.57E-05	895	2.96E-05
R6	2	1978	4.13E-05	1990	3.21E-05	1831	2.38E-05	1933	3.24E-05
R6	2	2808	4.19E-05	2820	3.72E-05	2856	3.68E-05	2828	3.86E-05
R7	1	0	0	0	0	0	0	0	0
R7	2	0	0	0	0	0	0	0	0
R8	1	988.8	1.31E-04	1001	1.29E-04	988.8	1.33E-04	993	1.31E-04
R8	1	1428	5.09E-05	1477	5.83E-05	1416	5.61E-05	1440	5.51E-05
R8	2	1038	1.33E-04	988.8	1.52E-04	988.8	1.43E-04	1005	1.43E-04
R8	2	1514	7.72E-05	1453	7.81E-05	1440	5.81E-05	1469	7.11E-05
R9	1	1025	3.93E-04	1025	3.79E-04	1062	3.49E-04	1037	3.74E-04
R9	2	1013	4.87E-04	1025	4.87E-04	1025	5.25E-04	1021	5.00E-04
5		*frequency*	*power*	*frequency*	*power*	*frequency*	*power*	*frequency*	*power*

L1	1	0	0	0	0	0	0	0	0
L1	2	0	0	0	0	0	0	0	0
L2	1	1965	3.30E-05	1965	3.43E-05	1990	3.46E-05	1973	3.40E-05
L2	1	2161	2.21E-05	2148	1.98E-05	2148	2.17E-05	2152	2.12E-05
L2	2	1978	3.70E-05	1978	3.43E-05	1965	3.78E-05	1974	3.64E-05
L2	2	2173	2.61E-05	2185	2.23E-05	2161	2.61E-05	2173	2.48E-05
L4	1	927.7	3.55E-05	927.7	3.55E-05	939.9	4.06E-05	932	3.72E-05
L4	1	2063	2.83E-05	2063	2.66E-05	2051	3.50E-05	2059	3.00E-05
L4	2	952.1	4.62E-05	927.7	4.56E-05	927.7	4.40E-05	936	4.53E-05
L4	2	2124	2.25E-05	2026	5.53E-05	2051	5.00E-05	2067	4.26E-05
L5	1	964.4	1.61E-04	976.6	1.50E-04	964.4	1.83E-04	968	1.65E-04
L5	1	1160	2.15E-04	1172	2.19E-04	1160	2.18E-04	1164	2.17E-04
L5	2	988.8	1.98E-04	964.4	1.73E-04	964.4	2.07E-04	973	1.93E-04
L5	2	1172	2.10E-04	1160	2.31E-04	1160	2.33E-04	1164	2.25E-04
L6	1	0	0	0	0	0	0	0	0
L6	2	0	0	0	0	0	0	0	0
L7	1	1001	1.36E-04	1001	9.86E-05	1001	1.10E-04	1001	8.20E-05
L7	1	1978	7.92E-05	1990	6.68E-05	1978	8.15E-05	1982	5.36E-05
L7	1	2366	3.25E-05	2966	2.46E-05	2954	3.35E-05	2762	2.20E-05
L7	2	1025	8.78E-05	1013	1.18E-04	1013	1.13E-04	1017	1.06E-04
L7	2	2148	5.33E-05	2002	8.30E-05	1990	8.64E-05	2047	7.42E-05
L7	2	2979	2.89E-05	2966	4.66E-05	2966	4.74E-05	2970	4.10E-05
L8	1	976.6	2.77E-04	976.6	2.78E-04	976.6	2.84E-04	977	2.80E-04
L8	1	2002	3.74E-05	2002	4.02E-05	1965	4.43E-05	1990	4.06E-05
L8	2	1001	2.99E-04	1001	2.97E-04	988.8	2.90E-04	997	2.95E-04
L8	2	1990	4.71E-05	2002	4.77E-05	1990	5.26E-05	1994	4.91E-05
L9	1	1160	3.15E-04	1172	3.18E-04	1160	3.27E-04	1164	3.20E-04
L9	2	1172	3.09E-04	1160	3.42E-04	1160	3.49E-04	1164	3.33E-04
M3	1	0	0	0	0	0	0	0	0
M3	2	0	0	0	0	0	0	0	0
R1	1	0	0	0	0	0	0	0	0

R1	2	0	0	0	0	0	0	0	0
R2	1	976.6	9.89E-05	1001	8.00E-05	964.4	9.43E-05	971	9.66E-05
R2	1	1953	2.81E-05	2002	1.74E-05	1965	1.70E-05	1959	2.26E-05
R2	2	976.6	6.66E-05	964.4	9.90E-05	964.4	9.28E-05	968	8.61E-05
R2	2	1941	1.09E-05	1978	1.93E-05	1965	2.19E-05	1961	1.73E-05
R4	1	1172	1.99E-05	1147	1.33E-05	1172	1.44E-05	1164	1.59E-05
R4	2	1160	1.03E-05	1147	9.63E-06	1172	1.18E-05	1160	1.06E-05
R5	1	1013	4.25E-04	1013	2.85E-04	1025	2.82E-04	1019	3.53E-04
R5	1	1685	9.30E-05	1733	6.85E-05	1697	7.59E-05	1705	7.91E-05
R5	2	1038	1.94E-04	1038	2.15E-04	1025	2.39E-04	1034	2.16E-04
R5	2	1685	9.40E-05	1685	1.09E-04	1685	1.29E-04	1685	1.11E-04
R6	1	988.8	3.25E-05	1001	3.21E-05	1013	4.22E-05	1001	3.56E-05
R6	2	1013	4.75E-04	1001	4.05E-05	1013	5.04E-05	1009	1.89E-04
R7	1	0	0	0	0	0	0	0	0
R7	2	0	0	0	0	0	0	0	0
R8	1	964.4	7.93E-05	976.6	8.57E-05	964.4	7.46E-05	968	7.98E-05
R8	1	1965	4.54E-05	1978	6.02E-05	1953	6.28E-05	1965	5.61E-05
R8	2	1001	6.50E-05	1001	7.63E-05	1001	8.54E-05	1001	7.55E-05
R8	2	1990	4.54E-05	2002	4.56E-05	1978	5.47E-05	1990	4.86E-05
R9	1	1013	1.07E-03	1013	7.28E-04	1013	7.14E-04	1013	8.92E-04
R9	2	1025	5.05E-04	1025	5.52E-04	1025	6.32E-04	1025	5.63E-04

Table E.9: The frequencies and corresponding poweres of all frequencies pulled from the frequency spectra of specimen 1622. The average values in the last two columns are the values used in the cluster analysis and the ANOVA tests.

Site	Gauge	Height	Strike 1		Strike 2		Strike 3		Average	
3			*frequency*	*power*	*frequency*	*power*	*frequency*	*power*	*frequency*	*power*
	L1	1	0	0	0	0	0	0	0	0
	L1	2	0	0	0	0	0	0	0	0
	L2	1	0	0	0	0	0	0	0	0
	L2	2	0	0	0	0	0	0	0	0
	L4	1	1013	7.15E-05	1013	5.52E-05	1013	6.97E-05	1013	6.55E-05
	L4	2	1038	6.80E-05	1001	7.35E-05	1038	7.07E-05	1026	7.07E-05
	L5	1	1147	6.84E-05	1147	5.01E-05	1135	6.37E-05	1143	6.07E-05
	L5	2	1147	6.64E-05	1135	7.15E-05	1135	6.53E-05	1139	6.77E-05
	L6	1	0	0	0	0	0	0	0	0
	L6	2	0	0	0	0	0	0	0	0
	L7	1	1233	5.58E-05	1245	5.70E-05	1221	3.66E-05	1111	4.80E-05
	L7	2	0	0	0	0	0	0	0	0
	L8	1	1123	8.99E-05	1123	6.91E-05	1123	8.29E-05	1123	8.06E-05
	L8	1	2576	2.50E-05	2600	1.65E-05	2527	1.83E-05	2568	1.99E-05
	L8	2	1123	7.90E-05	1123	8.56E-05	1123	8.22E-05	1123	8.23E-05
	L8	2	2551	1.46E-05	2539	2.15E-05	2637	1.96E-05	2576	1.85E-05
	L9	1	0	0	0	0	0	0	0	0
	L9	2	1733	1.42E-05	1697	1.68E-05	1709	1.64E-05	1713	1.58E-05
	M3	1	0	0	0	0	0	0	0	0
	M3	2	0	0	0	0	0	0	0	0
	R1	1	0	0	0	0	0	0	0	0
	R1	2	0	0	0	0	0	0	0	0
	R2	1	0	0	0	0	0	0	0	0
	R2	2	0	0	0	0	0	0	0	0
	R4	1	1135	6.70E-05	1147	7.25E-05	1147	7.03E-05	1143	6.99E-05
	R4	1	3442	1.42E-05	3491	1.89E-05	3430	1.53E-05	3454	1.62E-05

	R4	2	1147	7.30E-05	1147	7.64E-05	1147	7.51E-05	1147	7.49E-05
	R4	2	1721	1.72E-05	1758	1.73E-05	1758	2.02E-05	1746	1.82E-05
	R4	2	2258	1.70E-05	2246	1.72E-05	2258	1.85E-05	2254	1.75E-05
	R5	1	1038	1.01E-04	1135	1.01E-04	1135	9.91E-05	1103	1.00E-04
	R5	1	2295	2.77E-05	2271	2.65E-05	2246	2.68E-05	2271	2.70E-05
	R5	2	1074	1.04E-04	1038	1.10E-04	1062	1.07E-04	1058	1.07E-04
	R5	2	1733	1.99E-05	1758	2.26E-05	1746	2.76E-05	1746	2.34E-05
	R5	2	2258	3.21E-05	2271	3.42E-05	2246	3.48E-05	2258	3.37E-05
	R6	1	1050	1.33E-04	1160	1.08E-04	1135	1.08E-04	1115	1.16E-04
	R6	2	1050	1.57E-04	1050	1.62E-04	1172	1.56E-04	1091	1.58E-04
	R7	1	1086	8.64E-05	1086	9.07E-05	1086	1.05E-04	1086	9.39E-05
	R7	1	1709	4.59E-05	1709	5.55E-05	1685	4.99E-05	1701	5.04E-05
	R7	2	1086	1.44E-04	1074	1.60E-04	1074	1.54E-04	1078	1.53E-04
	R7	2	1709	6.75E-05	1660	8.10E-05	1624	6.36E-05	1664	7.07E-05
	R8	1	0	0	0	0	0	0	0	0
	R8	2	0	0	0	0	0	0	0	0
	R9	1	1013	5.20E-05	1013	5.43E-05	1050	4.84E-05	1025	5.16E-05
	R9	2	1025	5.49E-05	1038	5.69E-05	1038	5.47E-05	1034	5.55E-05
	R9	2	1721	1.29E-05	1758	1.52E-05	1758	1.73E-05	1746	1.51E-05
	R9	2	2258	1.77E-05	2234	1.93E-05	2258	2.08E-05	2250	1.92E-05
4			*frequency*	*power*	*frequency*	*power*	*frequency*	*power*	*frequency*	*power*
	L1	1	0	0	0	0	0	0	0	0
	L1	2	0	0	0	0	0	0	0	0
	L2	1	1294	8.59E-05	1294	9.00E-05	1294	9.26E-05		
	L2	1	2588	5.12E-05	2588	5.24E-05	2563	5.45E-05		
	L2	2	1294	9.03E-05	1270	8.94E-05	1270	9.80E-05		
	L2	2	2563	5.53E-05	2539	4.11E-05	2515	3.80E-05		
	L2*	1	1257	5.82E-05	1245	6.13E-05	1245	7.14E-05	1272*	7.66e-05*
	L2*	1	2478	4.27E-05	2441	5.08E-05	2466	6.72E-05	2521*	5.31E-05*
	L2*	2	1270	9.02E-05	1270	7.23E-05	1245	7.37E-05	1270*	8.56E-05*
	L2*	2	2417	5.96E-05	2466	4.49E-05	2466	4.56E-05	2494*	4.74E-05*

L4	1	1099	1.00E-04	1099	1.14E-04	1099	1.04E-04	1099	1.06E-04
L4	1	1294	1.02E-04	1270	1.17E-04	1294	1.13E-04	1286	1.11E-04
L4	1	2466	4.18E-05	2490	6.27E-05	2515	6.29E-05	2490	5.58E-05
L4	2	1074	1.34E-04	1074	1.39E-04	1074	1.36E-04	1074	1.36E-04
L4	2	1270	9.64E-05	1270	9.44E-05	1270	9.47E-05	1270	9.52E-05
L4	2	2319	5.24E-05	2319	6.11E-05	2295	5.81E-05	2311	5.72E-05
L5	1	1245	1.55E-04	1245	1.68E-04	1245	1.59E-04	1245	1.61E-04
L5	1	2466	3.46E-05	2490	4.72E-05	2466	4.43E-05	2474	4.20E-05
L5	2	1221	2.17E-04	1221	2.13E-04	1196	2.23E-04	1213	2.18E-04
L5	2	2319	4.04E-05	2319	4.80E-05	2295	4.67E-05	2311	4.51E-05
L6	1	1221	6.05E-04	1221	8.19E-04	1221	6.66E-04	1221	6.97E-04
L6	1	2490	1.17E-04	2441	1.26E-04	2466	1.01E-04	2466	1.14E-04
L6	2	1233	6.71E-04	1233	6.85E-04	1233	7.38E-04	1233	6.98E-04
L6	2	2454	1.21E-04	2454	1.45E-04	2454	1.50E-04	2454	1.38E-04
L7	1	1221	4.78E-01			1196	4.59E-01	1209	4.68E-01
L7	1	2417	1.64E-01			2417	1.26E-01	2417	1.45E-01
L7	2	0	0	0	0	0	0	0	0
L8	1	1270	2.24E-04	1270	2.73E-04	1245	2.69E-04	1262	2.55E-04
L8	1	2783	1.15E-04	2856	9.03E-05	2856	1.02E-04	2832	1.03E-04
L8	2	1245	2.99E-04	1245	2.99E-04	1245	3.02E-04	1245	3.00E-04
L8	2	2832	1.35E-04	2856	1.31E-04	2832	1.36E-04	2840	1.34E-04
L9	1	1074	4.66E-05	1099	4.99E-05	1074	4.89E-05	1082	4.85E-05
L9	1	1709	3.61E-05	1709	3.35E-05	1685	2.72E-05	1701	3.23E-05
L9	1	2661	2.80E-05	2539	2.07E-05	2563	1.81E-05	2588	2.23E-05
L9	2	1074	6.24E-05	1074	6.21E-05	1074	6.49E-05	1074	6.31E-05
L9	2	1660	3.29E-05	1709	3.71E-05	1660	3.93E-05	1676	3.64E-05
L9	2	2734	3.27E-05	2710	3.41E-05	2686	3.83E-05	2710	3.50E-05
M3	1	2563	8.27E-05	2563	8.23E-05	2563	8.10E-05		
M3	2	2539	7.98E-05	2515	7.54E-05	2515	8.04E-05		
M3*	1	2478	5.16E-05	2490	6.28E-05	2466	6.69E-05	2521*	7.12E-05*
M3*	2	2466	8.06E-05	2466	6.32E-05	2466	6.72E-05	2495*	7.44E-05*

R1	1	0	0	0	0	0	0	0	0
R1	2	0	0	0	0	0	0	0	0
R2	1	1221	8.87E-05	1221	8.75E-05	1221	8.96E-05	1221	8.86E-05
R2	1	2417	4.63E-05	2417	4.69E-05	2441	5.08E-05	2425	4.80E-05
R2	2	1221	1.06E-04	1221	1.04E-04	1233	1.10E-04	1225	1.07E-04
R2	2	2454	4.95E-05	2441	4.94E-05	2454	5.05E-05	2450	4.98E-05
R4	1	1196	1.50E-04	1221	1.12E-04	1221	1.09E-04	1213	1.24E-04
R4	1	1685	8.86E-05	1611	9.13E-05	1648	7.88E-05	1648	8.62E-05
R4	1	2539	4.06E-05	2539	3.30E-05	2527	2.88E-05	2535	3.41E-05
R4	2	1221	1.25E-04	1221	1.33E-04	1221	1.26E-04	1221	1.28E-04
R4	2	1672	1.24E-04	1685	1.14E-04	1648	1.12E-04	1668	1.17E-04
R4	2	2515	3.91E-05	2515	3.86E-05	2539	4.25E-05	2523	4.01E-05
R5	1	1196	7.15E-04	1221	5.21E-04	1221	5.24E-04	1213	5.87E-04
R5	1	1587	2.24E-04	1611	1.88E-04	1611	1.76E-04	1603	1.96E-04
R5	1	2417	1.72E-04	2441	1.08E-04	2429	1.10E-04	2429	1.30E-04
R5	2	1233	5.50E-04	1221	5.55E-04	1233	5.56E-04	1229	5.54E-04
R5	2	1611	2.53E-04	1636	2.24E-04	1624	2.34E-04	1624	2.37E-04
R5	2	2417	1.05E-04	2417	1.35E-04	2429	1.36E-04	2421	1.25E-04
R6	1	1221	4.41E-04	1221	5.65E-04	1221	4.73E-04	1221	4.93E-04
R6	1	1685	1.04E-04	1636	1.32E-04	1636	9.70E-05	1652	1.11E-04
R6	1	2417	9.00E-05	2393	1.16E-04	2368	9.16E-05	2393	9.92E-05
R6	2	1221	5.34E-04	1221	5.40E-04	1208	5.69E-04	1217	5.48E-04
R6	2	1648	1.33E-04	1660	1.17E-04	1697	1.43E-04	1668	1.31E-04
R6	2	2393	1.09E-04	2356	1.08E-04	2356	1.24E-04	2368	1.14E-04
R7	1	1172	2.72E-04			1172	3.00E-04	1172	2.86E-04
R7	2	1147	2.65E-04	1135	2.76E-04	1147	2.73E-04	1143	2.71E-04
R8	1	1196	1.80E-04	1196	1.22E-04	1196	1.25E-04	1196	1.42E-04
R8	1	1587	1.08E-04	1563	8.89E-05	1538	8.14E-05	1563	9.28E-05
R8	1	2368	6.56E-05	2417	4.14E-05	2417	4.74E-05	2401	5.15E-05
R8	2	1233	1.18E-04	1196	1.25E-04	1233	1.29E-04	1221	1.24E-04
R8	2	1599	1.23E-04	1611	1.16E-04	1636	1.22E-04	1615	1.20E-04

	R8	2	2319	6.15E-05	2344	5.29E-05	2344	5.17E-05	2336	5.53E-05
	R9	1	1172	2.49E-04	1099	1.86E-04	1086	1.75E-04	1119	2.03E-04
	R9	1	1587	1.62E-04	1587	1.78E-04	1599	1.49E-04	1591	1.63E-04
	R9	2	1111	2.87E-04	1123	3.11E-04	1123	2.85E-04	1119	2.94E-04
	R9	2	1599	2.07E-04	1611	1.66E-04	1636	1.89E-04	1615	1.87E-04
5			*frequency*	*power*	*frequency*	*power*	*frequency*	*power*	*frequency*	*power*
	L1	1	0	0	0	0	0	0	0	0
	L1	2	0	0	0	0	0	0	0	0
	L2	1	1318	3.39E-05	1306	2.98E-05	1306	3.47E-05		
	L2	2	1318	3.55E-05	1306	3.68E-05	1318	4.23E-05		
	L2*	1	1294	2.92E-05	1270	2.75E-05	1306	3.13E-05	1300*	3.11E-05*
	L2*	2	1257	4.15E-05	1294	4.16E-05	1306	3.93E-05	1300*	3.95E-05*
	L4	1	1184	6.88E-05	1196	7.67E-05	1172	7.21E-05	1184	7.25E-05
	L4	1	2454	1.89E-05	2478	2.36E-05	2478	2.04E-05	2470	2.10E-05
	L4	1	3357	1.59E-05	3113	1.79E-05	3186	1.07E-05	3219	1.48E-05
	L4	2	1172	7.80E-05	1160	8.66E-05	1160	7.73E-05	1164	8.06E-05
	L4	2	2241	1.99E-05	2405	1.90E-05	2441	2.07E-05	2362	1.99E-05
	L4	2	3149	2.30E-05	3113	2.61E-05	3125	2.35E-05	3129	2.42E-05
	L5	1	1196	8.98E-05	1208	9.19E-05	1196	8.66E-05	1200	8.95E-05
	L5	2	1184	1.36E-04	1184	1.33E-04	1184	1.13E-04	1184	1.27E-04
	L6	1	1270	2.25E-04	1282	2.53E-04	1282	2.44E-04	1278	2.40E-04
	L6	2	1013	2.35E-04	1013	2.36E-04	1001	2.21E-04	1009	2.31E-04
	L6	2	1160	1.80E-04	1160	1.93E-04	1147	1.95E-04	1156	1.89E-04
	L6	2	1294	3.06E-04	1282	3.20E-04	1282	3.22E-04	1286	3.16E-04
	L7	1	1306	1.90E-04	1331	3.15E-04	1294	3.24E-04	1310	2.76E-04
	L7	2	1306	3.16E-04	1294	2.80E-04	1282	2.58E-04	1294	2.85E-04
	L8	1	1184	1.20E-04	1172	1.29E-04	1184	1.31E-04	1180	1.27E-04
	L8	1	3174	4.39E-05	3174	5.00E-05	3125	4.24E-05	3158	4.54E-05
	L8	1	4053	2.17E-05	4102	2.14E-05	4163	1.72E-05	4106	2.01E-05
	L8	2	1160	2.02E-04	1172	1.92E-04	1147	1.92E-04	1160	1.95E-04
	L8	2	3162	7.92E-05	3113	7.40E-05	3125	7.38E-05	3133	7.56E-05

L8	2	4077	4.19E-05	4053	4.88E-05	4089	3.98E-05	4073	4.35E-05
L9	1	1282	1.91E-05	1294	2.07E-05	1270	1.99E-05	1282	1.99E-05
L9	1	3259	1.59E-05	3320	1.49E-05	3540	1.53E-05	3373	1.54E-05
L9	2	1270	2.56E-05	1257	2.67E-05	1257	2.71E-05	1261	2.65E-05
L9	2	3198	2.24E-05	3174	2.14E-05	3198	1.98E-05	3190	2.12E-05
L9	2	4346	1.15E-05	4382	1.41E-05	4370	1.58E-05	4366	1.38E-05
M3	1	0	0	0	0	0	0	0	0
M3	2	0	0	0	0	0	0	0	0
R1	1	0	0	0	0	0	0	0	0
R1	2	0	0	0	0	0	0	0	0
R2	1	0	0	0	0	0	0	0	0
R2	2	0	0	0	0	0	0	0	0
R4	1	1025	2.40E-05	1025	2.91E-05			1025	2.66E-05
R4	1	1294	3.13E-05	1282	2.66E-05			1288	2.89E-05
R4	2	1038	6.27E-05	1025	7.80E-05	1025	7.93E-05	1029	7.33E-05
R4	2	1257	3.50E-05	1282	5.12E-05	1270	5.28E-05	1270	4.63E-05
R5	1	1123	1.45E-04	1123	1.42E-04			1123	1.44E-04
R5	2	1123	2.04E-04	1111	2.10E-04	1099	2.15E-04	1111	2.10E-04
R5	2	2393	4.59E-05	2466	3.92E-05	2441	4.21E-05	2433	4.24E-05
R6	1	1245	1.85E-04	1282	1.89E-04	1282	1.71E-04	1270	1.82E-04
R6	2	1282	1.85E-04	1245	2.56E-04	1270	2.54E-04	1266	2.32E-04
R6	2	2612	3.84E-05	2576	5.65E-05	2563	5.19E-05	2584	4.89E-05
R7	1	1147	1.47E-04	1147	1.48E-04	1147	1.40E-04	1147	1.45E-04
R7	2	1147	1.85E-04	1160	1.93E-04	1147	1.94E-04	1151	1.90E-04
R8	1	1147	7.85E-05	1147	7.23E-05			1147	7.54E-05
R8	2	1147	1.06E-04	1147	9.77E-05	1147	1.04E-04	1147	1.02E-04
R9	1	1208	1.01E-04	1208	8.26E-05			1208	9.16E-05
R9	2	1025	1.41E-04	1038	1.75E-04	1.04E+03	1.77E-04	1034	1.64E-04

Table E.10: The frequencies and corresponding poweres of all frequencies pulled from the frequency spectra of specimen 1652. The average values in the last two columns are the values used in the cluster analysis and the ANOVA tests.

Site	Gauge	Height	Strike 1		Strike 2		Strike 3		Average	
3			*frequency*	*power*	*frequency*	*power*	*frequency*	*power*	*frequency*	*power*
	L1	1	0	0	0	0	0	0	0	0
	L1	2	0	0	0	0	0	0	0	0
	L2	1	0	0	0	0	0	0	0	0
	L2	2	0	0	0	0	0	0	0	0
	L4	1	1489	2.44E-05	1453	2.36E-05	1477	2.78E-05	1473	2.53E-05
	L4	1	2014	3.36E-05	1978	3.65E-05	2051	3.87E-05	2014	3.63E-05
	L4	2	1477	3.20E-05	1416	2.81E-05	1416	2.91E-05	1436	2.97E-05
	L4	2	1990	5.32E-05	1990	5.53E-05	1941	5.03E-05	1974	5.29E-05
	L5	1	1440	9.65E-05	1428	1.10E-04	1440	1.16E-04	1436	1.07E-04
	L5	1	3027	2.74E-05	3027	2.74E-05	3040	3.85E-05	3031	3.11E-05
	L5	2	1440	1.39E-04	1440	1.44E-04	1440	1.40E-04	1440	1.41E-04
	L5	2	2966	5.78E-05	2979	5.60E-05	3027	5.47E-05	2991	5.62E-05
	L6	1	0	0	0	0	0	0	0	0
	L6	2	0	0	0	0	0	0	0	0
	L7	1	0	0	0	0	0	0	0	0
	L7	2	0	0	0	0	0	0	0	0
	L8	1	1331	9.34E-05	1367	1.09E-04	1367	1.09E-04	1355	1.04E-04
	L8	1	2161	3.93E-05	2124	4.26E-05	2136	4.75E-05	2140	4.31E-05
	L8	1	3040	3.50E-05	3052	3.86E-05	3076	3.64E-05	3056	3.66E-05
	L8	2	1331	1.13E-04	1343	1.24E-04	1343	1.18E-04	1339	1.18E-04
	L8	2	2161	7.44E-05	2148	7.40E-05	2148	7.25E-05	2152	7.36E-05
	L8	2	3052	2.80E-05	2991	4.11E-05	2979	3.90E-05	3007	3.61E-05
	L9	1	1355	1.58E-04	1379	1.68E-04	1367	1.67E-04	1367	1.64E-04
	L9	1	2026	7.23E-05	2051	7.34E-05	2100	7.19E-05	2059	7.25E-05
	L9	1	2832	6.06E-05	2869	8.12E-05	2832	7.87E-05	2844	7.35E-05
	L9	2	1367	1.90E-04	1379	2.10E-04	1379	2.06E-04	1375	2.02E-04

	L9	2	2136	9.12E-05	2112	8.96E-05	2124	9.58E-05	2124	9.22E-05
	L9	2	2869	1.29E-04	2869	1.06E-04	2869	1.03E-04	2869	1.13E-04
	M3	1	0	0	0	0	0	0	0	0
	M3	2	0	0	0	0	0	0	0	0
	R1	1	1245	2.94E-05	1245	2.94E-05	1306	3.05E-05	1265	2.98E-05
	R1	2	1221	3.69E-05	1221	3.60E-05	1282	3.42E-05	1241	3.57E-05
	R2	1	0	0	0	0	0	0	0	0
	R2	2	0	0	0	0	0	0	0	0
	R4	1	0	0	0	0	0	0	0	0
	R4	2	0	0	0	0	0	0	0	0
	R5	1	1428	1.98E-04	1465	2.11E-04	1453	2.17E-04	1449	2.08E-04
	R5	2	1465	2.53E-04	1477	2.51E-04	1465	2.57E-04	1469	2.54E-04
	R6	1	0	0	0	0	0	0	0	0
	R6	2	0	0	0	0	0	0	0	0
	R7	1	0	0	0	0	0	0	0	0
	R7	2	0	0	0	0	0	0	0	0
	R8	1	1550	9.55E-05	1538	9.57E-05	1550	9.42E-05	1546	9.51E-05
	R8	2	1538	1.04E-04	1538	1.05E-04	1526	1.09E-04	1534	1.06E-04
	R9	1	1343	2.46E-04	1343	2.60E-04	1331	2.52E-04	1339	2.52E-04
	R9	2	1331	3.00E-04	1331	2.99E-04	1331	3.04E-04	1331	3.01E-04
4			*frequency*	*power*	*frequency*	*power*	*frequency*	*power*	*frequency*	*power*
	L1	1	0	0	0	0	0	0	0	0
	L1	2	0	0	0	0	0	0	0	0
	L2	1	0	0	0	0	0	0	0	0
	L2	2	0	0	0	0	0	0	0	0
	L4	1	0	0	0	0	0	0	0	0
	L4	2	0	0	0	0	0	0	0	0
	L5	1	0	0	0	0	0	0	0	0
	L5	2	0	0	0	0	0	0	0	0
	L6	1	0	0	0	0	0	0	0	0
	L6	2	0	0	0	0	0	0	0	0

L7	1	0	0	0	0	0	0	0	0
L7	2	0	0	0	0	0	0	0	0
L8	1	1721	2.14E-05	1721	5.48E-05	1697	6.81E-05	1713	4.81E-05
L8	1	2930	1.29E-05	3174	2.43E-05	3101	2.41E-05	3068	2.04E-05
L8	2	1758	8.84E-05	1746	9.32E-05	1697	9.23E-05	1734	9.13E-05
L8	2	3076	3.71E-05	3088	3.91E-05	3052	3.62E-05	3072	3.75E-05
L9	1	1086	1.13E-04	1111	1.20E-04	1123	1.41E-04	1107	1.24E-04
L9	1	1758	4.79E-05	1611	9.13E-05	1672	1.06E-04	1680	8.18E-05
L9	2	1135	1.72E-04	1135	1.69E-04	1135	1.63E-04	1135	1.68E-04
L9	2	1709	1.39E-04	1709	1.37E-04	1672	1.29E-04	1697	1.35E-04
M3	1	0	0	0	0	0	0	0	0
M3	2	0	0	0	0	0	0	0	0
R1	1	1318	1.03E-05	1367	1.22E-05	1379	1.41E-05	1355	1.22E-05
R1	1	2393	9.34E-06	2393	8.70E-06	2429	8.95E-06	2405	9.00E-06
R1	2	1428	2.24E-05	1379	2.04E-05	1416	2.05E-05	1408	2.11E-05
R1	2	2405	1.44E-05	2454	1.29E-05	2332	1.37E-05	2397	1.37E-05
R2	1	1929	2.47E-05	1941	2.09E-05	1941	2.84E-05	1937	2.47E-05
R2	1	2795	1.25E-05	2783	8.42E-06	2869	9.93E-06	2816	1.03E-05
R2	2	1782	2.43E-05	1965	2.78E-05	1929	3.13E-05	1892	2.78E-05
R2	2	2673	1.52E-05	2808	1.59E-05	2795	1.84E-05	2759	1.65E-05
R4	1	1794	6.56E-05	1636	4.91E-05	1733	7.07E-05	1721	6.18E-05
R4	2	1782	8.15E-05	1782	1.07E-04	1794	1.19E-04	1786	1.02E-04
R5	1	1599	1.18E-04	1685	1.05E-04	1709	1.32E-04	1664	1.18E-04
R5	2	1514	1.24E-04	1514	1.71E-04	1526	1.67E-04	1518	1.54E-04
R6	1	0	0	0	0	0	0	0	0
R6	2	0	0	0	0	0	0	0	0
R7	1	0	0	0	0	0	0	0	0
R7	2	0	0	0	0	0	0	0	0
R8	1	1465	3.82E-05	1453	4.10E-05	1453	4.35E-05	1457	4.09E-05
R8	2	1550	4.81E-05	1514	6.95E-05	1514	6.68E-05	1526	6.15E-05
R9	1	1453	9.75E-05	1428	7.77E-05	1477	8.40E-05	1453	8.64E-05

	R9	1	2185	5.51E-05	2185	5.64E-05	2173	5.76E-05	2181	5.64E-05
	R9	2	1501	7.10E-05	1501	1.11E-04	1489	1.27E-04	1497	1.03E-04
	R9	2	2209	6.58E-05	2161	8.63E-05	2161	6.95E-05	2177	7.38E-05
5			*frequency*	*power*	*frequency*	*power*	*frequency*	*power*	*frequency*	*power*
	L1	1	0	0	0	0	0	0	0	0
	L1	2	0	0	0	0	0	0	0	0
	L2	1	0	0	0	0	0	0	0	0
	L2	2	0	0	0	0	0	0	0	0
	L4	1	0	0	0	0	0	0	0	0
	L4	2	0	0	0	0	0	0	0	0
	L5	1	0	0	0	0	0	0	0	0
	L5	2	0	0	0	0	0	0	0	0
	L6	1	0	0	0	0	0	0	0	0
	L6	2	0	0	0	0	0	0	0	0
	L7	1	0	0	0	0	0	0	0	0
	L7	2	0	0	0	0	0	0	0	0
	L8	1	1318	1.39E-04	1331	1.42E-04	1331	1.57E-04	1327	1.46E-04
	L8	1	2649	9.01E-05	2637	8.49E-05	2661	8.91E-05	2649	8.80E-05
	L8	1	3992	3.09E-05	3992	3.08E-05	4004	3.47E-05	3996	3.21E-05
	L8	2	1294	1.88E-04	1331	1.81E-04	1318	1.88E-04	1314	1.86E-04
	L8	2	2673	1.00E-04	2637	1.03E-04	2612	9.16E-05	2641	9.82E-05
	L8	2	4004	3.99E-05	3943	3.08E-05	3918	2.84E-05	3955	3.30E-05
	L9	1	2332	4.57E-05	2319	4.49E-05	2405	4.84E-05	2352	4.63E-05
	L9	2	2454	6.86E-05	2563	7.52E-05	2539	7.81E-05	2519	7.39E-05
	M3	1	0	0	0	0	0	0	0	0
	M3	2	0	0	0	0	0	0	0	0
	R1	1	2368	2.45E-05	2417	3.03E-05	2344	3.05E-05	2376	2.84E-05
	R1	2	0	0	0	0	0	0	0	0
	R2	1	0	0	0	0	0	0	0	0
	R2	2	0	0	0	0	0	0	0	0
	R4	1	1282	3.54E-05	1306	4.00E-05	1294	4.20E-05	1294	3.91E-05

R4	1	1782	1.77E-05	1782	2.82E-05	1721	2.33E-05	1762	2.31E-05
R4	1	2258	1.32E-05	2185	2.47E-05	2161	1.99E-05	2201	1.93E-05
R4	2	1331	5.33E-05	1318	6.33E-05	1318	6.45E-05	1322	6.04E-05
R4	2	1782	4.49E-05	1672	3.28E-05	1843	3.52E-05	1766	3.76E-05
R4	2	2197	3.33E-05	2100	3.41E-05	2136	4.25E-05	2144	3.66E-05
R5	1	1746	6.08E-05	1709	7.18E-05	1721	8.12E-05	1725	7.13E-05
R5	1	1953	3.07E-05	1917	5.31E-05	1917	4.59E-05	1929	4.32E-05
R5	1	2673	3.41E-05	2637	5.10E-05	2625	5.33E-05	2645	4.61E-05
R5	2	1758	1.01E-04	1770	5.76E-05	1709	8.23E-05	1746	8.03E-05
R5	2	1953	7.48E-05	1953	5.93E-05	1929	5.25E-05	1945	6.22E-05
R5	2	2673	6.92E-05	2686	6.54E-05	2649	6.33E-05	2669	6.60E-05
R6	1	0	0	0	0	0	0	0	0
R6	2	0	0	0	0	0	0	0	0
R7	1	1318	3.65E-05	1318	3.44E-05	1318	3.27E-05	1318	3.46E-05
R7	2	0	0	0	0	0	0	0	0
R8	1	1294	7.80E-05	1294	8.33E-05	1294	8.91E-05	1294	8.35E-05
R8	2	1306	1.16E-04	1331	1.38E-04	1306	1.27E-04	1314	1.27E-04
R9	1	1294	1.10E-04	1306	1.28E-04	1282	1.46E-04	1294	1.28E-04
R9	2	1318	1.78E-04	1318	2.32E-04	1306	2.11E-04	1314	2.07E-04

Table E.11: The frequencies and corresponding poweres of all frequencies pulled from the frequency spectra of specimen 1653. The average values in the last two columns are the values used in the cluster analysis and the ANOVA tests.

Site	Gauge	Height	Strike 1		Strike 2		Strike 3		Average	
3			*frequency*	*power*	*frequency*	*power*	*frequency*	*power*	*frequency*	*power*
	L1	1	0	0	0	0	0	0	0	0
	L1	2	0	0	0	0	0	0	0	0
	L2	1	0	0	0	0	0	0		
	L2	2	1978	1.05E-04	1978	9.27E-05	2100	1.19E-04		
	L2*	1	0	0	0	0	0	0	0*	0*
	L2*	2	2002	1.27E-04	2002	1.65E-04	2002	1.32E-04	2010*	1.23e-04*
	L4	1	2002	2.39E-05	2002	2.94E-05	2002	3.10E-05	2002	2.81E-05
	L4	2	2002	3.03E-05	1978	2.59E-05	2002	2.68E-05	1994	2.77E-05
	L5	1	1953	5.95E-05	1929	5.81E-05	1929	5.96E-05	1937	5.90E-05
	L5	2	1929	7.10E-05	1929	7.76E-05	1904	7.34E-05	1921	7.40E-05
	L6	1	1514	3.77E-05	1538	3.16E-05	1538	3.57E-05	1530	3.50E-05
	L6	1	1929	3.93E-05	1953	3.44E-05	1929	3.90E-05	1937	3.76E-05
	L6	2	1514	6.31E-05	1514	6.08E-05	1514	5.85E-05	1514	6.08E-05
	L6	2	1929	4.22E-05	1929	4.55E-05	1929	4.06E-05	1929	4.28E-05
	L7	1	0	0	0	0	0	0	0	0
	L7	2	0	0	0	0	0	0	0	0
	L8	1	0	0	0	0	0	0	0	0
	L8	2	0	0	0	0	0	0	0	0
	L9	1	1978	7.57E-05	1978	7.89E-05	1953	8.74E-05	1970	8.07E-05
	L9	2	1978	7.77E-05	1978	6.65E-05	1953	6.30E-05	1970	6.91E-05
	M3	1	0	0	0	0	0	0	0	0
	M3	2	0	0	0	0	0	0	0	0
	R1	1	0	0	0	0	0	0	0	0
	R1	2	0	0	0	0	0	0	0	0
	R2	1	0	0	0	0	0	0	0	0
	R2	2	0	0	0	0	0	0	0	0

	R4	1	1440	3.17E-05	1343	5.16E-05	1318	3.25E-05	1367	3.86E-05
	R4	2	1416	4.92E-05	1367	5.18E-05	1367	4.96E-05	1383	5.02E-05
	R5	1	1929	8.95E-05	1953	9.85E-05	1929	7.95E-05	1937	8.92E-05
	R5	2	1953	1.05E-04	1929	1.11E-04	1929	1.10E-04	1937	1.08E-04
	R6	1	0	0	0	0	0	0	0	0
	R6	2	0	0	0	0	0	0	0	0
	R7	1	0	0	0	0	0	0	0	0
	R7	2	0	0	0	0	0	0	0	0
	R8	1	2002	4.38E-05	1978	5.20E-05	1929	4.41E-05	1970	4.66E-05
	R8	2	1978	6.12E-05	1978	6.14E-05	1978	5.81E-05	1978	6.02E-05
	R9	1	2124	1.02E-05	2197	1.27E-05	2100	1.29E-05	2140	1.19E-05
	R9	2	2173	1.72E-05	2148	1.49E-05	2148	1.83E-05	2156	1.68E-05
4			*frequency*	*power*	*frequency*	*power*	*frequency*	*power*	*frequency*	*power*
	L1	1	0	0	0	0	0	0	0	0
	L1	2	0	0	0	0	0	0	0	0
	L2	1	2039	2.60E-05	2026	3.26E-05	2051	3.26E-05		
	L2	2	2039	4.23E-05	2039	3.69E-05	2051	2.43E-05		
	L2*	1	2014	2.64E-05	2026	4.45E-05	2026	2.77E-05	2030*	3.16E-05*
	L2*	2	2026	4.72E-05	2039	2.94E-05	2014	4.61E-05	2035*	3.77E-05*
	L4	1	1440	2.94E-05	1465	2.81E-05	1453	3.03E-05	1453	2.92E-05
	L4	2	1440	2.34E-05	1453	3.59E-05	1453	3.78E-05	1449	3.24E-05
	L5	1	1489	6.03E-05	1465	6.06E-05	1465	6.08E-05	1473	6.05E-05
	L5	1	1965	7.39E-05	1990	6.82E-05	1953	6.33E-05	1969	6.84E-05
	L5	1	3149	2.83E-05	3149	2.62E-05	3162	2.97E-05	3153	2.81E-05
	L5	2	1489	5.33E-05	1453	8.34E-05	1453	9.13E-05	1465	7.60E-05
	L5	2	1965	5.58E-05	1953	9.18E-05	2002	9.52E-05	1973	8.09E-05
	L5	2	3174	1.40E-05	3174	2.70E-05	3113	3.38E-05	3154	2.49E-05
	L6	1	1489	6.61E-05	1453	6.71E-05	1440	5.68E-05	1461	6.33E-05
	L6	1	1965	7.71E-05	1953	9.39E-05	1978	7.82E-05	1965	8.31E-05
	L6	1	3394	4.07E-05	3442	3.63E-05	3430	2.33E-05	3422	3.34E-05
	L6	2	1501	6.23E-05	1489	9.13E-05	1477	6.48E-05	1489	7.28E-05

L6	2	1990	6.66E-05	1953	9.54E-05	1990	6.87E-05	1978	7.69E-05
L6	2	3442	3.24E-05	3442	4.73E-05	3455	3.84E-05	3446	3.93E-05
L7	1	1489	6.61E-05	1453	6.71E-05	1440	5.68E-05	1461	6.33E-05
L7	1	1965	7.71E-05	1953	9.39E-05	1978	7.82E-05	1965	8.31E-05
L7	1	3394	4.07E-05	3442	3.63E-05	3430	2.33E-05	3422	3.34E-05
L7	2	1501	6.23E-05	1489	9.13E-05	1501	6.45E-05	1497	7.27E-05
L7	2	1990	6.66E-05	1953	9.54E-05	1990	6.87E-05	1978	7.69E-05
L7	2	3442	3.24E-05	3442	4.73E-05	3455	3.84E-05	3446	3.93E-05
L8	1	1514	8.35E-05	1538	7.76E-05	1477	7.67E-05	1510	7.93E-05
L8	1	1953	1.01E-04	1917	9.76E-05	1929	9.16E-05	1933	9.66E-05
L8	1	3455	2.82E-05	3455	2.92E-05	3479	2.23E-05	3463	2.66E-05
L8	2	1501	6.99E-05	1526	9.10E-05	1514	9.39E-05	1514	8.50E-05
L8	2	1953	7.47E-05	1953	1.20E-04	1929	1.20E-04	1945	1.05E-04
L8	2	3430	2.53E-05	3442	3.40E-05	3467	3.23E-05	3446	3.05E-05
L9	1	1428	9.56E-05	1416	9.12E-05	1392	8.81E-05	1412	9.16E-05
L9	1	3455	2.96E-05	3479	2.29E-05	3467	1.81E-05	3467	2.35E-05
L9	2	1392	7.94E-05	1428	1.03E-04	1440	1.10E-04	1420	9.75E-05
L9	2	3430	2.07E-05	3442	3.00E-05	3430	3.02E-05	3434	2.70E-05
M3	1	0	0	0	0	0	0	0	0
M3	2	0	0	0	0	0	0	0	0
R1	1	0	0	0	0	0	0	0	0
R1	2	0	0	0	0	0	0	0	0
R2	1	1379	2.37E-05	1343	2.47E-05	1367	2.29E-05	1363	2.38E-05
R2	1	1978	2.86E-05	1990	2.73E-05	1941	2.01E-05	1970	2.53E-05
R2	2	1355	3.29E-05	1367	4.93E-05	1367	3.30E-05	1363	3.84E-05
R2	2	1990	3.28E-05	1953	4.41E-05	1953	3.08E-05	1965	3.59E-05
R4	1	1416	3.84E-05	1404	4.03E-05	1379	4.20E-05	1400	4.02E-05
R4	1	1880	2.29E-05	1855	2.71E-05	1831	3.02E-05	1855	2.67E-05
R4	2	1367	5.84E-05	1392	5.76E-05	1379	9.39E-05	1379	7.00E-05
R4	2	1831	3.65E-05	1831	3.85E-05	1843	5.67E-05	1835	4.39E-05
R5	1	1440	4.41E-05	1428	3.41E-05	1453	5.34E-05	1440	4.39E-05

	R5	1	1990	6.68E-05	2002	7.61E-05	1965	8.07E-05	1986	7.45E-05
	R5	2	1453	7.85E-05	1440	5.89E-05	1453	1.04E-04	1449	8.04E-05
	R5	2	1990	8.32E-05	1953	8.60E-05	1990	1.26E-05	1978	6.06E-05
	R6	1	1355	5.18E-05	1392	5.20E-05	1379	5.38E-05	1375	5.25E-05
	R6	1	1868	3.69E-05	1868	3.69E-05	1868	3.32E-05	1868	3.56E-05
	R6	1	2478	4.32E-05	2490	3.97E-05	2490	3.76E-05	2486	4.02E-05
	R6	2	1367	7.09E-05	1367	1.08E-04	1367	1.13E-04	1367	9.72E-05
	R6	2	1843	3.52E-05	1855	5.43E-05	1855	6.51E-05	1851	5.15E-05
	R6	2	2502	3.74E-05	2429	6.37E-05	2490	5.33E-05	2474	5.15E-05
	R7	1	1331	3.81E-05	1367	3.71E-05	1355	3.86E-05	1351	3.79E-05
	R7	1	1831	2.91E-05	1868	3.66E-05	1831	3.31E-05	1843	3.30E-05
	R7	2	1367	4.67E-05	1355	7.59E-05	1355	7.58E-05	1359	6.61E-05
	R7	2	1758	3.51E-05	1843	5.07E-05	1831	6.04E-05	1811	4.87E-05
	R8	1	1416	3.32E-05	1428	3.34E-05	1428	3.49E-05	1424	3.38E-05
	R8	1	1990	4.77E-05	2014	4.84E-05	1978	5.25E-05	1994	4.95E-05
	R8	2	1404	5.14E-05	1404	4.78E-05	1416	7.52E-05	1408	5.81E-05
	R8	2	1978	5.20E-05	2014	5.77E-05	1978	8.05E-05	1990	6.34E-05
	R9	1	1428	9.53E-06	1453	1.53E-05	1392	8.33E-06	1424	1.11E-05
	R9	1	2014	1.76E-05	2173	1.78E-05	1978	2.16E-05	2055	1.90E-05
	R9	2	1416	2.03E-05	1404	2.14E-05	1404	2.97E-05	1408	2.38E-05
	R9	2	2161	2.36E-05	2185	2.18E-05	2148	3.26E-05	2165	2.60E-05
5			*frequency*	*power*	*frequency*	*power*	*frequency*	*power*	*frequency*	*power*
	L1	1	0	0	0	0	0	0	0	0
	L1	2	0	0	0	0	0	0	0	0
	L2	1	1453	1.28E-05	1477	1.46E-05	1489	1.29E-05	1473	1.34E-05
	L2	1	3015	9.50E-06	2991	1.00E-05	3003	9.94E-06	3003	9.83E-06
	L2	2	1514	1.80E-05	1440	1.80E-05	1465	1.64E-05	1473	1.74E-05
	L4	1	1489	2.13E-05	1477	2.92E-05	1477	2.68E-05	1481	2.58E-05
	L4	1	2588	1.62E-05	2710	2.91E-05	2515	2.86E-05	2604	2.46E-05
	L4	2	1416	3.36E-05	1489	3.13E-05	1428	3.18E-05	1444	3.22E-05
	L4	2	2612	4.62E-05	2600	4.15E-05	2612	4.01E-05	2608	4.26E-05

L5	1	1477	1.52E-04	1489	1.88E-04	1489	1.79E-04	1485	1.73E-04
L5	1	2563	2.39E-05	2539	2.40E-05	2527	3.41E-05	2543	2.73E-05
L5	2	1501	1.50E-04	1501	1.69E-04	1489	1.80E-04	1497	1.67E-04
L5	2	2563	4.05E-05	2576	4.37E-05	2515	3.82E-05	2551	4.08E-05
L5	2	4028	4.48E-05	4077	4.47E-05	4114	3.66E-05	4073	4.20E-05
L6	1	1489	5.93E-05	1501	5.96E-05	1489	5.91E-05	1493	5.93E-05
L6	1	3003	2.26E-05	3003	2.24E-05	2991	2.05E-05	2999	2.18E-05
L6	2	1477	6.41E-05	1489	6.75E-05	1489	6.93E-05	1485	6.70E-05
L6	2	2942	2.22E-05	2942	2.53E-05	2917	2.44E-05	2934	2.40E-05
L7	1	1465	4.10E-05	1538	3.48E-05	1526	3.84E-05	1510	3.80E-05
L7	1	3479	1.85E-05	3528	2.19E-05	3467	2.34E-05	3491	2.13E-05
L7	2	1489	3.22E-05	1538	4.68E-05	1489	4.64E-05	1505	4.18E-05
L7	2	2441	2.09E-05	2490	2.70E-05	2502	2.17E-05	2478	2.32E-05
L7	2	3577	1.46E-05	3516	1.61E-05	3516	1.99E-05	3536	1.69E-05
L8	1	1428	6.18E-05	1440	6.57E-05	1440	5.90E-05	1436	6.22E-05
L8	1	1892	2.63E-05	1917	3.06E-05	1917	3.18E-05	1909	2.96E-05
L8	1	2612	2.25E-05	2722	2.82E-05	2661	2.24E-05	2665	2.43E-05
L8	2	1453	6.16E-05	1416	6.31E-05	1477	7.47E-05	1449	6.65E-05
L8	2	1953	4.32E-05	1892	4.17E-05	1917	4.41E-05	1921	4.30E-05
L8	2	2893	4.66E-05	2722	4.58E-05	2698	3.88E-05	2771	4.37E-05
L9	1	1501	3.42E-05	1440	3.08E-05	1489	2.53E-05	1477	3.01E-05
L9	1	2087	2.00E-05	2173	1.95E-05	2026	2.55E-05	2095	2.17E-05
L9	1	2576	2.39E-05	2722	2.65E-05	2734	1.89E-05	2677	2.31E-05
L9	2	1355	2.42E-05	1514	2.22E-05	1501	3.03E-05	1457	2.56E-05
L9	2	2222	2.37E-05	2283	1.94E-05	2222	2.36E-05	2242	2.22E-05
L9	2	4199	1.93E-05	4211	1.89E-05	4236	1.73E-05	4215	1.85E-05
M3	1	0	0	0	0	0	0	0	0
M3	2	0	0	0	0	0	0	0	0
R1	1	0	0	0	0	0	0	0	0
R1	2	0	0	0	0	0	0	0	0
R2	1	1465	2.98E-05	1477	2.93E-05	1440	2.42E-05	1461	2.78E-05

R2	2	1477	2.19E-05	1514	2.59E-05	1477	2.78E-05	1489	2.52E-05
R4	1	1794	5.64E-05	1807	5.50E-05	1770	4.88E-05	1790	5.34E-05
R4	1	2686	1.44E-05	2600	1.40E-05	2637	1.59E-05	2641	1.48E-05
R4	2	1526	4.86E-05	1526	5.50E-05	1538	5.46E-05	1530	5.28E-05
R4	2	1807	5.79E-05	1819	6.00E-05	1807	6.08E-05	1811	5.96E-05
R4	2	2942	2.25E-05	2966	2.14E-05	2942	2.18E-05	2950	2.19E-05
R5	1	1489	1.37E-04	1489	1.31E-04	1489	1.11E-04	1489	1.26E-04
R5	1	2478	2.55E-05	2539	3.05E-05	2539	2.79E-05	2519	2.80E-05
R5	1	3955	1.54E-05	3906	1.70E-05	3784	1.87E-05	3882	1.70E-05
R5	2	1501	1.03E-04	1501	1.09E-04	1501	1.07E-04	1501	1.06E-04
R5	2	2612	4.15E-05	2612	3.54E-05	2539	3.89E-05	2588	3.86E-05
R5	2	3870	1.89E-05	3870	1.64E-05	3882	1.21E-05	3874	1.58E-05
R6	1	0	0	0	0	0	0	0	0
R6	2	2051	4.25E-05	2051	4.72E-05	2051	4.17E-05	2051	4.38E-05
R7	1	1477	4.41E-05	1477	4.01E-05	1477	4.29E-05	1477	4.23E-05
R7	2	1477	3.98E-05	1489	4.55E-05	1489	4.65E-05	1485	4.39E-05
R8	1	1404	6.44E-05	1416	7.04E-05	1404	7.16E-05	1408	6.88E-05
R8	1	1782	3.59E-05	1782	3.82E-05	1794	3.05E-05	1786	3.49E-05
R8	2	1465	7.42E-05	1465	7.92E-05	1477	7.15E-05	1469	7.50E-05
R8	2	2930	4.31E-05	2917	4.15E-05	2917	4.13E-05	2921	4.20E-05
R9	1	1465	3.75E-05	1465	3.66E-05	1477	3.34E-05	1469	3.58E-05
R9	1	4126	1.18E-05	4053	1.08E-05	4028	9.17E-06	4069	1.06E-05
R9	2	1465	3.16E-05	1477	3.29E-05	1501	2.98E-05	1481	3.15E-05
R9	2	2917	7.76E-06	2881	8.59E-06	2917	1.18E-05	2905	9.38E-06
R9	2	4138	9.11E-06	4077	1.16E-05	4028	9.23E-06	4081	9.99E-06

Curriculum Vitae

Name:	Claudia Blandford
Post-Secondary Education and Degrees:	University of Virginia, Charlottesville VA 2007 - 2011 BSc The University of Western Ontario, London ON 2011-2014, MESc
Honours and Awards:	Academic All-Region, 2009-2011 Deans List, 2009-2010 Canadian Merit Scholarship, 2007
Related Work Experience:	Teaching Assistant The University of Western Ontario 2012-2014

Publications:

Blandford C., Neuert M., Balsdon M., Yazdani A., Jenkyn TR. Resonant frequencies excited in the craniofacial skeleton due to impact are not dependent on impact site or impact severity. *submitted to the Journal of Cranio-Facial Surgery*.